SOLVENT VAPOR ASSISTED SELF ASSEMBLY OF PATTERNABLE BLOCK COPOLYMERS

A Dissertation

Presented to the Faculty of the Graduate School

of Cornell University

In Partial Fulfillment of the Requirements for the Degree of

Doctor of Philosophy

by

Joan K. Bosworth

August 2009

SOLVENT VAPOR ASSISTED SELF ASSEMBLY OF PATTERNABLE BLOCK COPOLYMERS

Joan K. Bosworth, Ph.D.

Cornell University, 2009

Block copolymer self assembly presents a method for patterning and templating applications on the 10-50 nm length scale, a smaller scale than can be easily achieved by photolithography. Here we investigate the use of functionalized polar-nonpolar block copolymers both as photopatternable self-assembling materials and for selective infiltration of one block for patterning. Block copolymer thin films with defect-free self-assembled morphology over large domains combined with careful control of the orientation of the morphology are critical for these patterning applications.

Self assembly of block copolymers is facilitated by polymer chain mobility, commonly achieved by heating block copolymer films above the glass transition temperature of the blocks. However, many block copolymer systems, including those discussed here, are thermally incompatible. Swelling in a solvent vapor, called solvent annealing, provides sufficient mobility for self assembly. Solvent annealing proved critical to forming ordered structures of functional polar-nonpolar block copolymer thin films.

Thermal instability initially led to limited self assembly of combined top-down/bottom-up block copolymer systems. In this case, photolithographic functionality has been designed into block copolymers, allowing the majority component of a block copolymer to behave as a negative-tone photoresist. Solvent vapor annealing has provided a simple and inexpensive method for allowing the bottom-up self assembly of these top-down photopatternable materials. An additional

benefit of solvent annealing is the ability to reversibly tune the morphology formed using the selectivity of different swelling solvents to the two blocks: that is, the choice of solvent for annealing directs the formation of different morphologies in the dried film, here spherical and cylindrical. This behavior is reversible, alternating annealing sessions lead to switching of the morphology in the film. Secondary ordering techniques applied in tandem with solvent annealing can be used to further control the self assembly and give highly ordered block copolymer domains. Here we demonstrate the use of graphoepitaxy to align block copolymer self assembly to patterns in substrates.

The combination of block copolymer self assembly with lithographic crosslinking in films was initially pursued to allow precise location of assembled patterns. Taking this behavior a step further, we combine solvent annealing, used to reversibly tune the self-assembled morphology, and lithographic patterning, used to prevent switching in exposed regions. This combined process has provided a method for selectively patterning 100 nm-wide domains of spherical morphology within regions of parallel-oriented cylindrical morphology.

We also investigate solvent annealing of a block copolymer blended with a hydrogen bonding material that selectively segregates into the polar block. Blending provides a method of tuning the periodicity upon solvent annealing for self assembly, with morphology control again possible by solvent selectivity. Selective extraction of the blended material forms voids displaying the tunable periodicity, and the pattern is then transferred by templating to inorganic materials.

BIOGRAPHICAL SKETCH

A native of Houston, Texas, Joan K. Bosworth (Katy) graduated from Houston's High School for the Performing and Visual Arts in 1997. There she participated in pre-professional dance training and still had time for an excellent education. Priorities at this small arts school limited the science and math faculty, occasionally making it a challenge to schedule advanced classes in either area. It was in an advanced chemistry class, held before school for a handful of very determined students by an equally determined teacher, that Katy developed her love of chemistry.

Katy received a B.A. in chemistry and art history from Rice University in 2001. There she participated in research in the laboratory of Prof. Vicki L. Colvin, working on several projects, including templating self-assembled colloidal materials as well as protein and virus crystals. She also completed a semester of independent study with the support of Prof. John L. Margrave, studying the chemistry of art materials, with particular emphasis on understanding their degradation over time and steps for their conservation.

In 2001, interested in pursuing a career in art conservation, she took a position as a laboratory technician in the laboratory of Prof. Colvin, a job that offered flexibility while she also worked as a gallery assistant at Houston's Lawndale Art Center and interned in a private art conservation workshop. The sciences became far more attractive upon observing the contrast in job security between her chemistry and art world compatriots, and she decided to pursue a Ph.D. in materials chemistry in the Department of Chemistry and Chemical Biology at Cornell University.

In 2003, Katy began work in the laboratory of Prof. Christopher K. Ober in the Department of Materials Science & Engineering, studying block copolymer self assembly. Katy has worked closely with collaborator Dr. Charles T. Black, completing

internships both at IBM's Watson Research Center in Yorktown Heights, NY and The Center for Functional Nanomaterials at Brookhaven National Laboratory.

As much as she loves her native Houston (the friendly, quirky, doesn't-take-itself-seriously side), Katy has relished living in a place completely unlike her hometown. Ithaca has hills, colorful fall leaves, snow, lakes, waterfalls, and a large population of free-spirited folk, all of which have provided her unending amusement. Katy anticipates her graduation in January 2009 with both sadness to leave and great excitement about the adventure ahead.

ACKNOWLEDGEMENTS

Shortly after graduating from Rice, a friend with an offer for buy-one-get-one-free plane tickets invited me to come with her on a trip to Ithaca to visit a friend. I asked if Ithaca was somewhere near New York City (a common mistake for those unfamiliar with Ithaca), and decided that the trip could be a fun adventure. We arrived in Ithaca for a mid-October weekend of spectacular fall color and blue skies. I spent the weekend walking around Cornell and Ithaca, thinking that I could very much see myself living here. Allie King and her friend Eric Ryan are now married and remain two of my favorite people. I am very thankful that Allie offered me a cheap ticket to Ithaca on a whim, a small event that has had an enormous impact.

Two years later, I was torn about accepting my offer to Cornell. I had fallen in love with Cornell – its location in Ithaca, its great reputation, its friendly atmosphere. However, I knew I would miss my family and my then-boyfriend Brian. Brian encouraged my desire to move across the country in search of a wild academic adventure. When I moved to Ithaca, Brian and I expected that we would live apart until I finished graduate school, as there are not many opportunities in Ithaca for programmers creating software entirely for the Macintosh. After we spent three years racking up frequent flyer miles, Brian decided to branch out into independent software development and moved to Ithaca. We were married at the Johnson Museum of Art on Cornell's campus on a spectacular blue-sky fall day, a day not unlike my first trip to Ithaca. Brian is a pun-filled self-described geek, smart and sweet and thoughtful. He is the funniest person I know, and I blame him for my emerging smile lines. I love him dearly and am unendingly grateful for his continuing love and support.

I would also like to thank my parents, two nonconformist semi-reformed (yet conservative) hippies. Truly, there are no two other people like them. My two

siblings, Kelly and Will, and I have all turned out to be very different individuals, yet we exemplify the biggest lessons that our parents taught us. These lessons are nose-to-the-grindstone hard work, strong individuality, and a love of the arts – but only as a hobby. Our parents were afraid for a period of time that each of their children would become artists, and that they would have to financially support their artist children forever. The three of us are all semi-gainfully employed now (Kelly as a certified public accountant, and Will recently graduated with a B.S. in mechanical engineering from MIT), much to our parents' pleasure. Mom & Dad: many thanks for patiently teaching all of these things to your occasionally free-spirited daughter (and to Kelly & Will too).

My class of fellow chemistry graduate students was a particularly smart, hardworking, and humble group among a school filled with smart, hardworking, humble students. We supported each other through our first year of classes and teaching, and continued our tradition of Friday night dinners until we began to graduate and move to our new jobs. To Jaci Greimann, Lara Liou, Lindsay Batory, Jeff Rose, Stephanie Hammond, and Jay Henderson: I feel particularly blessed to have had your friendship.

From the time I first learned of his research, Prof. Chris Ober's group felt like home. I am grateful that Chris allowed me the chance to work in his group, and I have always appreciated Chris's even-keeled and respectful approach to advising. My coworkers in the Ober group have backgrounds variously in chemistry, materials science, chemical engineering and physics, and I have loved being able to work in a field with fluid boundaries. Working in this group has also allowed exposure to the best facilities Cornell has to offer, including the Cornell NanoScale Facility (CNF) and the Cornell High Energy Synchrotron Source (CHESS).

I would also like to thank my coworkers in the Ober group. In my time at Cornell, I have worked alongside roughly 50 fellow students and postdocs. I would like to thank my current labmates: Dr. Jin Kyun Lee, Dr. Eisuke Murotani, Dr. Woo Jin Bae, Dr. Harihara Subramanian, Dr. Young Jin Cho, Dr. Heloise Therien-Aubin, Craig Weinman, Marvin Paik, Dr. Anuja De Silva, Drew Forman, Rong Dong, Evan Schwartz, Ethan Chiang, Abhinav Rastogi, Jing Sha, Michelle Chavis, Priscilla Taylor, Zhaoli Zhou, Marie Krysak, Carol Newby, Christine Ouyang, Lin Chen, Hao Chen, Liz Welch, Reinhard Berger, and Diana Wang, and my many other former labmates. I also appreciate the help I received from undergraduates Albert Ko and Jenny Huang, as well as summer student James McDonough. In particular, I would like to thank my current and former coworkers in the block copolymer self assembly project: Marvin Paik, Michelle Chavis, Evan Schwartz, Diana Wang, Dr. Mingqi Li, Dr. Xavier Andre, and Dr. Peter Busch; also Dr. Detlef-M Smilgies from CHESS has been a very helpful collaborator. Dr. Lewis Fetters provided insightful advice on anionic polymerization. I also particularly appreciated Jing Sha and Drew Forman, both of whom have demonstrated expertise with photo- and electron-beam lithography.

I traveled to the University of Bayreuth in Germany twice over the course of my studies for collaborations, and was generously hosted by profs. Hans-Werner Schmidt and Larisa Tsarkova. Dr. Frauke Pfeiffer, a former student of the Schmidt Group, took great care of me while I was there, and I was happy to reciprocate when she visited Cornell. I still treasure her friendship.

Dr. Chuck Black has served as a collaborator and mentor for several years. He facilitated a fellowship and an internship from IBM, and then sponsored a second internship at Brookhaven National Laboratory after he had moved there. Chuck's great advice and encouragement have provided continuous motivation.

TABLE OF CONTENTS

LIST OF FIGURES

LIST OF SCHEMES

LIST OF TABLES

SYMBOLS AND TERM ABBREVIATIONS

α	exponent in dilution approximation, $\chi_{EFF} = \chi_{AB}*\phi^{\alpha}$, corrects experimental behavior
bcc	body-centered cubic crystal packing
C	cylindrical morphology
χ	Flory-Huggins interaction parameter
χ_{AB}	Flory-Huggins interaction parameter for blocks of an AB diblock copolymer
d	spatial period of a block copolymer; in literature also called d, D, or L_0. Here *d* is used to avoid confusion with other abbreviations.
D	disordered state
d_0	spatial period in polymer bulk; in literature also called L_0
f_A	volume ratio of block A in a block copolymer
fcc	face-centered cubic
fco	face-centered orthorhombic
ϕ_s	solvent volume fraction (in solvent polymer blend)
G	gyroid morphology
h	wall spacing in sandwiched thin film confinement studies; film thickness in thin films supported on a substrate
K	indicates "kg/mol" - follows number. For example 11K means 11 kg/mol
L	lamellar morphology
M_n	number-average molecular weight
MST	microphase separation temperature
N	degree of polymerization
n	number of layers
ODT	order-disorder transition

OOT	order-order transition
R_G	radius of gyration
S	spherical morphology
SCF	self-consistent mean-field
T_g	glass transition temperature
T_m	melting temperature
ϕ_p	block copolymer volume fraction (in solvent mix); also called ϕ in literature

CHEMICAL ABBREVIATIONS

2MOE	2-methoxyethanol
DBP	di-*n*-butyl phthalate
DOP	dioctyl phthalate
HABA	2-(4-hydroxyphenylazo)benzoic acid
P2VP	poly(2-vinylpyridine)
PAA	poly(acrylic acid)
PαMS	poly(α-methylstyrene)
PαMS-*b*-PHOST	poly(α-methylstyrene)-*block*-poly(4-hydroxystyrene)
PB	polybutadiene
PDMS	poly(dimethylsiloxane)
PEO	poly(ethylene oxide)
PEO-*b*-PPO-*b*-PEO	poly(ethylene oxide)-*block*-poly(propylene oxide)-*block*-poly(ethylene oxide)
PEP	poly(ethylene-alt-propylene)
PEP-*b*-PEE	poly(ethylenepropylene)-*block*-poly(pethylethylene)
PFS	poly(ferrocenyldimethylsilane)
PHOST	poly(4-hydroxystyrene)
PI	polyisoprene
PLA	poly($_{D,L}$-lactide)
PLLA	poly($_{L}$-lactide)
PMMA	poly(methyl methacrylate)
PMMA-*b*-PHEMA	poly(methyl methacrylate)-*block*-poly(hydroxyethyl methacrylate)

PPO	poly(propylene oxide)
PS	polystyrene
PS-*b*-P2VP	polystyrene-*block*-poly(2-vinylpyridine)
PS-*b*-P2VP-*b*-PtBMA	poly(styrene)-*block*-poly(2-vinylpyridine)-block-poly(*tert*-butyl methacrylate)
PS-*b*-P4VP	polystyrene-*block*-poly(4-vinylpyridine)
PS-*b*-PAA	polystyrene-*block*-poly(acrylic acid)
PS-*b*-PB	polystyrene-*block*-polybutadiene
PS-*b*-PB-*b*-PS	polystyrene-*block*-polybutadiene-*block*-polystyrene
PS-*b*-PDMS	polystyrene-*block*-poly(dimethylsiloxane)
PS-*b*-PEB-*b*-PS	polystyrene-*block*-poly(ethylene-butylene)-*block*-polystyrene
PS-*b*-PEO	polystyrene-*block*-poly(ethylene oxide)
PS-*b*-PEP	polystyrene-*block*-poly(ethylene-alt-propylene)
PS-*b*-PFS	polsytyrene-*block*-polyferrocenyldimethylsilane
PS-*b*-PI	polystyrene-*block*-polyisoprene
PS-*b*-PLA	polystyrene-*block*-poly($_{D,L}$-lactide)
PS-*b*-PLLA	polystyrene-*block*-poly($_{L}$-lactide)
PS-*b*-PMMA	polystyrene-*block*-poly(methyl methacrylate)
PS-*b*-PtBA	polystyrene-*block*-poly(*tert*-butyl acrylate)
PS-*b*-PtBMA	polystyrene-*block*-poly(*tert*-butyl methacrylate)
PS-*r*-PMMA	polystyrene-*ran*-poly(methyl methacrylate)
PtBA	poly(*tert*-butyl acrylate)
PtBMA	poly(*tert*-butyl methacrylate)
THF	tetrahydrofuran

TMMGU	tetramethoxymethyl glycoluril
TPST	triphenylsulfonium triflate

CHAPTER 1

BLOCK COPOLYMER SELF ASSEMBLY IN THIN FILMS: CONTROL OF SELF ASSEMBLY AND PATTERNING APPLICATIONS

1.1 Block Copolymer Self Assembly for Patterning Applications

Self-assembled materials, such as block copolymers, hold promise for patterning on length scales that are difficult to achieve by photolithography. As described in further detail below, block copolymers can self-assemble into a variety of morphologies including those that are spherical, cylindrical, and lamellar. In order for block copolymer self assembly to be realistically applicable for templating applications in thin films, defect free self assembly must be obtained over large domains, in addition to control of the orientation of morphology formed in the thin films.

Self assembly is facilitated by imparting mobility to polymer chains, either by heating films or by annealing in a solvent vapor. Solvent vapor infiltrates block copolymers and induces mobility, but also alters the phase behavior of block copolymers from the neat state. This phase behavior alteration requires special attention, but it also provides a method for tuning phase behavior in films. Secondary ordering techniques such as graphoepitaxy and chemical epitaxy can be combined with polymer mobility techniques to cause defect-free ordering and to control orientation in thin films. Pattern transfer of the ordered self-assembled pattern to a wide variety of other materials is achieved using a small number of methods. Control of the location of self assembly is also possible using combined top-down/bottom-up patterning techniques by incorporating lithographic capabilities into block copolymer structures.

1.2 Block Copolymer Phase Behavior

1.2.1 Self Assembly in the Bulk

Block copolymers are made up of two or more polymer segments covalently bound in a single chain. The simplest and most studied set are linear diblock

copolymers, made up of two separate polymer species covalently bound in the center.[1] Self assembly of block copolymers only occurs when polymer chains are immiscible and have sufficient mobility, typically achieved by thermal annealing above the glass transition temperatures of the two blocks.

1.2.1.1 Diblock Copolymers

When sufficiently immiscible, linear block copolymers are known to form a variety of morphologies, commonly including those that are lamellar, cylindrical (hexagonal), and spherical (body-centered cubic); for a narrow range of parameters, they are also known to form gyroid morphologies.[1] Schematics of these morphologies can be seen in Figure 1.1. Theoretical work intersecting with experimental studies have found that block copolymer phase behavior can be described by a small number of parameters. In his mean field theory for weakly segregated block copolymers, Leibler found that phase behavior can be determined by the volume fraction of one of the blocks, f, and $\chi_{AB}N$, the product of the Flory-Huggins interaction parameter, χ_{AB} (a measure of the affinity, or lack thereof, of two blocks to each other) and the degree of polymerization N.[2] This theory works well for describing self assembly of block copolymers in the weak field regime.

Semenov created a phase diagram for strong segregation regimes, drawing a phase diagram using Liebler's weak-field phase diagram and his own strong field phase diagram with dotted lines connecting the two theories.[3] For strongly segregated polymers, in which the thickness of the interface is significantly less than the domain dimension, block copolymer morphology is largely determined by the volume fraction of the two blocks.[4] These theoretical calculations agree with experimental data for polystyrene-*block*-polybutadiene showing spherical morphology for less than 25% and

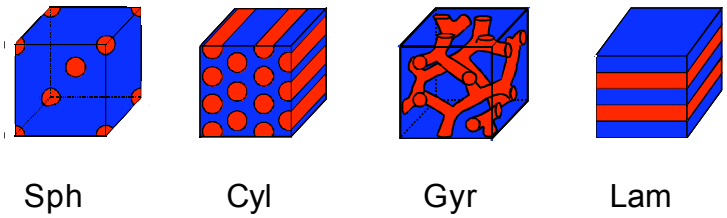

Figure 1.1. Morphologies formed by phase-separating block copolymers: body-centered cubic packed spheres (Sph), hexagonally packed cylinders (Cyl), double gyroid (Gyr), and lamellae (Lam). Inverse phases are not shown. Figure by Minqi Li, used with permission.

more than 85% PS, hexagonally-packed cylindrical morphology for 25 – 40% and 60-85% PS, and lamellar morphology for 40-60% PS.

With their self-consistent mean-field theory (also called self-consistent field theory or SCF theory), Matsen and Bates describe both the weak-field regime, where interfaces between morphologies curved in the phase diagram, as well as the strong segregation regime, where interfaces between morphologies run nearly vertical.[5] Their theoretical phase diagram can be found in Figure 1.2. In the case of symmetric block copolymers, phase separation occurs for $\chi ABN = 10.5$, called the mean-field critical point. Further reading on this subject can be found in a number of excellent reviews.[1,6,7]

Typical molecular weight ranges for self-assembling block copolymers are 20-100 kg/mol, yielding typical periodicity of morphologies of 20-50 nm.[8] The upper limit of spacing is due to the limited chain mobility caused by the high degree of entanglement in very large molecular weights, rendering self assembly on a practical time scale impossible. For the lower limit, the product of $\chi_{AB}N$ becomes small for lower molecular weights (small N), and for lower molecular weights, the interaction is not sufficiently strong for self assembly to occur.

The period spacing of lamellar morphology was found experimentally to scale with the 2/3 power of the molecular weight; i.e. for spatial period d and degree of polymerization N, $d \sim N^{2/3}$.[9] The 2/3 scaling law was confirmed in theoretical calculations in the strong segregation limit for lamellar, cylindrical, and spherical morphologies.[4] Notably, though, the 2/3 power only holds in the strong segregation limit, where the interfacial width (which is dependent on χ, the Flory-Huggins interaction parameter) is significantly smaller than the domain spacing. In cases of weaker segregation, spacing is more closely related to the radius of gyration of the copolymer molecule, which scales with one half power N, such that $d \sim R_G \sim N^{1/2}$.

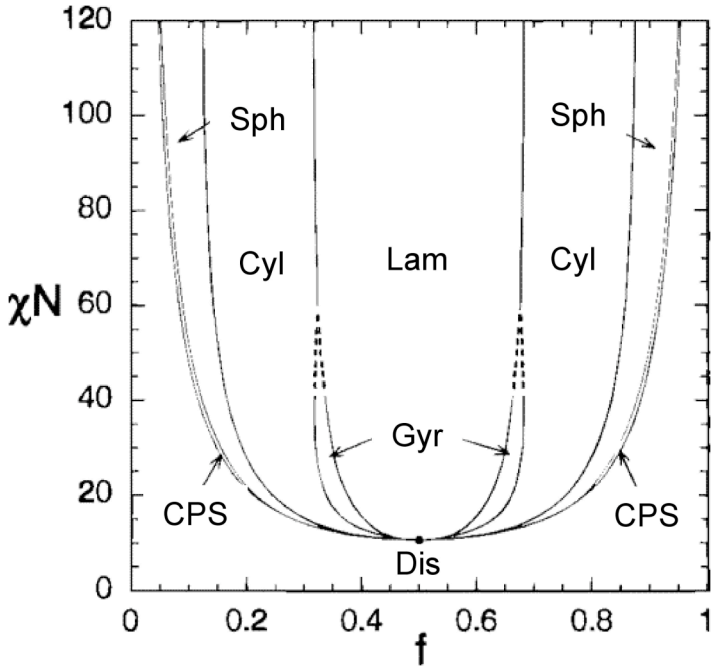

Figure 1.2. Phase diagram for diblock copolymer melts created using mean-field theory. Phases are labeled Lam (lamellar), Cyl (hexagonal cylinders), Gyr (double gyroid), Sph (bcc spheres), CPS (close-packed spheres), and DIS (disordered). Dashed lines denote extrapolated phase boundaries, and the dot denotes the mean-field critical point. Reprinted with permission from ref. 5, copyright 1996 American Chemical Society.

1.2.1.2 Triblock Copolymers

The phase behavior of linear ABA triblock copolymers is similar to that of AB diblock copolymers.[10,11] The same sequence of morphologies are expected for ABA triblocks as for AB diblocks, though some asymmetry in the phase diagram is expected, especially when the two A blocks in the ABA triblock possess different molecular weights.[12,13] Matsen and Schick noted differences in domain spacing between AB and ABA block copolymers due to chain bridging in the triblocks.[14] Further calculation by Matsen & Thompson noted that ABA triblocks (with symmetric A) have nearly identical phase behavior to AB diblocks, as demonstrated by the overlaid phase diagrams (Figure 1.3).[15] In the remainder of this review, ABA triblock copolymers will be discussed alongside AB diblock copolymers due to the similarity of their phase behavior.

In the case of linear triblock copolymers (also called triblock terpolymers) with ABC structure, and even more so with higher-order block copolymers (4 blocks and higher), the additional complexity allows the formation of many more structures than diblocks.[1] Many of the possible morphologies are displayed in Figure 1.4. However, understanding this complex behavior is more difficult due to the increased number of parameters to consider. First, there are significant structural differences depending on the ordering of the blocks, thus the structure of a triblock cppolymer, even with identical volume fractions, varies significantly for ABC, ACB, and BAC ordering. Furthermore, predicting the morphology in the case of triblocks requires accounting for the interactions of each block with the other two means must be considered, χ_{AB}, χ_{AC}, χ_{BC}, as well as knowing the volume fractions for two of the blocks, f_A and f_B. Finally, slow equilibration of ABC systems has been found to become even more complicated in the comparison of experimental studies with theoretical, making it

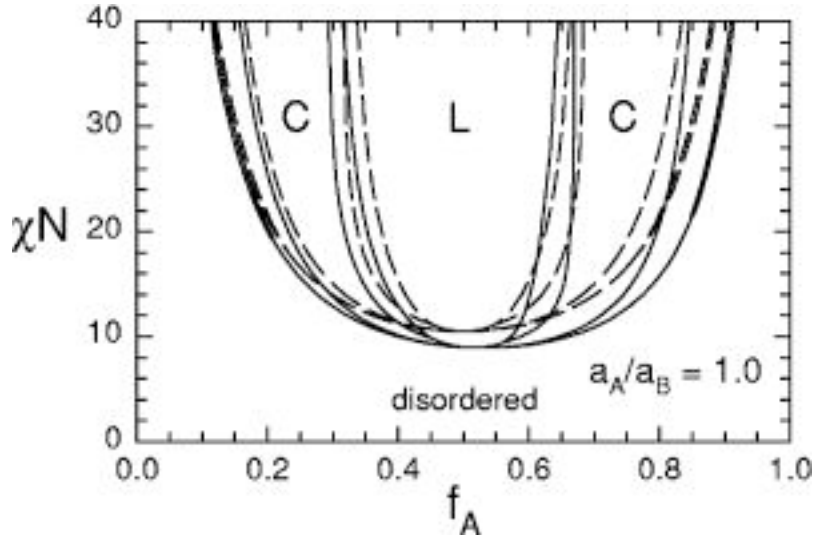

Figure 1.3. The mean-field phase diagram for an ABA triblock copolymer (solid curves) possesses very similar shape to one for an AB diblock copolymer (dashed curves). Reprinted with permission from ref. 15, copyright 1999, American Institute of Physics.

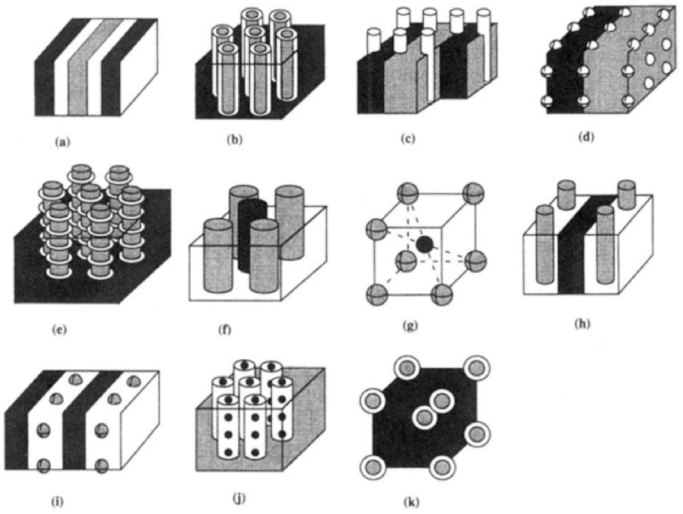

Figure 1.4. Examples of morphologies formed by ABC triblock copolymers[16]; gyroid morphologies have also been demonstrated (not shown here). Reprinted with permission from ref. 1, copyright 1995, American Chemical Society.

difficult to determine if structures formed in polymers are thermodynamically stable structures or simply metastable states. Those studying triblock copolymer self assembly have often turned to using solvent evaporation or solvent annealing to gain long range ordering due to the slow thermal equilibrium problem, both in the bulk and in thin films.

1.2.1.3 Nonlinear Architectures

Phase behavior of nonlinear polymers also varies significantly from those of linear polymers. Examples of nonlinear polymers are block copolymers in which one or more of the blocks are composed of star, comb, or dendrimer structures. While this subject is not covered in this work, more information can be found here.[17]

1.2.1.4 Thermal Annealing

Block copolymer self assembly, even when thermodynamically favorable, will only occur at an appreciable speed when the polymer chains are given sufficient mobility. Increased mobility is primarily achieved by heating to temperatures above the T_g for both polymers. This can become tricky when a block copolymer possesses both a high T_g and a low thermal degradation temperature.

It is interesting to note that reversibly tunable morphologies are possible for a single molecular weight sample by heating the block copolymer. The Flory-Huggins interaction parameter χ has an inverse-temperature component ($\chi = A/T + B$), which allows downward vertical movement in the phase diagram with increased temperature; this movement is reversible with a lowering of temperature. In symmetric block copolymers, the lamellar morphology shifts directly to a disordered state; in asymmetric polymers, for example those forming cylindrical morphologies, transitions from cylindrical to spherical morphology occur before the morphology becomes

disordered. Sakurai et al. demonstrated a transition in polystyrene-*block*-polyisoprene (PS-*b*-PI), with total number-average molecular weight (M_n) 82 kg/mol and 16% polystyrene, from cylindrical morphology at 150˚C to spherical morphology at 200˚C.[18] Kimishima et al. similarly observed PS-*b*-PI with M_n 44 kg/mol and 20% PS, which underwent a transition from cylinders to spheres occurring 115-16.7˚C.[19] Hajduk et al. demonstrated a transition from lamellae to cylinders, evenly spaced, to hexagonally-packed cylinders upon heating slightly asymmetric polystyrene-*block*-poly(ethene-co-butene).[20] Thermoreversible order-order transitions are only possible for a narrow range of polymer compositions, for polymers with Flory-Huggins interaction parameter (χ) and correct molecular weight (N) such that the barrier between molecular weights occurs for a temperature that lies between the glass transition temperature and the thermal degradation temperature for a polymer. This is, of course, only possible in the weak-field regime.

In the strong segregation regime, however, the interfaces between morphologies are nearly vertical in the phase diagram, and thermally induced transitions are not possible. Tuning morphology must be achieved by horizontal movement in the phase diagram, one involving a change in the relative sizes of the blocks. This can be achieved by blending with homopolymers or other materials prior to bulk or film casting; it can also be achieved by annealing in a selective solvent. Solvent annealing is particularly attractive due to its *in situ* tunability after bulk or film casting. The phase behavior of solvent and homopolymer blends are covered in more detail below (section 1.2.2).

1.2.1.5 Self Assembly in Thin Films: Confinement Effects

Many templating applications require patterning of block copolymer thin films. Block copolymer self assembly in thin films varies significantly from the bulk due to

interfacial interactions at the polymer-substrate and polymer-air interfaces. The important points are summarized below; for a more in-depth review of these materials, see Fasolka and Mayes.[21] In this section, we focus on film thicknesses (h) equal to or larger than the bulk spacing d_0.

1.2.1.5.1 Between Two Hard Walls: Surface Neutrality vs. Orientation

Russell et al. first observed the formation of multilayered parallel orientations of lamellae in films of symmetric polystyrene-*block*-poly(methyl methacrylate), (PS-*b*-PMMA), on silicon, referred to as surface-induced ordering.[22,23] No preferential orientation was observed in toluene-cast films, but parallel orientation was observed after thermal annealing.[23] This was accompanied by film thickness forming in steps, also known as island & hole formation or terracing. Parallel orientation from selective interactions with walls also occurs for films of cylinders.[24] In all of these films, films were formed on surfaces with a preferential interaction with one of the blocks.

Turner gave the first theoretical treatment of the equilibrium behavior of a symmetric block copolymer confined between two identical parallel plates with preferential attraction of the plates to one block of the polymer.[25] For the symmetric system, he found the formation of n number (A-B, B-A) lamellar layers aligned parallel to the plates. When the plate spacing corresponds to a half-odd integer number of layers, no frustration in spacing is observed.

Walton et al. went on to study the orientation of block copolymers as a function of interaction with blocks; when walls are preferential for one of the blocks, parallel orientation forms.[26] In the case of symmetric wetting of preferential walls, unfrustrated spacing occurs for wall spacing h, $h = nd_0$, which is the bulk spatial period d_0 multiplied by the number of layers n. Alternatively, for asymmetric preferential walls (the walls attract opposite blocks), the unfrustrated system forms

when the plate spacing corresponds with $h = (n + ½)d_0$. This behavior was confirmed experimentally with polystyrene-*block*-poly(methyl methacrylate) sandwiched between two walls treated with random copolymers of polystyrene-*ran*-poly(methyl methacrylate), or PS-*r*-PMMA, with varying composition and thus varying block interaction.[27,28]

In thick films, i.e. $h >> d_0$, with preferential walls, competing effects can lead to mixed orientations of the morphologies. Konrad et al. studied polystyrene-*block*-polybutadiene-*block*-polystyrene, or PS-*b*-PB-*b*-PS, films on silicon, and found parallel orientation near the substrate, but mixed perpendicular and parallel orientations at the air interface.[29] Xu et al. studied thick films of PS-*b*-PMMA confined between two walls of PS-*r*-PMMA random copolymers of varying composition; they observed that parallel orientation occurs near the walls, and proceeds throughout the film thickness for thinner films.[30] However, a mixed morphology is found for thicker films, with parallel orientation near the walls and perpendicular orientation far from the selective wall wetting influence.

Walton et al. also found that for neutral walls, lamellar block copolymers are expected to form perpendicular orientations for any plate spacing.[26] Pickett & Balasz found that for neutral walls, perpendicular morphology forms for all film thicknesses, and Monte Carlo simulations by Sommer et al. agree with this finding.[31,32] Kellogg et al. confirmed this behavior experimentally with PS-*b*-PMMA sandwiched between two walls treated with random copolymer brushes: nearly neutral walls formed perpendicular morphology.[28]

1.2.1.5.2 Substrate Surface Neutrality for Perpendicular Orientation

Surface-neutralizing techniques have been used extensively to gain perpendicular orientation of both cylindrical and lamellar morphologies by eliminating

preferential attraction of one block. In the case of substrate-supported films, which for practical purposes are the most common, the polymer-substrate interface can be controlled, though the polymer-air interface cannot. In some cases, however, the energy effect from the substrate neutralization is enough to induce perpendicular orientation, though this effect largely breaks down for $h > d_0$.

Manksy et al. systematically changed the substrate interactions with lamellar PS-*b*-PMMA using silicon to which PS-*r*-PMMA random copolymers with different compositions (f_{PS}) were grafted.[33] Neutral wetting conditions were acheived with random copolymer substrate treatment containing fraction of polystyrene, f_{PS}, $0.5 < f_{PS} < 0.65$. for film thicknesses 2.5 to 3.5 times d_0. Lamellae near the substrate are oriented perpendicular, though lamellae at the air interface still have parallel orientation. Mansky et al. confirmed the same behavior for cylindrical PS-*b*-PMMA, and found that neutral wetting conditions were also possible.[34] The surface tensions of PS and PMMA were found to be nearly equal at 225˚C, leading to neutral wetting at both the substrate and air interfaces.

The exact composition of random copolymer graft for neutral wetting conditions was revisited recently, and was found to be slightly different for cylindrical and lamellar morphologies.[35] In cylinder-forming PS-*b*-PMMA (M_n 88K, f_{PS} 0.72), perpendicular orientations found for brushes with f_{PS} 0.52 to 0.72, with the neutrality condition f_{PS} 0.64. On the other hand, lamellae-forming polymers (M_n 50K, f_{PS} 0.5) became perpendicular for 0.48 to 0.78, with neutrality condition f_{PS} 0.55.

The initial, and still most commonly used, method for control surface wetting is the grafting of random copolymers of hydroxyl-terminated PS-*r*-PMMA to the native silicon oxide surface layer present on silicon wafers.[36] This approach makes use of a hydroxyl-functionalized TEMPO initiator, which is then used to initiate the random copolymerization of styrene and methyl methacrylate by nitroxide-mediated

radical polymerization. Each polymer chain has one hydroxyl functionality, necessary for surface grafting onto the silicon oxide surface layer on silicon with sufficient density for surface modification.

Grafting is achieved by spin-coating a film of the hydroxyl-terminate random copolymer onto a silicon substrate with a native silicon oxide layer. The film is heated to facilitate binding of the polymer to the substrate. Before applying the block copolymer, any unbound material is rinsed away.

A variety of other surface neutralization techniques for PS-*b*-PMMA films have been used, including the following:

- Surface-tethered TEMPO initiators for random copolymerization of PS-*r*-PMMA brushes[37]
- Varying the grafting density of self-assembled monolayer films of non-polar octadecyltrichlorosilane to tune wetting on a polar silicon oxide substrate[38]
- Modification of a silicon oxide surface with a self-assembled monolayer that is neutral to PS-*b*-PMMA, 3-(*p*-methoxyphenyl)propyltrichlorosilane[39]
- Inclusion of crosslinkable benzocyclobutene monomer with the random copolymerization of styrene and methyl methacrylate initiated from unfunctionalized TEMPO; the benzocyclobutene component crosslinks with heat, rendering heated films insoluble.[40,41] An advantage to this method is that bond-formation to the substrate is not required; therefore this technique can be extended to substrates other than silicon oxide. Use of photolithographic techniques to pattern gold on top of this solvent-resistant neutral layer gives selective orientation control with resolution demonstrated to 6 μm.[40]
- Inclusion of a small quantity of hydroxyethyl methacrylate (HEMA) monomer with the styrene and methyl methacrylate initiated from unfunctionalized

TEMPO; with inclusion of 1-2% HEMA, more than one hydroxyl group per polymer chain may be achieved, ensuring better surface adhesion.[42,43]

- Blending of two different random copolymers (each PS-*r*-PMMA-*r*-"monomer3") which crosslink together into a mat upon UV exposure; the two additional monomers are methacrylates with acryloyl side chains and glycidyl side chains. Photopattern resolution of 100 μm was demonstrated.[43,44]
- Blending hydroxyl-end-functionalized polymers of PMMA and PS.[45]
- Inclusion of an azide-functionalized styrene monomer with the random copolymerization of styrene and methyl methacrylate initiated from unfunctionalized TEMPO; crosslinking of the films, which can be initiated using heat or UV, renders them insoluble with UV pattern resolution demonstrated to 7 μm.[46]

Substrate modification has been demonstrated for a small number of other block copolymers. Use of tunable substrate surface energy from grafted PS-*r*-PMMA was studied for neutralization polystyrene-*block*-polyisoprene and polystyrene-*block*-poly(*n*-butyl methacrylate).[47] For a symmetric block copolymer of polystyrene-*block*-poly(2-vinylpyridine), PS-*b*-P2VP, a random copolymer composed of PS-*r*-P2VP-*r*-PHEMA (with PHEMA 2 mol % for substrate grafting) led to perpendicular orientations in thin films near the substrate.[48] These were not able to overcome selective wetting interactions at the air interface, leading to parallel interactions near the film surface. PS-*r*-PMMA surface neutralization using hydroxyl-terminated PS-*r*-PMMA caused perpendicular orientation of polystyrene-*block*-poly(ethylene oxide), PS-*b*-PEO, with PEO cylinders after solvent annealing in nonselective solvent benzene and water vapor.[49] One final method for controlling interfacial interactions has been briefly demonstrated: blending a small quantity (2.5% or less) of hydroxyl-terminated

polystyrene was found to neutralize the air interface of PS-*b*-PEO, leading to perpendicular orientation of cylinders applied to an untreated substrate upon annealing in benzene.

1.2.1.5.3 Incommensurate Thicknesses: Shift Happens

As described above in section 1.2.1.5.1, parallel orientations of lamellar block copolymers form when sandwiched between walls that display either a symmetric or asymmetric preference for one of the blocks, as long as the wall spacing h matches the repeat distance of the polymer. However, when h does not match the repeat distance of the polymer, the shifts in the self assembly from the bulk behavior can occur in order to minimize the strain within the polymer. These changes include shifting the polymer spacing d from the bulk value d_0, formation of perpendicular orientation, and in films supported on one side only, the formation of discrete film thicknesses, called island and hole formation or terracing.

Shull predicted that for lamellae-forming morphologies, domain spacing d would shift from the bulk value d_0 for incommensurate wall spacing thicknesses, that is, $h \neq nd_0$ for symmetric wall wetting, or $h = (n + ½)d_0$ for asymmetric wall wetting.[50] This behavior was first observed by Russell et al. in thin films of symmetric PS-*b*-PMMA on silicon substrates.[51] Lambooy et al. observed this experimentally for PS-*b*-PMMA confined between two solid surfaces a shift in the parallel lamellae spacing d from the bulk value spacing d_0. [27,52] This shift varied in a cyclic manner relative to the wall spacing h as it shifted between commensurate and incommensurate film thicknesses. They also observe that the deviation from d_0 decreases as h becomes much larger – an explanation that makes sense considering that the deviation would be distributed over a larger number of polymer chains. Koneripalli et al. also demonstrated this behavior for lamellar poly(ethylenepropylene)-*block*-

poly(ethylethylene) (PEP-*b*-PEE) in confinement with PEE-selective walls.[53] Knoll, Tsarkova & Krausch reported the same behavior for cylindrical morphology; using polystyrene-*block*-polybutadiene, PS-*b*-PB and PS-*b*-PB-*b*-PS, that form parallel cylinders of PS on silicon, *d* was found to vary cyclically with *h*.[54]

In thin films supported by a substrate (that is, not sandwiched between two walls), an alternative method to subvert frustration from incommensurate thicknesses is discretization of the film thickness into islands or holes, sometimes also called terracing.[23,55] Koneripalli et al. demonstrate the concept of island and hole formation nicely, as seen in Figure 1.5.[53] Carvalho and Thomas demonstrated that terracing occurred for thin films of a variety of lamellae-forming block copolymers, including PS-*b*-PMMA, PS-*b*-P2VP, and PS-*b*-PB.[56]

Several groups have predicted transitions in the orientation from strained parallel lamellae to distorted perpendicular lamellae in a symmetric block copolymer constrained between highly selective, symmetric wetting walls (i.e. walls made of the same material as one of the blocks) in the case of small, but incommensurate, wall spacing *h*.[31,57-61] Suh et al. explain this behavior in terms of film thickness.[61] The deviation to reach a full period thickness is the same value for thick and thin films; for thick films, however, this deviation is distributed over a larger number of layers so the compression or expansion of each layer is small. In thin films, the deviation is very large. For these thin films, the entropic cost of film chains stretching or compressing to adjust the film thickness in the parallel orientation can become larger than the cost of being oriented perpendicular to the walls. Wang et al. use Monte Carlo simulations to further study this phenomenon, as reproduced in Figure 1.6.[62] In experimental support of this behavior, Carvalho & Thomas both observed for some cases the formation of nonparallel orientation at edges between terrace steps.[56]

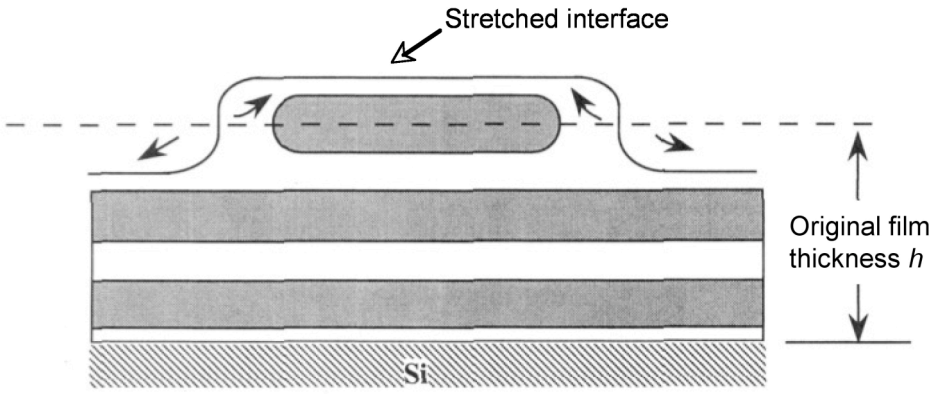

Figure 1.5. Schematic of island formation in a diblock copolymer film. The arrows indicate how material movement occurs as the flat, as-cast film with thickness h (incommensurate for discrete film thickness) forms the island. The height of the island is equal to the equilibrium domain thickness d_0. Alternatively, hole formation occurs similarly. Reprinted with permission from ref. 53, copyright 1995, American Chemical Society.

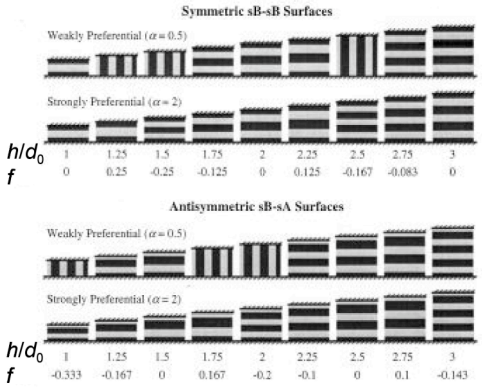

Figure 1.6. Illustration of simulated morphology behavior of symmetric diblock copolymer thin films confined between two hard and homogeneous surfaces of varying degree of attraction (weakly and strongly preferential). Light regions represent A blocks and dark regions represent B blocks. When the wall spacing h is commensurate with bulk periodity d_0, lamellae with parallel orientations form. When film wall spacing is incommensurate with polymer periodicity, the lamellar orientation and periodicity (d) shift to relieve frustration (f). Reprinted with permission from ref. 62, copyright 2000, American Institute of Physics.

Brown & Chakrabarti used a coarse-grained model to simulate self assembly of a symmetric block copolymer between walls, varying the wall attraction and separation.[58] In the case of identical walls, either parallel or perpendicular orientation was found. When the walls that attract opposite morphologies, termed asymmetric wetting, they also observe the formation of distorted lamellae, nicknamed "egg carton" and "twisted perpendicular," in addition to the parallel and perpendicular orientations. Using self-consistent field theory, Matsen showed similar behavior for symmetric and asymmetric wetting, including the formation of a distorted morphology for asymmetric wetting of a symmetric block copolymer with high potentials (strong block attraction).[59] This distorted morphology was described as being parallel at one wall and perpendicular at the other, identical to the morphology that Koneripalli found experimentally for $h = d_0$ under asymmetric confinement.[63] Russell et al. was the first to observe this mixed-phase morphology experimentally for very thin films, found in thin films of PS-*b*-PMMA on silicon.[51]

Formation of perpendicular orientation was also shown experimentally for symmetric PS-*b*-PMMA with $h \sim d_0$ supported on a substrate, rather than sandwiched between walls; this morphology is understood with parallel orientation of PMMA at the surface and slightly capped lamellae at the air interface.[64] This behavior was studied in more detail both theoretically and experimentally by Fasolka et al., and they observed the formation of the hybrid structures not observed in the bulk for $h \sim \frac{1}{2}d_0$,[21,65] which can be seen in Figure 1.7. Kim & Russell studied the behavior of thin films of bulk-cylinder forming PS-*b*-PMMA supported by a silicon substrate, a condition found to be only weakly attractive to the blocks; in addition to the possible parallel and perpendicular structures predicted by theory, a hybrid structure was observed of half-cylinders at the air surface possible with the surface energies of the two blocks is not too large.[66]

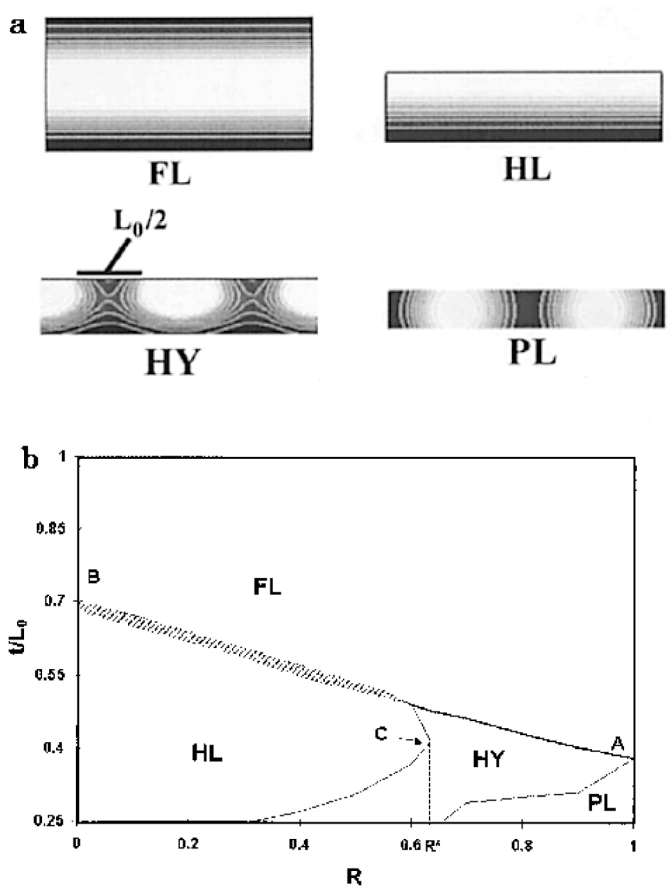

Figure 1.7. a) Mean-field prediction of morphologies formed in films with thickness (*t* in figure, *h elsewhere in text)* approaching periodicity (L_0 in figure, d_0 elsewhere in text). Cross-section views of the following morphologies are observed: symmetric surface-parallel full lamella (FL), half-lamella (HL), symmetric hybrid structure (HY), and surface-perpendicular lamellae (PL). b) An example of a phase diagram of the ratio of film thickness *h* to bulk periodity d_0 versus R, the ratio of the preferential interaction strength of the top (S_1) and bottom interfaces (S_2): $R = \frac{S_2}{(S_1)^2}$. In this example, the degree of polymerization N is 200, and the Flory-Huggins interaction parameter χ is 0.1 Reprinted with permission from ref. 65, copyright 2000, American Chemical Society.

In the case of cylinder-forming polystyrene-*block*-polybutadiene-*block*-polystyrene, a perpendicular orientation was observed for $h < 2d_0$ and for incommensurate thicknesses for $h < 2d_0$.[24] Khanna et al. later compared AB diblock copolymers to ABA triblock copolymers in thin films; they found that AB diblocks form thickness-distorted parallel orientations, while ABA triblocks form perpendicular orientations.[67] The difference in behavior is attributed to the entropic cost of looping chains in the ABA triblocks.

Spherical morphologies also undergo thin film effects even for $h > d_0$ despite the fact that spheres are anisotropic. Yokoyama et al. observed surface-induced ordering –the spherical morphology assembles into a body-centered cubic packing, which aligns to the substrate and and forms terracing, in this case for polystyrene-*block*-poly(2-vinylpyridine) (PS-*b*-P2VP) with P2VP minor phase.[68] Stein et al. later found that the packing of spherical morphology varies with film thickness.[69,70] A body-centered cubic (bcc) lattice forms for film thickness greater than 23 layers, in agreement with the bulk structure. Deformation from the bcc lattice is observed as the film becomes thinner, progressing from increasingly deformed face-centered orthorhombic (fco) between 23 and 4 layers, and below 4 layers, hexagonal close-packed symmetry.

1.2.1.5.4 Thin Film Formation: Modification of T_g, ODT, and OOT

Huinink notes that all studies agree that in the case of selective wetting of block copolymers that form cylindrical morphology in the bulk, parallel cylinders form on selective substrates (those with a preferential interaction for one of the blocks) for all thicknesses higher than two repeat distances.[71] For thinner films a variety of behavior has already been described by which films adjust to make up for strain caused by incommensurate film thicknesses. The physical properties of polymers, in

addition to the phase behavior of block copolymers, are also affected by the degree of attraction to wetting walls.

Glass transition temperatures of polymer thin films with thickness near the radius of gyration of the polymer chains can be altered from the bulk values, largely due to confinement effects and interfacial attraction to substrates.[72-75] In all of these examples, attraction of a thin film of a homopolymer to a substrate causes an increase in T_g in thin films, while the opposite occurs when polymer chains are repulsed by the surface. Tsui et al. used surface-grafted PS-*r*-PMMA with varying composition to modify the chain interactions of a thin layer of polystyrene toward the substrate, and found that the T_g of polystyrene could be effectively controlled.[76]

Wall interfaces have also been found to alter the phase separation of nearby symmetric block copolymer chains. Fredrickson used SCF theory to demonstrate that a block copolymer melt in the vicinity of a solid wall or free surface (one with selective attraction) possessed a modified Flory-Huggins interaction parameter.[77] Due to the connectivity of the blocks and the incompressibility of the material (an assumption of the calculation), the calculated interaction parameters have an oscillatory component with period $2\pi/d_0$, normal to the wall plane, which decays exponentially from the interface. Milner and Morse also predicted this oscillatory profile normal to the surface for bulk-cylindrical morphology as well (corresponding to thickness commensurability), though they also observed that the decay length is longer closer to the mean-field critical point.[78]

Foster et al. observed experimental evidence of alteration of χ in the vicinity of walls – for thin films of symmetric poly(ethylene-propylene)-*block*-poly(ethylethylene) (PEP-*b*-PEE) in which the PEE block preferentially segregates to both the substrate and air interfaces, the polymer near the polymer/air interface and the polymer/substrate interfaces display induced microstructure while the center of the

film is disordered, indicating a shift in the order-disorder transition (ODT) near interfaces corresponding to an increase in the Flory-Huggins interaction parameter χ.[79]

Theoretical studies predict that the modification of χ near interfaces can drive an order-order transition from cylindrical to lamellar morphologies in thin films in the case of asymmetric block copolymers (e.g. cylinder-forming in the bulk) in the weak segregation limit.[80] Heckmann and Drossell also point out that the strong interaction of polymer chains toward walls leads to an increased wetting of one block at the wall, causing a shift in the available volume fraction near interfaces, shifting the morphology as well.[81]

Huinink et al. modeled the behavior of bulk-cylindrical block copolymer films with bulk spatial period d_0, confined between walls separated by a distance h, where $d_0 < h < 2d_0$.[71,82] They established a phase diagram dependent entirely on the distance between the walls and the strength of interaction of the blocks with the walls, demonstrating the formation of parallel cylinders, perpendicular cylinders, parallel lamellae, and parallel perforated lamellae. Yin et al. also used simulations to study asymmetric diblock copolymer films forming gyroid morphologies in the bulk.[83] They observed multiple morphological transitions depending on the film thickness and polymer/wall interactions, including the formation of hybrid morphologies, as well as parallel cylinders, perforated lamellae and lamellae.

Tsarkova et al. investigated this behavior experimentally with cylinder-forming polystyrene-*block*-polybutadiene, f_{PS} 25.5% on weakly- and strongly- PB attractive substrates.[84] On weakly interacting substrates, parallel cylinders form up to 5 layers thick, though the bottom layer is found to have half-cylinders stabilized at the substrate. Strongly interacting substrates lead to a transition from parallel cylinders to lamellae and perforated lamellae, depending on film thickness h. This behavior has also been studied for ABA triblocks [85-87] as well as ABC triblocks.[88]

Yang et al. used self-consistent field theory to study morphology formation of a bulk-cylindrical ($f = 0.3$) block copolymer while confined between symmetric walls with both weak and strong substrate preferences.[89] They observed the existence of phases previously observed theoretically and experimentally, including parallel and perpendicular cylinders and parallel flat lamellae. They also observed three new morphologies: undulated cylinders, undulated lamellae, and parallel cylinders with non-integer period ($1.5C_{||}$, or 1.5 times the d_0 for a parallel cylinder), none of which have been observed elsewhere. These newly-observed morphologies are observed at specific film thicknesses h undergoing very strong polymer-substrate interaction; the $1.5C_{||}$ forms with weak substrate preference for the long block and $1.6R_G < h < 2.8R_G$. Under weak polymer-substrate preference, when the longer block preferentially wets the substrate, parallel and perpendicular cylinders alternate with changing thickness h, though when the minor phase selectively wets, parallel cylinders and lamellar phases alternate with h.

1.2.2 Phase Behavior of Block Copolymer Blends

Bulk block copolymer phase behavior may be tuned by blending block copolymers with other materials. Common components are solvents (with selective or nonselective preference for the blocks) and homopolymers composed of one of the blocks. We primarily focus on blending with solvents due to their aid in understanding solvent annealing to gain long-range ordering in block copolymer thin films, which is discussed in section 1.2.3. Though beyond the scope of this work, it is worth noting that much interesting work in recent years has shown that blends of bulk block copolymers with metal oxide precursors[90-94] and nanoparticles[95-99] can modify the self assembly behavior of the block copolymers and form interesting composite and porous materials.

1.2.2.1 Nonselective Solvent Swelling: Vertical Phase Diagram Shift

When swelling with nonselective solvents, those that are good solvents for all blocks in a block copolymer, theoretical studies have found little effect on the overall shape and structure of the phase diagram, as long as the effect of the dilution is factored into the χN y-axis of the phase diagram. Helfand and Tagami first introduced the concept of the dilution approximation for the behavior of the order-disorder transition (ODT) as well as order-order transitions (OOT) in block copolymers.[100] In unblended symmetric block copolymers, the order disorder transition occurs for the condition

$$\chi_{AB}N = 10.5. \qquad \text{Eqn. 1.1}$$

for a block copolymer with Flory-Huggins interaction parameter χ_{AB} and degree of polymerization N. The dilution approximation describes the modification of the phase behavior upon blending with a nonselective good solvent with an additional factor, the polymer volume fraction in the polymer-solvent mixture, ϕ_p:

$$\chi_{AB}N\phi_p = 10.5. \qquad \text{Eqn. 1.2}$$

The inverse temperature component of χ_{AB} means the order-disorder transition of a swollen block copolymer occurs at a lower temperature than that of a neat polymer. This behavior occurs because the solvent segregates at the interface between the two blocks, moderating the strength of their interaction.

Whitmore and Noolandi studied the bulk behavior of symmetric block copolymers swollen with solvents, both by using self-consistent field (SCF) theory and by comparison to experimental results with polystyrene-*block*-polyisoprene (PS-*b*-PI) plus neutral solvent toluene, confirming the dilution approximation for concentration solutions of lamellar morphology.[102] Whitmore and Vavasour took this a

step further by establishing a phase diagram for a block copolymer and nonselective solvent blend using SCF theory of polymer blends.[103] For the y-axis of the phase diagram, the χN component has been replaced with $\chi N\phi_p$, but otherwise the shape and location of the transitions are similar to the solvent-free phase diagram. Huang and Lodge confirm this behavior for neutral solvents by theoretical calculations, as seen in Figure 1.8.[101]

Huang & Lodge also point out that it is possible to shift vertically through multiple morphologies of the phase diagram, much like for thermoreversible phase transitions (section 1.2.1.4), by increasing the concentration of a solvent blended with a block copolymer.[101] In a simplification of the dilution approximation, this can be visualized as a downward vertical shift in the phase diagram for a neat polymer upon blending with solvent. When a block copolymer possesses an asymmetric composition, this can lead to transitions between morphologies.

The dilution approximation is expected to fail in two cases. In the first, the use of a neutral, but poor solvent, leads to macrophase separation into solvent-rich and solvent-poor regions.[104] In the second, Fredrickson and Liebler as well as Olvera de la Cruz observed that the dilution approximation requires modification in semidilute solutions due to chain swelling effects.[105,106] Inhomogeneous solvent concentrations develop at interfaces between the blocks, and the solvent at the interfaces acts to screen unfavorable AB interactions.[105] In this case, the concentration of block copolymer in the weak field regime at constant temperature is found to scale $\phi_p \sim N^{-0.62}$ in good solvents and $\phi_p \sim N^{-0.5}$ in θ solvents, and ϕ_p is found in good solvents to have an exponent of 1.59, such that

$$\chi_{AB}N\phi_p^{1.59} = 10.5. \qquad \text{Eqn. 1.3}$$

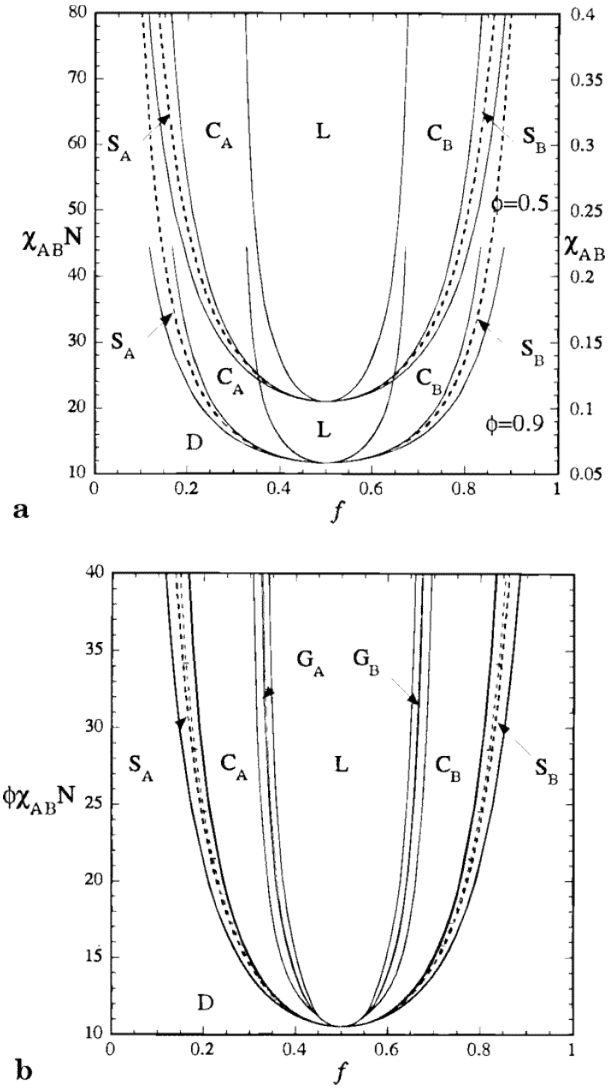

Figure 1.8. a) Two-dimensional mean-field phase diagrams for a diblock copolymer swollen in a neutral good solvent with two different polymer volume fractions $\phi_p = 0.5$ & 0.9. b) The phase diagrams from (a) overlay perfectly with each other and with the melt when the dilution approximation is taken into account – that is, when ploted in terms of $\phi_p\chi_{AB}N$. Reprinted with permission from ref. 101, copyright 1998, American Chemical Society.

Lodge et al. found the ϕ_p scaling factor disagreed somewhat with experimental results of lamellar polystyrene-*block*-polyisoprene (PS-*b*-PI) swollen with neutral solvent dioctylphthalate (DOP), regardless of dilution, and that the dilution approximation requires the addition of an exponent to properly describe the phase behavior. The experimentally-measured dilution factor for the order-disorder transition (ODT) scales with $\phi_p^{1.6}$ for PS-*b*-PI swollen with toluene and DOP, but with $\phi_p^{1.2}$ for poly(ethylene propylene)-*block*-poly(ethylethylene) (PEP-*b*-PEE) swollen with squalane.[107] They later studied PS-*b*-PI in solution with nonselective toluene using SANS to study the solvent formed at the block interfaces; PS-*b*-PI swollen with toluene also displays the ODT shift that scales with $\phi_p^{1.6}$.[108] Lodge et al. went on to demonstrate experimentally with PS-*b*-PI with a variety of compositions in DOP that the dilution factor for order-disorder transition (ODT) actually scales with ϕ_p^{α}, where α varies from 1.3 to 1.6, thus demonstrating that the dilution approximation fails for a variety of morphologies.[109]

They also studied the dilution fluctuation with order-order transitions (OOT) between cylinder to sphere, gyroid to cylindrical, and lamellae to gyroid, and found that the effective Flory-Huggins parameter of the order-order transition scales with $\phi_p^{1.0}$, as predicted theoretically.[109] Thus, order-order transitions decrease less quickly than the order-disorder transition, indicating that experimental phase diagrams for swollen polymers would possess a shape that does not exactly map to the neat block copolymer phase diagram in the weak segregation regime. Certain ordered phases expected near the ODT are not present in the swollen state due to the differences in OOT and ODT shift with solvent. In plotting the value of the exponent α with the degree of polymerization, they observe an increase in α with increasing N, which is opposite to the expectation that α should decrease to 1.0 as the separation increases.

A summary of the phase behavior of a block copolymer swollen with a nonselective solvent follows: the dilution approximation says that interaction

parameter in a polymer scales with the volume fraction of the polymer in the solvent-polymer blend. This is attributed to the alteration of the interaction of the two blocks due to selective segregation of the solvent to the interface between the blocks. Comparison of this theory with experimental results for the shift in ODT has found that an exponent must be added to adjust for non-ideal behavior, such that $\chi_{EFF} = \chi_{AB}\phi_P^{\alpha}$ where α can be 1.2 to 1.6. The value of the exponent cannot be predicted, but depends on the solvent and block copolymer system. This non-ideal behavior is only observed for order-disorder transitions; order-order transitions follow the dilution approximation with α equal to 1.

1.2.2.2 Selective Solvent Swelling: Morphology Shift by Solvent Partitioning

Solvent selectivity also plays a very strong role in the morphology formed by solvent-swollen block copolymers. For each block of a polymer, solvents may be good solvents, poor solvents (near θ conditions), or non-solvents. Of course, if it is a non-solvent for both blocks, the solvent does not affect the film at all.

When the two blocks are both soluble in a solvent, though to different degrees, shifts in the morphology in the swollen state occur due to unequal swelling of the blocks. As such, the phase behavior not only depends the Flory-Huggins interaction parameter between the two blocks χ_{AB}, the degree of polymerization N and the polymer volume fraction ϕ_p, but it also depends on the interaction parameter between each of the blocks and the solvent, termed here χ_{AS} and χ_{BS}.[101,110] Lai et al. suggested a clever method of determining solvent selectivity: measuring the glass transition temperature of the two blocks in a sealed cell (for example, by differential scanning calorimetry) can provide information on the degree of swelling of each block.[111] The solvent behaves as a plasticizer, lowering its glass transition temperature, T_g. The depression of the T_g in each block indicates the degree of swelling in each block.

Lodge et al. showed theoretically that for lamellar PS-*b*-PI swollen in PI-selective cyclohexane, an increase in the degree of swelling of the PI block is observed.[108] Cyclohexane is a good solvent for PI, but a θ solvent for PS at 34.5˚C. Thus, they calculate a strong temperature dependence on the preferential swelling, with a smaller preference above the θ temperature, though the preference is not completely eliminated.

This selective partitioning can be expected to affect the volume fraction of the block copolymer, *f*. Huang and Lodge studied the effect of solvent selectivity on phase formation using SCF theory.[101] A two-dimensional phase diagram for a solvent-swollen diblock copolymer is reproduced in Figure 1.9. In this case, they chose ϕ_p of 0.5 and χ_{AS} and χ_{BS} of 0.6 and 0.4, respectively, indicating a slight preference for the B block. Consequently, the phase diagram of the solvent-swollen polymer shifts to the right. Also, the shape of the solvent-swollen phase diagram is asymmetric, such that the location of the transitions do not map on top of a neat block copolymer phase diagram.

Huang & Lodge also reported a change in the degree of stabilization of block copolymer morphology.[101] In their SCF study, they held χ_{BS} at a constant value and varied χ_{AS}. There exists a critical value of χ_{AS}^{*} that is determined by the intersection of the spinodal curves of $\chi_{AB}N$, χ_{AS}, and ϕ_p. For $\chi_{AS} > \chi_{AS}^{*}$, or weak selectivity, increasing ϕ_p causes the stable microphase separation region to become made smaller, which corresponds to narrower phase diagram, or a lower position on it. On the other hand, for $\chi_{AS} > \chi_{AS}^{*}$, corresponding to a strongly selective solvent, increasing ϕ_p has the opposite effect – the stable region becomes larger.

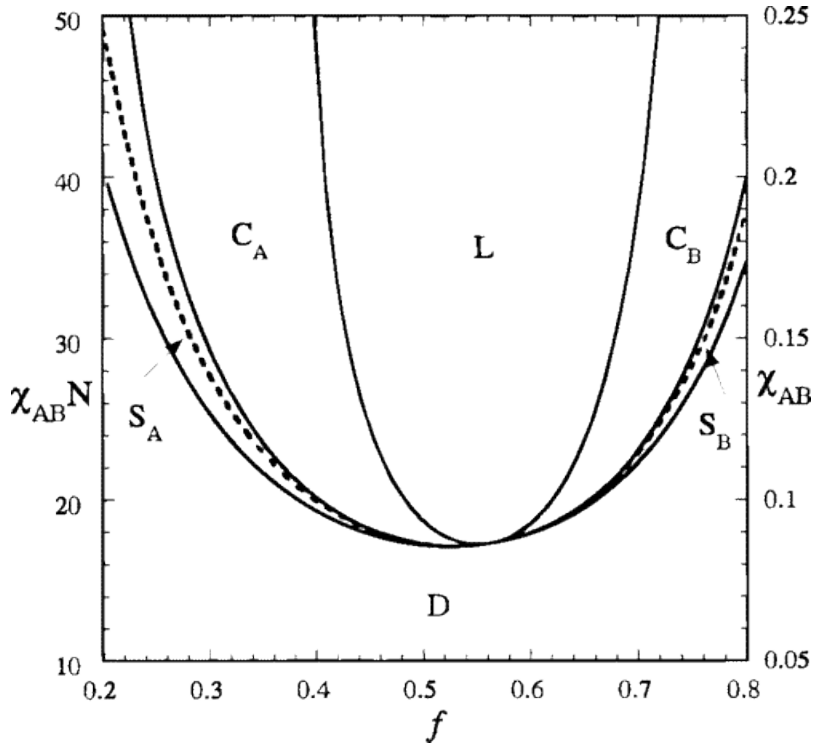

Figure 1.9. Two-dimensional phase diagram for a diblock copolymer swollen with a selective solvent. The diagram displays a shift in the mean-field critical point and possesses an asymmetric shape. Reprinted with permission from ref. 101, copyright 1998, American Chemical Society.

They further predict morphology tunability, forming multiple structures for high solvent selectivity, for example, $\chi_{BS} = 0.4$ and $\chi_{AS} > 0.7$ (solvent preference for the B block). For a polymer that forms lamellar morphology in the melt, one would expect a morphology transition with increasing solvent volume in the B block to change the morphology from lamallae (L) to cylinders of block A (C_A), to spheres (S_A), and finally to disordered state, corresponding to a shift in *f*. This maybe be envisioned as a horizontal walk across the phase diagram. Also, for a polymer with asymmetric morphology forming cylinders of block B (C_B) in the melt, one could expect a shift through C_B, L, C_A, S_A, micelles, and disordered state.

This morphology-shifting behavior has been demonstrated experimentally in many cases.[111-117] Hanley and Lodge report swelling of symmetric PS-*b*-PI in di-*n*-butyl phthalate (DBP), slightly selective for PS.[112] DPB is a θ solvent for PI around 90˚C, and so it is selective below that temperature but negligibly selective above 100˚C. Varying both the selective solvent concentration and the temperature, they observed shifts that can be visualized a diagonal shift of position in the phase diagram, where the x-axis volume component is caused by the solvent selectivity and the y-axis shift is due to the inverse-temperature component of χ. For example, for $\phi_p = 0.9$, they observe shifts from lamellae (75˚C), perforated lamellae (100˚C, metastable state), gyroid (150˚C) and cylinders (180˚C). They suggest swelling with a selective solvent is akin to a horizontal trajectory across the phase diagram, while combining solvent swelling with thermal annealing, as they do, corresponds with a diagonal trajectory.

Hanley, Lodge & Huang go on to point out that asymmetric PS-*b*-PI swollen with DBP forms inverse versions of their morphology: L → G_{inv} → C_{inv} → S_{inv}, moving in the opposite direction as the thermoreversible morphology shift G → C → Disordered.[114] Swelling with tetradecane, selective for PI, allows access to the G → C

→ D shift. Lai et al. go on to show as many as five ordered phases for a single block copolymer by swelling PS-*b*-PI with tetradecane.[111]

1.2.2.3 Solvent Blending Shifts Polymer Spacing

Bulk blends of solvent and block copolymers not alter phase behavior from the neat block copolymer, but they also change the equilibrium spacing of the polymers. These changes in periodicity have been found to vary depending on solvent selectivity. Swelling with a solvent leads to a decrease in the periodicity of the block copolymer, though the degree varies depending on the solvent selectivity for the different blocks.

Hashimoto et al. demonstrated this behavior experimentally with PS-*b*-PI swollen with nonselective solvent dioctyl phthalate (DOP).[118] They observed changes in the periodicity *d* to vary with degree of polymerization N, the temperature T, and the polymer volume fraction ϕ_p according to

$$d/b \sim N^{0.67} [\phi_p/T]^{0.33} \qquad \text{Eqn. 1.4}$$

where b is the statistical Kuhn length.

Shibayama et al. also observe a critical $[\phi_p/T]$ value with different swelling behavior of PS-*b*-PI swollen with neutral solvents toluene and DOP.[119,120] This value, approximately $\phi_p = 70\%$, separates two regimes of spacing.[119] At dilute polymer concentrations $\phi_p < 70\%$, an increase in ϕ_p corresponds to a decrease in *d*, in agreement with spacing trends found previously. (Also of note – a homogenous solution is found for $\phi_p < 20\%$, indicating ODT suppression to room temperature.) Concentrated polymer solutions, $\phi_p > 70\%$, on the other hand, show the opposite trend. They go on to describe the dilute region as an equilibrium regime, one thermodynamically controlled; the other regime, where spacing increases with increasing solvent concentration, is found to be kinetically controlled.[120] This

difference is evidence that the solvent is acting to lower the glass transition of the blocks (and especially that of PS, with its higher T_g) to below room temperature, allowing polymer mobility at room temperature at sufficiently high solvent concentration, thus sufficient mobility for self assembly is observed at higher swelling.

Using self-consistent field theory, Whitmore and Noolandi modeled the behavior of symmetric polymers swollen by a nonselective good solvent.[121] They found:

$$d/b \propto [\chi_{AB}]^p N^q [\phi_p]^r \qquad \text{Eqn. 1.5}$$

where b is the statistical Kuhn length and the exponents p, q, and r vary depending on the segregation strength. For weak segregation, p≈0.33, q≈0.8, and r≈0.4, while for strong segregation p≈0.2, q≈0.67, and r≈0.22. Between weak-field and strong-field extremes, the exponent r smoothly evolves between r = 0.33 in weak field segregation (up to $\chi_{AB}N\phi_p \leq 15$) and r = 0.2 for strong field segregation.

This behavior of different scaling of *d* with strong and weak segregation has been observed experimentally with solvent-swollen melts.[110,122] Whitmore & Noolandi point out that that as ϕ_p approaches 1 – that is, neat polymer without solvent – the equation collapses to an expression very similar to that by Helfand for unblended block copolymer self assembly.[10]

$$d/b \approx \gamma^{2/3} N^{9/14} \qquad \text{Eqn. 1.6}$$

where γ is the interfacial tension, and $\gamma \approx [\chi_{AB}]^{0.5}$

$$d/b \approx [\chi_{AB}]^{0.14} N^{0.64} \qquad \text{Eqn. 1.7}$$

Whitmore & Noolandi's results are in agreement with those by Shibayama and Hashimoto, as long as the polymers are self-assembling in the thermodynamically-directed ranges (that is, sufficient swelling for mobility at the experimental

temperature). Lodge et al. also observed agreement of experimental results of PS-*b*-PI swollen with DOP, in which *d* scales with $\phi_p^{0.33}$ independent of morphology.[109]

Swelling with a nonselective solvent causes modification of *d* as well. Banaszak & Whitmore extended earlier self-consistent field theory studies to selective solvent swelling of symmetric block copolymers, assuming $\chi_{AB} = \chi_{SB}$ and $\chi_{SA} = 0$ (non-interacting).[110] They found the same basic relationships as for swelling with selective solvent,

$$d/b \propto [\chi_{AB}]^p N^q [\phi_p]^r \qquad \text{Eqn. 1.8}$$

where for strong segregation p≈0.2, q≈0.7, and r≈0.2 (the almost identical to values for a nonselective solvent), and weak segregation, p≈0.5, q≈0.9, and r≈0.5.

The weak field phase behavior was confirmed experimentally - *d* was found to scale with $\phi_p^{0.5}$ in PS-*b*-PI swollen with di-*n*-butyl phthalate (DPB), slightly selective for PS.[112]

Lai et al. experimentally studied the effect of solvent selectivity on the r exponent of $d \sim \phi^r$, and found that the value decreases with increasing solvent selectivity, even into negative values. Negative values of r indicate that the spacing increases with selective solvent blending, rather than decreasing as with a nonselective solvent. They conclude that r also varies with the block composition (*f*) and the mesophase formed upon swelling, and that it is not possible to make a simple sum of the contributions from these three related variables.[123]

1.2.2.4 Mixed Solvents: Morphology Tuning and Phase Behavior

It is not always possible to find good nonselective solvents for immiscible diblock copolymers, especially when they possess a large interaction parameter. The ability to tune solvent morphology by swelling with a selective solvent is also

attractive, but the morphology formed is a function of the degree of selective attraction for the available solvents. Blending two different solvents, each completely selective for a different block, would allow tunability of selective swelling and thus the morphology formed, and even allow access to neutral swelling conditions at the correct solvent ratio.

However, one must consider the interactions of each of the four materials in the system with each other. In a neat block copolymer, phase separation is dictated by χ_{AB}, N, and *f*. When swollen with a single solvent, the behavior depends on N, *f*, and χ_{AB} as well as the interaction of the solvent with each block, χ_{AS} and χ_{BS}. With the two-solvent system (we will call the solvents X and Y), we not only consider the volume fraction *f*, the degree of polymerization N, and the Flory-Huggins interaction of the block copolymer χ_{AB}, but also the interaction of each solvent with each block (χ_{AX}, χ_{AY}, χ_{BX} & χ_{BY}) and the interaction of the two solvents, χ_{XY}.

Alexandridis et al. swelled block copolymers made of poly(ethylene oxide) and poly(propylene oxide), PEO-*b*-PPO-*b*-PEO, often considered nonionic surfactants due to their oligomeric molecular weight, with blends of totally selective solvents.[124] Changing the overall concentrations of each of the solvents, PEO-selective water and PPO-selective *p*-xylene, allowed the formation of the entire range of morphologies expected for a block copolymer, including spherical, cylindrical, gyroid, and lamellar, as observed in Figure 1.10.

Huang and Hsu used self-consistent mean-field theory to study the phase behavior of an AB block copolymer blended with two solvents, one a neutral solvent (X) and the other slightly B-selective (Y).[125] They found that χ_{XY} caused an effect in the phase separation of the swollen diblock copolymer – if χ_{XY} is large (i.e. the solvents are highly immiscible), the preferentiality of the polymer is enhanced.

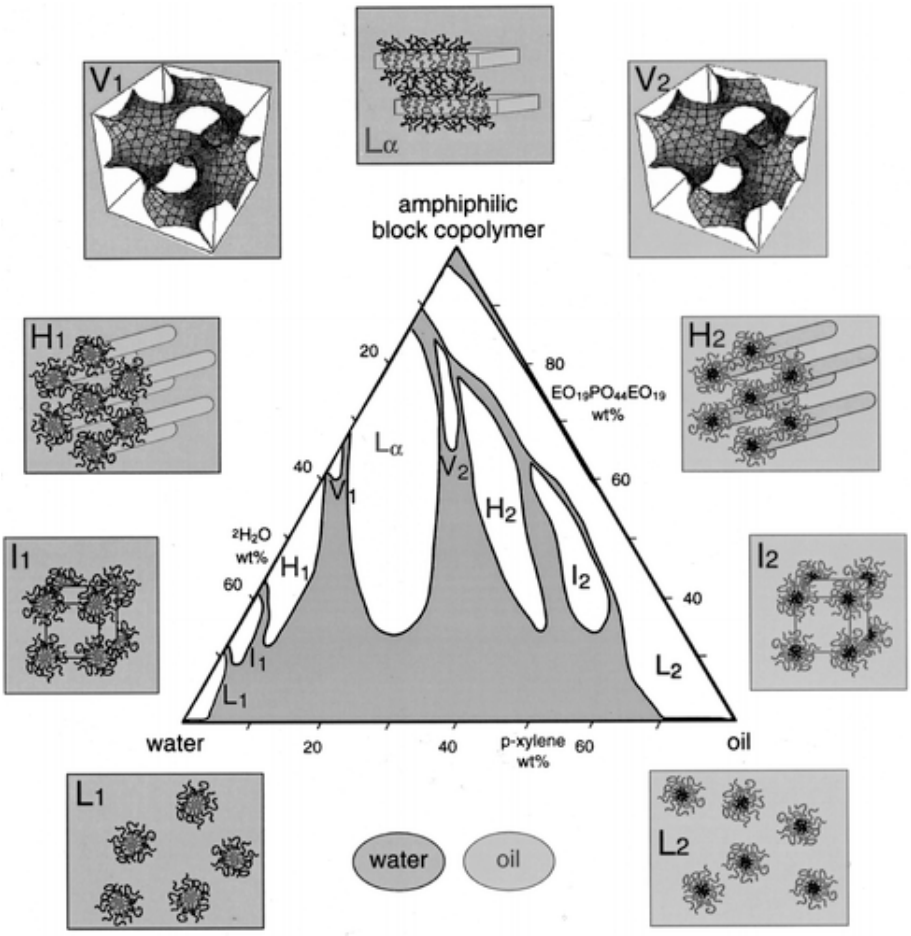

Figure 1.10. A phase diagram of PEO-*b*-PPO-*b*-PEO blended with PEO-selective water and PPO-selective *p*-xylene ("oil") at 25 °C. The phase boundaries of the one-phase regions are drawn with solid lines. I_1, H_1, V_1, L_α, V_2, H_2, and I_2 denote normal (oil-in-water) micellar cubic, normal hexagonal, normal bicontinuous cubic, lamellar, reverse (water-in-oil) bicontinuous cubic, reverse hexagonal, and reverse micellar cubic lyotropic liquid crystalline phases, respectively, while L_1 and L_2 denote water-rich (normal micellar) and water-lean/oil-rich (reverse micellar) solutions. The concentrations are expressed in weight percent. The samples whose compositions fall outside the one-phase regions are dispersions of two or three (depending on the location in the phase diagram) different phases. The line along the copolymer–oil axis indicates incomplete miscibility between the copolymer and the oil. Schematics of the different modes of self-organization of the amphiphilic block copolymers in the presence of solvents ("water" and "oil") are shown adjacent to the respective phases in the phase diagram. The amphiphiles are localized at the interfaces between the water and oil domains (denoted by dark grey and light grey, respectively). The gyroid minimal surface is used as a representation of the microstructure in the V_1 and V_2 phases. Reprinted with permission from ref. 124, copyright 1998, American Chemical Society.

Huang, Chiou & Lan modeled the behavior of an AB block copolymer [126] swollen with solvents X and Y, each totally selective for a different block. They again found that increased χ_{XY} drives macrophase separation of the blocks, possibly acting as a method to drive phase separation of poorly-segregated polymers, as well as increasing the degree of dilution possible for phase separation to still occur. Furthermore, they also observed the ability to tune the morphology formed by adjusting the ratio of the solvents.

1.2.2.5 Block Copolymers Blended with Non-Solvents: Homopolymers

Unlike solvent blending, which may be classified as selective or nonselective swelling, blending a block copolymer with a constituent homopolymer is classified as completely selective blending. Like solvent blending, Blending block copolymers with homopolymers has been found to alter phase behavior, changing the block copolymer spatial period and causing order-order transitions from the neat polymer state.

Zin and Roe observed PS-*b*-PB blended with PS with far lower molecular weight than the block copolymer.[127,128] Using PS-*b*-PB with M_n 27K and f_{PS} 0.27 swollen with PS (M_n 2K), an increase in the ODT temperature was observed, combined with an increase in the spatial period *d*. They also observed shifts in the morphology from spherical to lamellar morphology.

Hashimoto et al. and Winey, Thomas, & Fetters studied symmetric PS-*b*-PI swollen with PS (and sometimes PI).[129-133] They observed that low molecular weight PS molecules are distributed uniformly within the PS phase of lamellar PS-*b*-PI, and that the blending of PS can change the morphology formed.[129] Holding the homopolymer volume fraction ϕ_{HP} constant, the spatial period *d* was found to increase as the molecular weight of the PS blend increased; likewise, the morphology shifted

further with increased molecular weight of the blended PS homopolymer.[130] This was attributed to the miscibility of the PS homopolymer – as the molecular weight of the PS homopolymer increases, its miscibility with the PS block decreases, and the homopolymer segregates at the middle of the PS block domain, rather than distributing uniformly within the PS block domain.

Observing the width of each block domain as the PS homopolymer volume fraction increases, the PS block domain becomes larger as the PI domain becomes thinner, and the area per junction (that is, the surface area at the block interface per polymer chain) increases when the molecular weight of the PS homopolymer is small and distributes evenly within the PS block domain.[130] For constant PS homopolymer concentration, increasing the hompolymer molecular weight leads to increasing thickness in the PS and PI domains, and resulting from the selective partitioning of the homopolymer at the center, causing a decrease in the area per junction. As the PS concentration increases or as the M_n of the PS homopolymer increases, the PS homopolymer preferentially segregates at the center of the PS block rather than blending with the block copolymer PS chains. Observation of shifts in the morphology formed in blended films is observed – for example, for PS-*b*-PI 27K/22K (f_{PS} 0.55), transitions from lamellar morphology to bicontinuous double diamond, cylindrical, and spherical morphologies are observed, dictated not only by the overall PS volume fraction but also the M_n of the PS.[131] Mayes et al. also demonstrated that PS and PMMA homopolymers segregate into the corresponding blocks of PS-*b*-PMMA. Decreasing the molecular weight of the PS homopolymer led to better incorporation into the PS block; when the M_n of the homopolymer is larger than the block molecular weight, the homopolymer does not at all segregate into the block domains, existing as separate layer.[134] Thus for large homopolymer molecular weight,

the homopolymer causes a large increase in the periodicity, while a small homopolymer molecular weight causes little overall change in the periodicity.[132]

The mechanism of order-order transitions due to homopolymer blending is summarized nicely by Torikai et al, "… microdomains are extended by uniform solubilization of the homopolymers with considerably low [M_n], and the extension of either one of the two microdomains along the interface leaving the other one unchanged is the driving force of the morphological transitions observed in the binary blends."[135] In other words, volume changes in the blends caused by homopolymer blending has an effect on morphological transitions, but the molecular weight of the homopolymers and the resulting intercalation with blocks or partitioning at the center of the blocks is a major driving force as well. The biggest determining factor for morphology is the degree of curvature of the interface. Banaszak and Whitmore used SCF theory to demonstrate all of these things – homopolymers penetrate the block copolymer chains and cause lateral swelling the degree of which depends on the molecular weight of the homopolymer.[136]

Torikai also calculated the effect of block copolymer binary blends (A-*b*-B + A) versus ternary blends (A-*b*-B + A + B) on the periodicity *d* for the case of homopolymer completely segregated at the center of the block and for the case of homopolymer completely distributed within the blocks, and then compared the *d* spacing as molecular weight of the blending homopolymer was varied.[135] A difference in the degree of localization was observed between binary and ternary blends – binary blends segregate to the centers far more than ternary ones. Putting this behavior to practical use, Urbas et al. tuned domain spacing with ternary bends of PS-*b*-PI, PS and PI for photonic crystal applications, demonstrating an increase in spacing that nearly doubled while maintaining the lamellar morphology.[137]

1.2.3 Solvent Annealing

Block copolymer self assembly requires polymer chain mobility, typically achieved by heating above the glass transition temperature, T_g, for the two blocks. Another method of achieving block copolymer mobility is to swell it with a plasticizer (solvent), lowering the T_g of the polymer to below room temperature (or to easily achievable temperatures). This is particularly useful for diblock copolymers possessing both high T_g and low degradation temperatures. It has also proven important for gaining long range ordering in triblock copolymers due to the difficulty in accessing thermodynamically stable morphologies via thermal annealing.[1]

As described above in section 1.2.2.1, shifts in the phase behavior and periodicity of a block copolymer occur in the presence of a solvent. While this phase behavior must be taken into account, and certainly increases the degree of complication of the system over thermal annealing, it also provides a useful tool for tuning morphology and periodicity, and also for accessing difficult-to-achieve morphologies.

1.2.3.1 Polymer Mobility by Solvent Annealing Allows Self Assembly

As discussed many times in previous sections, block copolymer self assembly is facilitated by allowing polymer chains sufficient mobility to phase-segregate. For block copolymers with glass transition temerpatures (T_g) well above room temperature, heating the block copolymer above the blocks' glass transition temperatures renders sufficient mobility for self assembly. This is called thermal annealing.

Alternatively, swelling a polymer with a plasticizer (e.g., a solvent) causes suppression of the T_g.[138] If the polymer is swollen with sufficient material to lower the glass transition of the resulting material to below room temperature, the polymer

chains gain mobility, and in a block copolymer self assembly can occur. This is referred to as solvent annealing. The glass transition of a plasticized polymer is governed by:

$$T_g = \frac{T_{gP} + (KT_{gS} - T_{gP})\phi_S}{1 + (K-1)\phi_S} \qquad \text{Eqn. 1.9}$$

where T_{gP} is the glass transition temperature of the polymer, T_{gS} is the glass transition temperature of the solvent, ϕ_s is the volume fraction of solvent (plasticizer), and K is a constant with typical values between 1 and 3 governed by

$$K \approx \frac{\alpha_{1S} - \alpha_{gS}}{\alpha_{1P} - \alpha_{gP}} \qquad \text{Eqn. 1.10}$$

where α_1 is the volume coefficient of expansion above T_g, while α_g is the volume coefficient of expansion below T_g. Reorganization of the equation for T_g of the plasticized polymer for the depression of T_g in the swollen film gives

$$\frac{T_{gP} - T_g}{T_{gP} - T_{gS}} = \frac{1 - \phi_P}{1 - \phi_P(1 - \frac{1}{K})} \qquad \text{Eqn. 1.11}$$

where ϕ_P is the volume fraction of the polymer. Solvent T_{gS} values are only known for a few solvents, but the relationship between the T_g and the melting temperature T_m found for polymers can also be used to predict the T_{gS} from the freezing point of the solvent, T_{mS}:

$$\frac{T_g}{T_m} \approx \frac{2}{3} \qquad \text{Eqn. 1.12}$$

Zielinksi & Duda used a free-volume diffusion model to predict diffusion constants for mixtures of common solvents and polymers,[139] while Rauch & Köhler

carefully studied the interaction of polystyrene and toluene.[140] Both demonstrated that polymer diffusion increases as the T_g decreases upon addition of solvent. In other words, polymer chains gain mobility at room temperature when swollen with sufficient quantities of solvent. Mori et al. demonstrated that addition of nonselective solvent toluene to polystyrene-*block*-polyisoprene led to depression of the polystyrene block's T_g to below room temperature with 25% or more nonselective good solvent.[141]

Elbs et al. introduced the concept of the vitrification concentration, the concentration of polymer in a solvent-polymer blend above which a polymer is glassy and mobility is no longer possible.[142] Kim & Libera showed that PS-*b*-PB-*b*-PS (PS cylinders form by thermal annealing) forms parallel hexagonal cylinders when cast from solution and allowed to evaporate slowly.[143,144] Compression in the direction of film thinkness indicates that the film further shrinks after the polymer film reaches the vitrification concentration.

One final consideration is the efficacy of solvent annealing with selective solvents. For phase-segregating block copolymers, each block possess a T_g. Solvent annealing leads to self assembly when the ambient temperature is higher than the T_g of both blocks. For the sake of this description, we will discuss a block copolymer in which both blocks possess similar glass transition temperatures well above room temperature. When swelling a block copolymer film with a nonselective good solvent, the T_g of both blocks are suppressed and mobility is easily achieved. In the case of a block copolymer swollen with a completely selective solvent, only the soluble block experiences suppressed T_g, and so mobility for self assembly cannot be achieved at room temperature. In the case of a solvent that dissolves both blocks but displays preferential swelling of one block, sufficient mobility for self assembly cannot occur until the less soluble block swells enough for its T_g to lower below room temperature. In principle, the combination of thermal and solvent annealing techniques could lead

to polymer mobility at moderate annealing temperatures. This is not as useful in practice due to solvent flammability concerns.

1.2.3.2 Solvent Annealing: Thin Film Effects

In thin block copolymer films, solvent annealing in nonselective good solvents leads to self assembly behavior similar to that observed upon thermal annealing. Similar thin films effects are observed, including the formation of parallel orientation on preferentially-interacting substrates, island and hole formation, and occasionally perpendicular orientations at incommensurate film thicknesses. Some examples of this behavior in the literature:

- Terracing and formation of parallel cylinders were observed in PS-*b*-PB-*b*-PS (f_{PS} 0.26) swollen in nonselective good solvent chloroform.[145,146] Perpendicular orientations formed at incommensurate film thickness and stable non-bulk morphologies formed at thicknesses less than 1.5 domain spacings, including perforated lamellae.[145]
- Annealing polystyrene-*block*-poly($_{D,L}$-lactide), PS-*b*-PLA, with PLA cylindrical phase, leads to parallel cylinders upon annealing in benzene.[147]
- For poly(styrene)-*block*-poly(2-vinylpyridine)-*block*-poly(*tert*-butyl methacrylate), or PS-*b*-P2VP-*b*-PtBMA, terraces form upon annealing in chloroform.[148]
- Dioxane annealing polystyrene-*block*-poly(4-vinylpyridine), PS-*b*-P4VP blended with P4VP-miscible 2-(4-hydroxyphenylazo)benzoic acid, or HABA leads to parallel cylinder formation.[149,150] The block molecular weights of the PS-*b*-P4VP are 35.5 K for PS and 3.68 K for P4VP, which would be expected to form spherical morphology in the bulk (~10% P4VP by mass). Addition of ~18% HABA (1 mol HABA:1 mol P4VP subunits) lead to total polar

component 25.5% by mass. Density value for HABA is unknown, but this is likely to correspond to formation of cylindrical morphology in the bulk. Annealing in nonselective good solvent dioxane lead to formation of parallel cylinders containing the polar blend after annealing in dioxane

- Bosworth et al. observed parallel cylinder formation of poly(α-methylstyrene)-*block*-poly(4-hydroxystyrene) with 33% by mass PαMS after annealing in good solvent THF.[151]

1.2.3.3 Stability of Dried Films After Solvent Annealing

As described previously (section 1.2.2), blending block copolymers with either nonselective or selective solvents alters the polymer phase behavior. Stated another way, the thermodynamically stable state of a solvent-swollen block copolymer is different from that of a neat block copolymer. In the case of solvent annealing, the swollen state may be maintained upon evaporation of the solvent. After solvent evaporation, the block copolymer is no longer in a thermodynamically-stable state. However, as long as the glass transition temperature of the two blocks is sufficiently higher than the temperature at which the film is kept (typically, room temperature), there is little effective mobility of the polymer chains – the morphology is kinetically trapped. As discussed above, glass transition temperatures of polymer thin films can be altered from the bulk state strong interactions (attractive or unattractive) with the substrate (section 1.2.1.5.4).[72-75] However, if the T_g is sufficiently above room temperature, little mobility would be expected even in the case of very thin films.

One case in the literature does describe mobility of a polymer after solvent annealing. Niu & Saraf describe surface reconstruction of polystyrene-*block*-polyisoprene, PS-*b*-PI after solvent annealing in toluene, and this reconstruction is found to occur over a period of days after solvent annealing.[152] They neglect,

however, to discuss the glass transition temperature of the two block components. While the T_g of PS synthesized by anionic polymerization is known to be approximately 100˚C,[153] the T_g of PI is well below room temperature. The T_g varies somewhat depending on synthesis conditions, but is -68˚C for high 1,4 content[154] and well below room temperature for other PI compositions as well. The 1,4-PI content is not specified by Niu & Saraf,[152] but the surface reconstruction can be attributed to the mobility of the PI block at room temperature.

1.2.3.4 Solvent Blend: Phase Behavior Effects

As discussed in section 1.2.2.1, bulk block copolymer phase behavior is altered by blending with nonselective good solvents, effectively causing a vertical shift in the phase diagram. The modified dilution approximation describes the effective Flory-Huggins interaction parameter of the solvent-swollen block copolymer film such that $\chi_{EFF} = \chi_{AB}\phi_p^{\alpha}$, where χ_{AB} is the Flory-Huggins interaction parameter and ϕ_p is the polymer volume fraction, and the exponent α may be modified from its ideal value of one to describe real behavior. As the examples in section 1.2.3.2, annealing block copolymers in nonselective good solvents yields similar behavior to that of thermally annealed polymers.

Zhang et al. and Huang et al. attempted to use controlled solvent evaporation to kinetically trap different morphologies formed depending on χ_{EFF}.[155,156] Swelling PS-*b*-PB-*b*-PS with f_{PS} 0.245 in nonselective solvent toluene, the slowest evaporation rate gives the phase expected from thermal annealing, while higher concentrations of solvent lead to inverted cylindrical and inverted spherical phases.[155] They compared the same evaporation rate control with behavior of PS-*b*-PB block copolymers with f_{PS} in same range, forming cylinders of PS by thermal annealing. For fast evaporation rates, the diblock forms the same inverted sphere and cylinder morphologies

kinetically trapped from the swollen state. In more slowly dried films, morphologies more similar to those found in the bulk are found, though the mixed orientations suggest a solvent evaporation gradient is controlling the morphology. Inverted morphologies cannot be the thermodynamically stable state when swollen with a nonselective solvent (this is only possible for a selective solvent), and thus a gradient solvent evaporation effect must be driving non-thermodynamic structures. Gradient evaporation effects will be discussed further in 1.2.3.6.

1.2.3.5 Selective Solvent Anneal: Order-Order Transition

In section 1.2.2.2, we showed blending bulk block copolymers with a solvent entirely selective for one block causes order-order transitions to different morphologies from the morphology of the neat polymer. This can be visualized as a horizontal shift in the phase diagram.

In the case of solvent annealing block copolymer films, mobility must be achieved for both blocks in order for long range ordering to occur. Thus, even for a selective solvent, a solvent must swell both blocks sufficiently to surpass the vitrification concentration in both blocks. For solvent annealing, a solvent may show a preference toward one block, but must be at least to some degree a solvent for both blocks in order to achieve mobility for self assembly. This can be visualized as a diagonal shift in the phase diagram – selectivity shifts volume fraction (horizontal component), while solvent swelling causes a shift in χ_{AB} (vertical component) moderated by the dilution approximation.

When swelling a film in a completely selective solvent (a good solvent for one block, a nonsolvent for the other), no shift in morphology is observed. Immersion in completely selective solvents has been used to selectively swell the minor phase of polymers in thin films, causing partial pore formation, upon immersion in the

solvent.[157-159] Due to insolubility of the undissolved block, no change in the structure of the undissolved block occurs.

Order-order transitions have been observed in multiple block copolymer systems annealed in selective solvent vapor, including the following:

- PS-*b*-P2VP with f_{PS} 0.14 forms lamellar morphology swollen in THF and cylindrical in chloroform, despite volume fraction likely leading to spherical morphology in the bulk.[142]
- PS-*b*-P4VP (M_n of PS 35.5 K and P4VP 3.68 K) is blended with 2-(4-hydroxyphenylazo)benzoic acid, HABA, such that total polar component is 25.5% by mass; annealing in chloroform or toluene, both selective for the PS majority component, leads to spherical morphology in swollen state.[149,150] They report a collapse to perpendicular cylinders upon evaporation, discussed in section 1.2.3.6 below.
- Polystyrene-*block*-poly(ethylene-butylene)-*block*-polystyrene, or PS-*b*-PEB-*b*-PS, with f_{PS} 0.29-0.32, transition from ordered cylinders to spheres upon swelling in PEB-seletive cyclohexane.[160]
- Bosworth et al. observed PαMS sphere formation of poly(α-methylstyrene)-*block*-poly(4-hydroxystyrene) with 33% by mass PαMS after annealing in PHOST-selective solvent acetone.[151] The spherical morphology is kinetically trapped upon evaporation.

1.2.3.6 Solvent Evaporation Gradient Effects

The gradient caused by solvent evaporating from a film can cause non-equilibrium behavior in dried films. This was first investigated by Kim & Libera, who controlled the evaporation rate of PS-*b*-PB-*b*-PS films cast from carbon tetrachloride and toluene.[143] Deposition from carbon tetrachloride, which evaporates very quickly,

leads to a disordered morphology. Varying the evaporation rate of toluene (which has a much lower vapor pressure) leads to control of orientation: under slow evaporation, it behaves similarly to thermally annealed thin films – parallel cylinders form. Fast evaporation leads to perpendicular orientation of cylinders in these films, indicating a gradient evaporation effect. Intermediate evaporation rates lead to mixed orientations of cylinders. Kim & Libera also demonstrated that PS-*b*-PB-*b*-PS with perpendicular orientations after solvent evaporation have no selective wetting layer at the air interface; if these same films are then thermally annealed, a wetting layer forms.[144]

This behavior has been observed in other block copolymer systems. As mentioned in the section above, PS-*b*-P4VP which forms PVP spheres in the bulk is blended with sufficient HABA to gain 25.5% polar phase (by mass); annealing in chloroform forms spheres, which collapse to perpendicular cylinders upon evaporation. The film thickness is 45 nm, while the spatial period of the cylinders is 23 nm.[149,150]

The evaporation gradient is found to cause ordering in a block copolymer to propagate from the top air interface. In PS-*b*-PEO (f_{PS} 0.75) spin coated from benzene solution in benzene atmosphere (as well as benzene and water atmosphere), highly oriented arrays of perpendicular cylinders form upon evaporation.[161] The lattice period is 32 nm, while the thickness is 255 nm. They note that upon solvent evaporation, a front with ordered morphology extents from the surface into the film; thus, the perpendicular ordering is found to be substrate independent. A similar gradient with ordering beginning at the air interface is observed for polystyrene-*block*-poly($_L$-lactide) swollen in dichloromethane.[162]

1.2.3.7 Modification of Surface Tension by Solvent Annealing

Lin, Mueller and Binder used Monte Carlo simulations to study the air interface of a solvent-swollen polymer film, and found that the solvent modifies surface tensions.[163] Lin et al. found that the solvent swollen polymer (polymer-liquid) coexists with a solvent vapor and a solvent-rich liquid. This solvent-rich liquid, present at the air/solvent vapor interface, moderates the interaction with the air/solvent vapor.

Cavicchi et al. observed orientation control in films of polyisoprene-*block*-poly(D,L-lactide), PI-*b*-PLA with with $f_{PI} = 0.78$, thus likely to form a PLA cylindrical minor phase.[147,164] Annealing in benzene is found to cause sufficient mobility for parallel cylinders to form, but the parallel cylinders indicate that no surface energy mediation takes place in this system. Chloroform not only causes sufficient mobility for long range ordering, but also controls interfacial interactions. For commensurate film thicknesses, parallel orientations still form. However, for incommensurate thicknesses, the neutral air interface a can overcome preferential interactions at the substrate, leading to perpendicular orientations. While benzene and chloroform are selective for the PS nonpolar phase, slight differences in the solubility account for the behavior difference.

1.2.4 The Bag of Tricks: Controlling Self Assembly in Thin Films

Very precise control of self-assembled patterns in thin films is required for many applications, but particularly so for device patterning. The primary concerns are control of grain orientation and increasing grain size. Self-assembled large grains with very few defects cannot be achieved by thermal or solvent annealing alone. Application of secondary techniques to direct the self assembly have been applied in conjunction with annealing for mobility. The most commonly used techniques are

described below, including how the technique is applied and its corresponding advantages and disadvantages. Several review articles further summarize this subject matter.[165-170]

Perpendicular orientations of cylindrical and lamellar morphologies are particularly attractive, as they can form high-aspect ratio templates. Several methods for gaining perpendicular orientations of morphologies have already been discussed above. In thin films, preferential attraction of blocks to the substrate and air interfaces leads to parallel orientations of cylindrical and lamellar structures (section 1.2.1.5.1). Overcoming the tendency to orient parallel to the substrate has been the subject of significant work, as perpendicular orientations are particularly attractive for templating applications. Substrate neutralization can overcome the preferential attraction of blocks at the air interface to create perpendicular orientations of thermally annealed PS-*b*-PMMA (section 1.2.1.5.2). In solvent annealing, solvent evaporation gradients lead to perpendicular orientations of PS-*b*-PEO with PEO minor phase and PS-*b*-PLA (section 1.2.3.6). Also, air-interface neutralization by adsorbed solvent has been demonstrated for PI-*b*-PLA annealed in chloroform (section 1.2.3.7).

Other methods have been used to control grain size and orientation. Graphoepitaxy and chemical epitaxy make use of patterned substrates to direct self assembly. Other externally fields, such as shear forces and electric fields, can also direct alignment. While primarily used in conjunction with thermal annealing, many have been demonstrated with solvent annealing as well. Several of these techniques have also shown the ability to cause perpendicular orientations of cylindrical and lamellar morphologies as well.

1.2.4.1 Graphoepitaxy

Graphoepitaxy, also sometimes called self-aligned self assembly[171] or templated self assembly,[169] makes use of topographically patterned substrates. Self-assembling block copolymers can align parallel to the walls of the pattern, subdividing the larger pattern with a predictable number of repeat units. The substrate patterns may be significantly larger than the patterns (commonly up to 1 μm wide), allowing them to be created by inexpensive and common photolithographic techniques.

This behavior was first examined for spherical morphology alignment. Segalman et al. observed a lower number of defects extending 5 μm away from the wall as compared to a flat film of polystyrene-*block*-poly(2-vinylpyridine), PS-*b*-P2VP, with P2VP spheres.[172,173] As they describe, "the presence of a hard edge imparts translational order onto the hexatic, which has quasi-long range orientational order and short range translational order, and onto the liquid which has short-range translational and orientational order."[172]

Cheng et al., observing behavior of polsytyrene-*block*-poly(ferrocenyl dimethylsilane), PS-*b*-PFS, possessing PFS spheres in the bulk, forms a wetting layer of PFS on the substrate.[174] They understand the domain ordering to be driven by this preferential wetting layer on the vertical sidewalls, citing similar behavior for directing behavior of spherical morphology on flat substrates into the film.[68]

Studying the response of spherical PS-PFS ordering in response to the condition of the equilibrium period of the polymer not matching side wall width, they found that the period adjusts to match the width of the template – similar to behavior of thin films confined between two plates.[175] The authors created a plot of the number of sphere rows observed versus the trench width, and compared that value to the free energy of the adjustment of the trench width, reproduced in Figure 1.11.

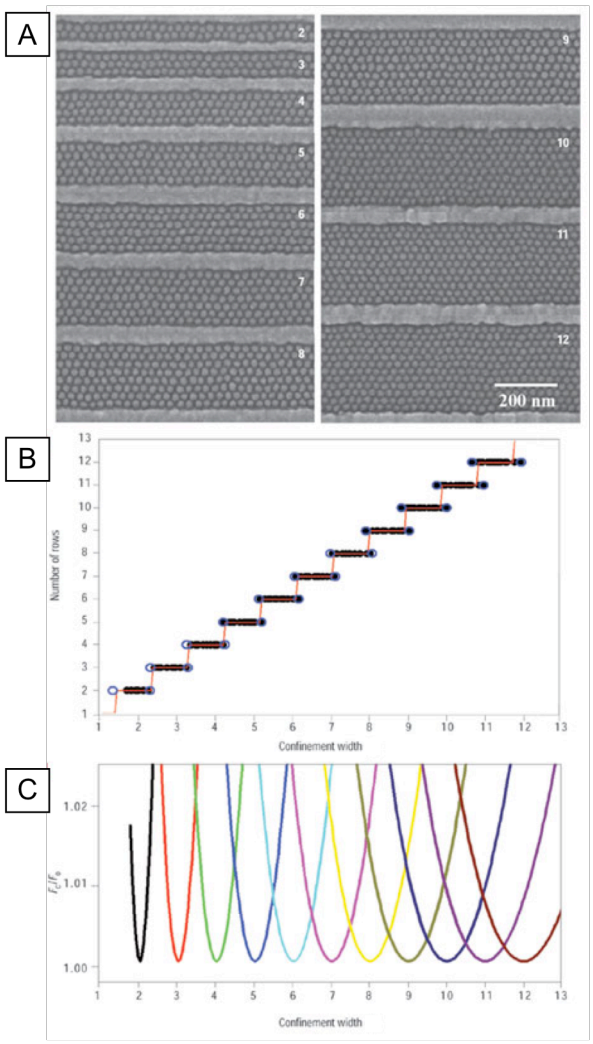

Figure 1.11. a) Plan-view scanning electron micrograph of ordered arrays of PFS spherical domains after calcining an assembled PS-*b*-PFS block copolymer confined to a trench in the substrate. Row width varies from 2 to 12 domains wide. b) The number of rows in the groove, N, plotted against confinement width, W, showing the widths at which arrays with N rows are stable. The confinement width (W) is expressed in terms of multiples of *d*, the equilibrium row spacing, which is 24.8 nm for this polymer. The open circles indicate the accessible states if a small energy fluctuation of 0.01kT per chain is available to the system. c) Energy vs. confinement width of block-copolymer system. The confined block-copolymer system, of a given W, will ideally select the value of N with the lowest free energy. A transition in the number of rows from N to N + 1 occurs when W = (N + 0.5)*d*, in agreement with the experimental data in (b). The free energy of the confined block copolymer (F_c) is presented relative to the free energy of the bulk block copolymer (F_0). Reprinted by permission from Macmillan Publishers Ltd.: Nature Materials, ref. 175, copyright 2004.

Bita et al. expanded the concept of graphoepitaxy to lithographically patterned posts, rather than trenches, which direct the assembly of spherical polystyrene-*block*-poly(dimethylsiloxane), PS-*b*-PDMS. [176] The posts are attractive to the PDMS spheres and behave as surrogates for the PDMS domains. Defect-free single grain alignment of the PS-*b*-PDMS is observed when the hexagonal array of posts is commensurate with the block copolymer periodicity, observed for posts separated by up to four times the polymer spatial period.

Extension of patterned substrates to cylindrical morphologies is also possible. Sundrani et al. observe that parallel cylinders align to parallel walls when confined to trench patterns, in this case using polystyrene-*block*-poly(ethylene-alt-propylene), PS-*b*-PEP, forming PS cylinders.[177,178] The end of the trench displays a curved shape, and the parallel cylinders were found to curve around this end, demonstrating alighment of parallel cylinders not only to straight walls. Other cases of ring or curved structures have been demonstrated for parallel cylinders of PS-*b*-PMMA with PMMA cylinders.[179,180]

Jung and Ross demonstrated differing alignment of PS-*b*-PDMS containing parallel cylinders of PDMS depending on surface treatment. In this case mobility was achieved by swelling in toluene, a good solvent for both blocks.[181] Films aligned on native silicon oxide display mixed orientation of parallel and perpendicular cylinders, relative to the plane of the film. Treatment of the substrate with grafted PS prior to block copolymer application leads to parallel orientation of the cylindrical domains, but alignment to the patterned substrate was not observed. PDMS-grafted substrates also possess parallel cylinders, but alignment to the walls varies depending on mesa width and degree of solvent swelling (and thus polymer mobility). Wider mesas combined with lower swelling ratios (less mobility) caused the parallel cylinders to align crosswise to the trench, perpendicular to the plane of the wall. Larger swelling,

thus more mobility, led to alignment of the parallel cylinders parallel to the walls. This behavior is attributed to mobility of the polymer on the surface, termed substrate pinning.[182] While the silicon oxide substrate does not impart significant mobility, PDMS leads to a high degree of mobility due to its low surface energy. Bosworth et al. observed similar behavior for cylindrical PαMS-*b*-PHOST upon annealing in good solvent THF: little alignment to silicon oxide trench walls is observed, but grafting a layer of PS to the substrate led to good alignment of the patterns.[151]

Alignment of perpendicular cylinders has been achieved using two methods. Treatment of substrates with PS-*r*-PMMA random copolymers brushes to neutralize surface interactions allows formation of perpendicular cylinders of PS-*b*-PMMA (PMMA cylinders).[183,184] Alternatively, block copolymers blended with homopolymers[185] or other block copolymers[186] are found to lead to perpendicular alignment for incommensurate film thicknesses; when confined in patterns on substrates further alignment of the perpendicular cylinders is observed.

Perpendicular alignment of PS-*b*-PMMA lamellae within trenches has also been demonstrated using surface neutrality techniques, though careful consideration of wetting interactions must be made.[187,188] If the random copolymer is on both the trench walls and bottom, lamellae perpendicular to the substrate occur, but these lamellae are also aligned perpendicular to the trench walls (crosswise alignment). The combination of walls that preferentially attract one of the blocks with a neutral trench bottom lead to formation of parallel lamellae that are aligned perpendicular to the walls of the trench.

1.2.4.2 Chemical Epitaxy

Chemical epitaxy refers to the use of a patterns of different materials on a substrate to direct ordering in a block copolymer film applied on top: this is possible

when each of the two areas of the pattern selectively attract a block. This results in the ability to control both the grain size and the orientation of BCP films. Patterns on substrates typically have the same spacing as the block copolymer spatial period, and patterning on this length scale requires expensive and low throughput techniques such as electron-beam lithography; since the chemical pattern must be created using these techniques one cannot argue that this technique allows patterning smaller length scales. The real application of this method is that these high-resolution patterning methods tend to have a large degree of defects, and the block copolymer applied on top is capable of healing these defects.[189-191] Recent demonstration of subdivision of more sparse patterns has improved the prospects for using this technique for patterning.[190,191]

Chemical epitaxy was first demonstrated to give perpendicular orientation of PS-*b*-PMMA lamellae using stripe patterns on substrates. This has been demonstrated using patterns of gold on silicon,[192,193] self-assembled monolayers,[194,195] polystyrene brushes on silicon oxide,[196] and patterns of polystyrene brushes with patterned poly(methyl methacrylate) on top.[189,197] Lamellae are found to align when the spatial period of the block copolymer matches the period of a striped chemical pattern. Lamellar PS-*b*-PMMA blended with corresponding homopolymers has also been demonstrated: redistribution of the homopolymer facilitates the defect-free assembly of the material when the spatial period does not match the period of the striped pattern.[198]

A thin layer of crosslinked block copolymer can also act as a pattern upon which a thicker lamellar morphology can assemble perpendicularly.[199,200] For the crosslinked underlayer, Park et al. used a monolayer of lamellar PS-*b*-PMMA oriented perpendicularly via a neutral substrate underlayer,[199] while Ruiz et al. used parallel cylinders, which form larger grains than perpendicular lamellae, to direct a block

copolymer with perpendicular lamellae deposited on top to form with large grain size.[200]

Expansion of chemical patterning for alignment of other morphologies was demonstrated later. Cylindrical morphologies of PS-*b*-PMMA with parallel and perpendicular orientations can be formed using patterned stripes with different widths. Parallel cylinders form on stripes with the same periodicity as the polymer, and complex structures such as alternating stripes of parallel and perpendicular orientations are formed when the surface pattern width is incommensurate with the spatial period of the block copolymer.[201] Perpendicular orientations of cylinders are also possible when the width of two materials in stripes are incommensurate with polymer periodicity.[202] Perpendicular orientation of cylindrical PS-*b*-PMMA is also possible on chemical patterns consisting of hexagonal arrays of dots.[203] Arrays of perpendicular morphologies with square, instead of hexagonal packing, are formed on chemical patterns of square array of dots.[204]

Alignment of spherical morphology was first observed by aligning parallel cylinders of polystyrene-*block*-poly(*tert*-butyl acrylate), PS-*b*-PtBA, with PtBA cylinders, along a surface pattern of chemically-patterned stripes.[205] Heating the PS-*b*-PtBA films causes deprotection of the *tert*-butyl group, forming polystyrene-*block*-poly(acrylic acid), PS-*b*-PAA. Thermal cleavage of the *tert*-butyl group results in a volume decrease in the polar block, and thus a transition to spherical morphology in which the spheres remain aligned to the chemical stripes. Later investigation of spherical PS-*b*-PMMA (PMMA spheres) demonstrates alignment of spherical PS-*b*-PMMA (PMMA spheres) on a striped chemical pattern with a hexagonal array of partial spherical domains.[206]

Use of chemical epitaxy to obtain novel shapes holds promise for integrated circuit fabrication.[207-209] A variety of different shapes needed for integrated circuit

design have been created in PS-*b*-PMMA using chemical epitaxy, demonstrated in Figure 1.12.

1.2.4.3 Electric Fields

Application of external fields such as electric fields and shear forces cause alignment block copolymer morphologies, both in bulk and in thin films. Here we describe the use of electric fields on lamellar and cylindrical morphologies to align morphology and to induce perpendicular orientations in thin films.

In the bulk, block copolymer morphologies align parallel to an applied electric field so long as the chains possess mobility (either above T_g or in solution) due to dielectric contrast between blocks of a block copolymer.[210-213] The mechanism by which chains align varies depending on the degree of phase separation in the block copolymer.[214,215] In strongly segregated block copolymers, alignment occurs by nucleation and growth of domains; in films near the order-disorder transition (weak segregation), alignment may also occur by grain rotation, leading to faster kinetics of ordering.

Application of an electric field perpendicular to block copolymer thin films has been used to align morphologies perpendicular to the plane of the film.[216,217] However, competing interfacial effects due to preferential surface wetting drive parallel alignment at film interfaces.[218,219] In thick films, electric fields drive perpendicular alignment of cylindrical PS-*b*-PI-*b*-PS (with PS cylinders)[218] and lamellar PS-*b*-PMMA[219] morphologies within the bulk of the film, but parallel orientations are still observed near the film surfaces.

Thurn-Albrecht et al. observed a threshold electric field above which selective

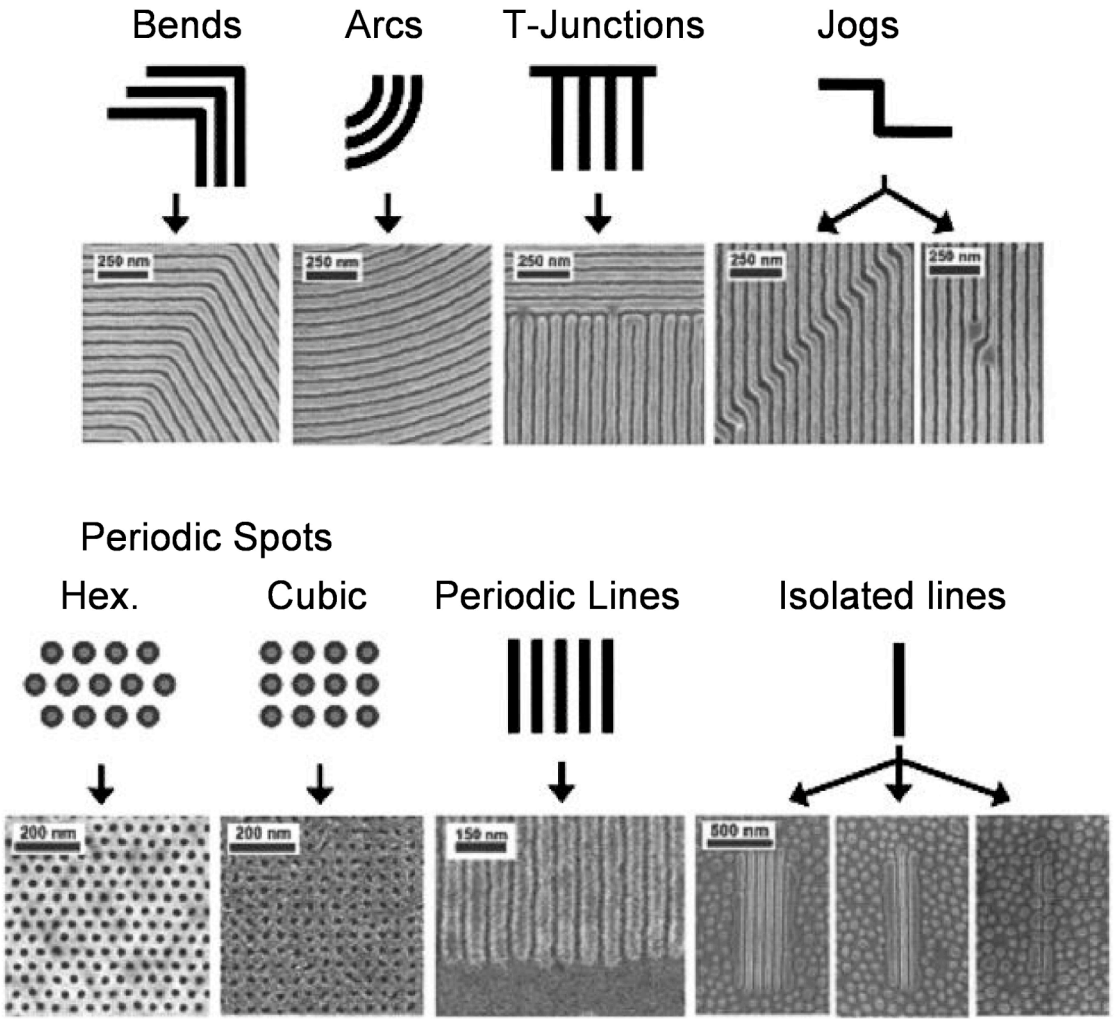

Figure 1.12. Examples of shapes of self-assembled PS-*b*-PMMA that can be formed using chemical epitaxy. The shapes correspond to the essential set of features required for integrated circuit fabrication. The PMMA domains are shown in dark gray, while the PS domains are shown in light gray or white. Adapted from refs. 207, 208.

surface wetting effects are overcome, leading to cylindrical PS-*b*-PMMA oriented perpendicular to the plane of the field; below this threshold value, the two orientations coexist in films.[217] Tsori & Andelman described two critical field values, E_1 and E_2 in the behavior of strongly segregated morphologies, in which $E_1 < E_2$.[220] Below E_1, only alignment parallel alignment is observed; above E_1, parallel alignment is still observed at the film interface, while perpendicular orientations are observed in the center of the film. Above E_2, however, the interfacial energies are entirely overcome, leading to perpendicular alignment throughout the film.

Several other methods have been used to further overcome interfacial effects, thus forming perpendicular morphologies in thin films. Surface neutralization by grafted random copolymers of PS-*ran*-PMMA mitigates preferential surface wetting of lamellar PS-*b*-PMMA.[221] Surface neutralization techniques alone can only be used for monolayer-thickness films, typically less than 100 nm (see section 1.2.1.5.2). When combined with electric fields, perpendicular alignment of films is observed for films approximately 1 μm thick, though some parallel alignment is still observed at the other (untreated) interface.

When lithium chloride is added to PS-*b*-PMMA, the lithium ions selectively segregate to the PMMA block due to coordination with its carbonyl groups.[222] Perpendicular orientations are easily possible when electric fields are applied,[222,223] and this behavior has been attributed to an increase in dielectric contrast from ion complexation.[224]

1.2.4.4 Shear Forces

Shear forces are another type of external field that have been used to align block copolymer morphology. In the bulk, elongational flow fields, often by roll casting, as well as large amplitude oscillatory shear, have been investigated. Large

amplitude oscillatory shear flow has been found to align bulk lamellar block copolymers of PS-*b*-PI, though the orientation of the alignment varies with the oscillatory frequency.[225-228] At low and high flow frequencies, alignment parallel to the plane of the shear occurs, while alignment perpendicular the shear plane occurs at intermediate frequencies.[225]

Bulk film studies with steady-shear elongational flow fields[229] and roll-casting experiments[230-233] have demonstrated that lamellar and cylindrical morphologies align parallel to the applied shear. Observation of a spherical morphology by simulations and in experiment demonstrate that spherical morphologies maintain a body-centered-cubic lattice at low stresses,[234] but at higher stresses the spheres undergo morphological transitions.[235-237] Sebastian et al. reports a critical shear stress similar to behavior of a block copolymer above its ODT temperature, suggesting a transition to disordered state.[235] Park and el al. and Zvelindovsky and Sevink observe elongation of the spheres, which then coalesce into cylinders aligned parallel to the plane of the shear as the shear rate increases.[236,237]

Thin films under steady shear have been investigated for alignment of block copolymer thin films. Shear-induced alignment of spherical domains has also been demonstrated, though alignment only occurs for thicknesses with 2 or more layers of spheres.[238-240] While spherical bilayers are not so useful for templating applications, etching away the top layer reveals a more useful monolayer.[241]

Parallel cylinders of polystyrene in a thin film polystyrene-*block*-poly(ethylene-alt-propylene), PS-*b*-PEP, are aligned parallel to a shear applied to the top surface of the film.[242] Use of a nonsolvent fluid to apply the strain allows alignment of the parallel cylinders within an arbitrary channel pattern in a polydimethylsiloxane pad applied to the polymer surface.[243]

1.2.4.5 Other External Alignment Methods

Other methods have been used to further control orientation of domains as well as the size and location of ordered domains, including temperature gradients, directional crystallization of solvents, and nanoimprint lithography. A temperature gradient can be used to orient block copolymer domains in the bulk[244] as well as in thin films.[245,246]

Directional crystallization of a solvent has been demonstrated with multiple diblock copolymers.[247-250] Combination of directional solvent solidification with a patterned substrate allows control of the thickness of the block copolymer forming between the two, and the thickness was found to direct orientation of cylinders of polystyrene-*block*-polyisoprene, PS-*b*-PI, with PI minor phase. At the tops of mesas perpendicular cylinders formed, while thicker regions away from the mesas form cylinders align perpendicular to the plane of the film.[251]

Nanoimprint lithography, sometimes called microembossing, has been used in a method similar to graphoepitaxy.[252-255] A patterned elastomeric mold is applied to a block copolymer solvent-swollen or melt film, and the block copolymer self assembly forms within trenches in the mold and aligns to the mold walls; after cooling or evaporating the solvent so that block copolymers no longer have mobility, the mold is removed.

1.3 Block Copolymer Templates

Block copolymer thin films have been used as structure-directing agents to pattern many different inorganic materials. Several reviews have created a comprehensive list of the resulting patterned materials and their applications.[256-258] While many different patterned inorganic materials have been formed, they have been created using only a few approaches to patterning. First, selective removal of one

block of a self-assembled diblock copolymer allows the remaining material to act as an etch resist or allows the voids to be filled with a new material. Alternatively, a foreign material infiltrated into a block copolymer thin film after self assembly of the block copolymer. A third method of directed assembly of inorganic materials is the self assembly of pre-blended block copolymer and inorganic metal oxide precurosors[90-94] or nanoparticles.[95-99] This has led to novel bulk composite materials and porous materials after removal of the block copolymer, often with the self assembly behavior tuned by the inorganic component. The "pre-blend, then self-assemble" method has been used on occasion for thin film patterning (the few examples are included in section 1.3.1.1, as their selective removal in thin films allows formation of a patterned monolith), though assembly of these materials could provide another robust means of thin film patterning.

1.3.1 Block Copolymer Lithography: Patterning After Selective Removal of a Block

The term "block copolymer lithography" was coined to describe pattern transfer from a block copolymer to inorganic materials by the same methods used in photolithography.[284] In photolithography, a photoresist is first selectively exposed and removed in a pattern using a light-induced solubility switch; this pattern is then transferred to a substrate material, primarily by dry etching methods or deposition plus lift-off techniques.[259-262] For block copolymer lithography, the method of pattern transfer is also a two-step process: 1) one block is selectively removed from the self-assembled block copolymer thin films, and 2) the resulting pattern is transferred either by use of the monolithic material as an etch resist or by backfilling the voids. Ito comments that block copolymer patterning does not allow formation of arbitrary patterns like those possible by photolithography, but it is useful for patterning repeating pattern shapes.[262]

1.3.1.1 Selective Removal of a Block From Self-Assembled Block Copolymer Film

Block copolymer lithography requires the selective removal of one block in an assembled block copolymer film in order to transfer the pattern to other materials. Four strategies for selective removal of one block from the self-assembled film are used, outlined below.

The first strategy for creating monolithic films is the selective degradation of one block in a self-assembled block copolymer, which is possible by careful selection of block copolymer material. The most common blocks for selective removal system are polyisoprene (or structurally similar polybutadiene) and poly(methyl methacrylate). Polyisoprene and polybutadiene components of polystyrene-*block*-polyisoprene and polystyrene-*block*-polybutadiene can be degraded by treatment with ozone.[263,264] Selective degradation of PMMA, most often from PS-*b*-PMMA, is achieved by its exposure to UV light followed by removal by acetic acid[265] or by selective reactive ion etching.[266,267] Some applications make use of these porous membranes without further modification after selective removal of one block, including for filtration applications[268] and optical waveguides.[269]

Several other block copolymer monoliths have been demonstrated. Selective degradation of polylactide from polystyrene-*block*-polylactide is possible by soaking in an aqueous solution of sodium hydroxide.[270] Poly(ethylene oxide) can be selectively removed from a triblock of polystyrene-*block*-poly(methyl methacrylate)-*block*-poly(ethylene oxide) in which the very small PMMA midblock can be selectively degraded, allowing the PMMA and PEO blocks to be washed away.[271]

A second strategy is the formation of pores without selective block degradation. Pores in diblock copolymers may also be formed by assembling a supramolecular assembly of a diblock copolymer such as polystyrene-*block*-poly(4-vinylpyridine) blended with a material that selectively segregates to the polar

block.[149,150,272,273] Extraction of the segregating material leaves pores within the diblock copolymer. Alternatively, partial pore formation in polystyrene-*block*-poly(methyl methacrylate)[157,158] and polystyrene-*block*-poly(4-vinylpyridine)[159] have been demonstrated by rinsing films in a solvent that is completely selective for the polar minor phase of the assembled block copolymer.

The third method for creating porous materials from self-assembled block copolymers is the use of polymers composed of inorganic materials such as silicon or iron in combination with an easily etched block such as PS, PI, or PMMA. Upon calcination or reactive ion etching of self-assembled films, the organic component of the films is removed and etch-resistant inorganic oxides are formed. Examples of some inorganic-containing etch-resistant blocks include:

- Poly(pentamethyldisilylstyrene)[274,275]
- Poly(ferrocenyldimethylsilane)[276,277] and poly(ferrocenylethylmethylsilane)[278,279]
- Poly(dimethylsiloxane)[181]
- Poly(silsesquioxanes)[280]

For the fourth method for patterning, a block copolymer is blended with a metal oxide precursor; upon self assembly in a thin film, the inorganic material selectively segregates into the polar block. Removal of the polymer leads to monolithic metal oxides. Du et al. created thin films of polyisoprene-*block*-poly(ethylene oxide) blended with an aluminum oxide precursor, leaving patterend aluminum oxide after calcination to remove the polymeric material.[94] Thin films of polystyrene-*block*-poly(ethylene oxide) blended with an organosilicate polymer,[281] an oligomeric titanate,[282] or an titanium tetra-isopropoxide[283] also self-assemble within the PEO block. Silicon oxide or titanium oxide patterns remain after removal of the

organic material, resulting in an etch-resistant oxide pattern similar to cases of blocks with silicon or iron-containing backbones.

1.3.1.2 Monolithic Polymer Used as an Etch Resist

Pattern transfer from the monolithic polymer film (described in section 1.3.3.1) to a variety of underlying substrate materials using etching techniques has been demonstrated; the following are examples of materials patterned by a monolithic etch resist:

- Silicon nitride[284,285]
- Silicon[264] for semiconductor capacitor fabrication[286-288]
- Germanium[264]
- Cobalt magnetic dot arrays[289]
- Nanotextured silver surfaces for enhanced Raman signals[290]
- Patterned catalysts for carbon nanotube array growth[291]
- Conducting polymer poly(3,4-ethylenedioxythiophane):poly(styrene-sulfonate)[292]
- Fabrication of a silicon field effect transistor.[171]

1.3.1.3 Patterning by Deposition in Pores

Back-filling pores formed by the selective removal of one block of an assembled block copolymer (described above) has also yielded a variety of patterned materials. All examples use one of the porous templates fabricated from self-assembled block copolymer films described above in 1.3.1.1. In some cases, the polymer template is subsequently removed; in other cases the polymer template is left in place

- Gallium arsenide nanostructures by metalorganic chemical vapor deposition[293,294]
- Ferromagnetic cobalt nanowires electrodeposited in pores for ultrahigh-denisty storage media[295,296]
- Gold deposited onto porous template by electron beam evaporation followed by lift-off of the remaining polymer, leaving gold nanoparticles[297]; the same method may be used to pattern chromium and layered gold and chromium.[298,299]
- Silicon oxide posts by chemical deposition of silicon precursors into pores[300]
- Cadmium selenide nanoparticles driven into pores by withdrawal of the patterned film from solutions containing particles[301] and by using electric fields[302]
- Poly(dimethylsiloxane) drawn into pores using an electric field[303]
- Chromium oxide formed in pores by sputtering[304]
- Metallic nickel nanowires embedded into pores both by washing in and by electrodeposition.[305]
- High density conducting polypyrrole fabricated in pores by electropolymerization[306]

1.3.2 Infiltration of a Self-Assembled Block Copolymer

The use of self-assembled block copolymers as structure directing agents by selective infiltration of one block is typically limited to thin film applications, as diffusion of the patterning material deep into the block copolymer film is problematic. In this technique, one of the blocks of an assembled block copolymer film is infiltrated by metal or oxide precursor materials.

Two examples of selective metal deposition follow. Parallel cylindrical polystyrene-*block*-poly(methyl methacrylate) is treated with a palladium colloid, which selectively deposits on top of the polystyrene domains.[307] Electroless deposition of nickel then forms on the palladium particles. Alternatively, polystyrene-*block*-poly(4-vinylpyridine) with cylindrical P4VP aligned parallel to the substrate is soaked in a weakly acidic aqueous solution of metal salts such as gold chloride, sodium tetrachloroplatinate and sodium tetrachloropalladate.[308,309] A plasma etch removes the polymer film and reduces the metal patterned in the P4VP domains.

Selective oxide formation within one domain follows similar methods. Kim et al. demonstrated titania and silica hybrid materials formed in self-assembled perpendicular cylinders of poly(ethylene oxide) in polystyrene-*block*-poly(ethylene oxide) upon exposure to titanium tetrachloride or silicon tetrachloride vapors.[310] Pai et al. used humidified supercritical carbon dioxide to infiltrate metal alkoxides such as tetraethylorthosilicate into poly(ethylene oxide)-*block*-poly(propylene oxide)-*block*-poly(ethylene oxide) and polyethylene-*block*-poly(ethylene oxide) containing trace amounts of *para*-toluenesulfonic acid.[311] The acid catalyzes silicon oxide formation in the more polar PEO block, which is left behind after calcination, and the small dielectric constant of the resulting mesoporous silicate film holds promise for applications for low-k dielectrics. Replacement of the *para*-toluenesulfonic acid in the film with a photoacid generator allows formation of the silicates only in UV-exposed regions.[312] Hayward et al. demonstrated similar infiltration of the polar majority component of cylinder-forming polystyrene-*block*-poly(2-vinylpyridine) by soaking in aqueous silica and titania precursor solutions, and removal of the polymeric material is then achieved by treatment in a UV/ozone cleaner.[313] Simple infusion of the assembled material with the precursor causes disruption in the ordered block

copolymer, which was ameliorated by crosslinking the P2VP component prior to swelling.

1.4 The Intersection of Block Copolymer Self Assembly With Lithography

The combination of top-down lithographic techniques with bottom-up block copolymer self assembly allows a single material to be patterned on two length scales. More specifically, lithographic patterning may precisely control the location of self-assembled block copolymer thin film domains. This combined patterning method requires careful choice of block copolymer materials that are also capable of lithographic patterning. Several reviews outline photoresist design and the development of photolithography for patterning down to the current state-of-the-art 30 nm patterns.[259-262]

An early example of combined patterning used polystyrene-*block*-poly(methyl methacrylate) with PMMA cylinders aligned perpendicular to the plane of a thin film by use of neutral substrates.[314] Electron-beam patterning both crosslinks the PS majority component and degrades the PMMA block, causing formation of pores only in patterned regions after development in acetic acid. Cobalt nanowires were then electrodeposited only in the porous regions.

Electron beam lithography has also been used to control the location of a monolayer of polystyrene-*block*-poly(2-vinylpyridine) micelles loaded with metal precursors.[315] An electron beam resist deposited on a substrate is patterned, and then the metal-loaded micelles are spin-coated on top on the patterned film. When the e-beam resist is removed, micelles deposited on the resist are selectively removed, and then the remaining patterned micelles are etched away to leave behind patterned metal dots. Alternatively, the a monolayer of metal-loaded micelles can themselves be used

as a negative tone electron-beam resist, with written patterns only a few micelles wide, approximately 200 nm.[316]

The design of a self-assembling block copolymer capable of behaving as a photoresist was previously reported by the Ober group.[94,317] Poly(α-methylstyrene)-*block*-poly(4-hydroxystyrene), PαMS-*b*-PHOST, self-assembles with perpendicular cylinders of PαMS upon spin coating from solution. PHOST, the majority component here, is a component of all high-resolution chemically amplified photoresists used for 248 nm lithography, whether they are positive tone (exposure induces solubility) or negative tone (exposure prevents solubility, often via crosslinking).[261] Inclusion of trace quantities of photoacid generator and crosslinker allow behavior of the block copolymer as a negative-tone photoresist, and patterns with 450 nm features have been demonstrated.[94,317] Selective removal of the PαMS block leads to the formation of pores in the crosslinked patterns, as demonstrated in Figure 1.13.

Use of solvent annealing to gain further control over the self assembly of PαMS-*b*-PHOST has allowed formation of parallel cylindrical morphology by annealing in THF as well as a kinetically-trapped spherical morphology by annealing in the majority-selective solvent acetone.[151] The morphology may be switched from spherical to cylindrical and vice versa using sequential solvent anneals in the two solvents. When combined with lithographic crosslinking behavior, spherical domains less than 100 nm wide are formed within cylindrical morphology by patterning with electron-beam lithography prior to morphology switching.[318]

The combined patterning technique can be extended to other block copolymer systems in which one block contains hydoxyl functionality. The critical components of photocrosslinking in a negative-tone photoresist are a) a photoacid generator, b) a crosslinker, and c) polymer with functional moiety capable of binding to crosslinker, most commonly a polymer containing hydroxyl groups.[259] In commercial

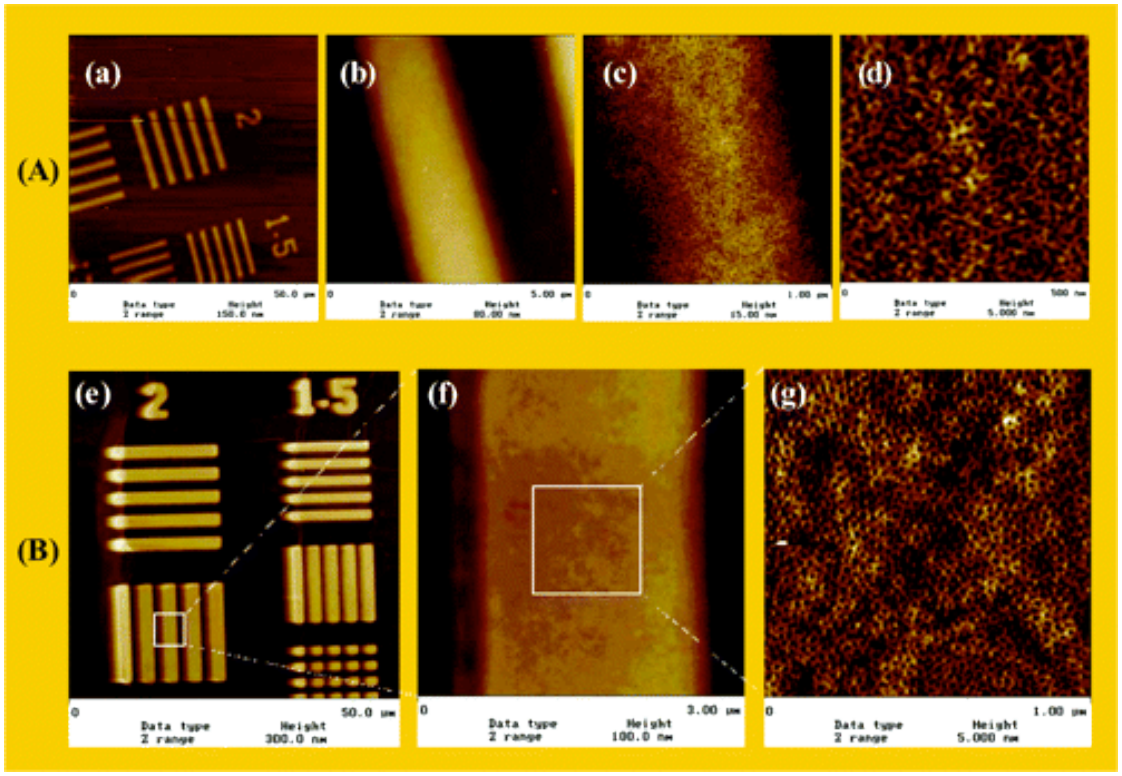

Figure 1.13. Photopatterns of porous material were formed using films of PαMS-*b*-PHOST on a silicon wafer. PαMS-*b*-PHOST (containing photoacid generator and crosslinker) with perpendicular cylinders of PαMS is patterned using a 248 nm stepper. Unexposed regions are developed away and then the PαMS is selectively removed to form pores in the photopatterned regions. (A) Film thickness is 39 nm, with (a) 2 and 1.5 μm lines shown. (b) A magnification of a 2 μm line. (c) A further magnification of the line. (d) A further magnification of the line. (B) Film thickness is 127 nm, with (e) 2 and 1.5 μm lines and dots shown. (f) A magnification of a 2 μm line. (g) A further magnification of the line. Reprinted with permission from ref. 317, copyright 2004, American Chemical Society.

photoresists, the photocrosslinking most commonly occurs by a condensation reaction, as is the case with PαMS-*b*-PHOST blended with the crosslinker tetramethoxymethyl glycoluril.[94,317] Alternatively, poly(hydroxyethyl methacrylate) is capable of behaving as a negative-tone photoresist with inclusion of the crosslinker tetramethoxymethyl glycoluril and a photoacid generator, [319,320] leading to another system capable of top-down/bottom up patterning, of poly(methyl methacrylate)-*block*-poly(hydroxyethyl methacrylate).[321]

La et al. studied a photopatternable block copolymer, polystyrene-*block*-poly(*tert*-butyl acrylate), PS-*b*-PtBA, which is capable of undergoing acid-catalyzed deprotection to polystyrene-*block*-poly(acrylic acid), rendering it soluble in an aqueous base developer.[322] When self-assembled films of PS-*b*-PtBA contain a photoacid generator, deprotection is catalyzed only in photopatterned regions, and the patterned regions containing PS-*b*-PAA are removed. The line edge roughness of this pattern is correlated to the size of the self-assembled microdomains, giving a method of controlling line edge roughness in at the edges of patterned regions.

1.5 Outlook and Summary

A wide variety of functional nanostructures have been fabricated using block copolymer self assembly, and many of these applications require a large degree of ordering in the block copolymer template. Self assembly of block copolymers is facilitated by polymer chain mobility, achieved by thermal or solvent annealing techniques. Once mobility allows self assembly, further control of domain alignment and grain size is possible using secondary techniques such as surface neutralization, graphoepitaxy, chemical epitaxy, electric fields, and shear forces.

Solvent annealing is particularly attractive for inducing ordering in block copolymer thin films as it allows them to self-assemble without risk of thermal

degradation. The solvent further affects the phase behavior by mitigating the interaction of the two blocks and by causing shifts in relative volume fraction (and thus morphology formed) depending on the selectivity of the solvent for each block. These methods offer the ability to tune the morphology formed in the block copolymer. Solvent annealing also leads to ordering mechanisms not available via thermal annealing techniques – gradient evaporation effects can cause perpendicular orientations, and the solvent can also moderate selective wetting of blocks at the air interface in films.

Several unexplored aspects to self assembly by solvent annealing remain. First, predicting when secondary effects such as gradient and interface-neutralization will occur in novel block copolymer systems for annealing would be useful. Second, an investigation of mixed solvent systems would provide a method not only for annealing block copolymers for which solvent common to the blocks are not found, but should also provide a method to continuously tune the selective-solvent induced morphology by altering the solvent mix. This complicated system requires extra consideration, since not only does the interaction between the two blocks have to be considered, but also the interaction of each solvent with each block (a total of 4 interactions for a diblock!) as well as the interaction of the two solvents with each other. However, this extra complication can be expected to yield rich control of self-assembled behavior.

Photolithography is used throughout the semiconductor industry to pattern inorganic components, but application for pattering polymeric components has been limited due to problems with solubility of underlying polymeric material during photoresist processing.[323] Likewise, pattern transfer using BCP templates is largely limited to inorganic materials. Recent development of fluorinated photoresists that are processable in supercritical carbon dioxide and hydrofluoroethers allows deposition

and development of the photoresist without damaging underlying non-fluorinated polymeric materials, termed orthogonal processing.[323-325] Orthogonal processing could be used to pattern a broad range of self-assembled block copolymer films, precisely controlling the location of the self-assembled pattern, without need to design photoresist capability into the assembling block copolymer. Alternatively, orthogonal processing capability could be incorporated into the design of a self-assembling block copolymer to allow pattern transfer to organic components.

REFERENCES

(1) Bates, F. S.; Fredrickson, G. H. *Phys. Today* **1999**, *52*, 32-38.

(2) Leibler, L. *Macromol.* **1980**, *13*, 1602–1617.

(3) Semenov, A. N. *Sov. Phys. JETP* **1985**, *61*, 733-742.

(4) Ohta, T.; Kawasaki, K. *Macromol.* **1986**, *19*, 2621-2632.

(5) Matsen, M. W.; Bates, F. S. *Macromol.* **1996**, *29*, 1091–1098.

(6) Abetz, V.; Simon, P. F. W. *Adv. Polym. Sci.* **2005**, *189*, 125-212.

(7) Daoulas, K. C.; Mueller, M.; de Pablo, J. J.; Nealey, P. F.; Smith, G. D. *Soft Matter* **2006**, *2*, 572-583.

(8) Edrington, A. C.; Urbas, A. M.; DeRege, P.; Chen, C. X.; Swager, T. M.; Hadjichristidis, N.; Xenidou, M.; Fetters, L. J.; Joannopoulos, J. D.; Fink, Y.; Thomas, E. L. *Adv. Mater.* **2001**, *13*, 421-425.

(9) Hashimoto, T.; Shibayama, M.; Kawai, H. *Macromol.* **1980**, *13*, 1237-1247.

(10) Helfand, E.; Wasserman, Z. R. *Macromol.* **1976**, *9*, 879-888.

(11) Helfand, E.; Wasserman, Z. R. *Macromol.* **1978**, *11*, 960-966.

(12) Mayes, A. M.; Olvera de la Cruz, M. *J. Chem. Phys.* **1989**, *91*, 7228-7235.

(13) Mayes, A. M.; Olvera de la Cruz, M. *J. Chem. Phys.* **1991**, *95*, 4670-4677.

(14) Matsen, M. W.; Schick, M. *Macromol.* **1994**, *27*, 187-192.

(15) Matsen, M. W.; Thompson, M. E. *J. Chem. Phys.* **1999**, *111*, 7139-7146.

(16) Zheng, W.; Wang, Z.-G. *Macromol.* **1995**, *28*, 7215-7223.

(17) Pitsikalis, M.; Pispas, S.; Mayes, J. W.; Hadjichristidis, N. *Adv. Polym. Sci.* **1998**, *135*, 1-137.

(18) Sakurai, S.; Kawada, H.; Hashimoto, T.; Fetters, L. J. *Macromol.* **1993**, *26*, 5796-5802.

(19) Kimishima, K.; Koga, T.; Hashimoto, T. *Macromol.* **2000**, *33*, 968-977.

(20) Hajduk, D. A.; Gruner, S. M.; Rangarajan, P.; Register, R. A.; Fetters, L. J.; Honeker, C.; Albalak, R. J.; Thomas, E. L. *Macromol.* **1994**, *27*, 490-501.

(21) Fasolka, M. J.; Mayes, A. M. *Annu. Rev. Mater. Res.* **2001**, *31*, 323-355.

(22) Anastasiadis, S. H.; Russell, T. P.; Satija, S. K.; Majkrzak, C. F. *Phys. Rev. Lett.* **1989**, *62*, 1852-1855.

(23) Coulon, G.; Russell, T. P.; Deline, V. R.; Green, P. F. *Macromol.* **1989**, *22*, 2581-2589.

(24) van Dijk, M. A.; van den Berg, R. *Macromol.* **1995**, *28*, 6773-6778.

(25) Turner, M. S. *Phys. Rev. Lett.* **1992**, *69*, 1788-1791.

(26) Walton, D. G.; Kellogg, G. J.; Mayes, A. M.; Lambooy, P.; Russell, T. P. *Macromol.* **1994**, *27*, 6225-6228.

(27) Lambooy, P.; Russell, T. P.; Kellogg, G. J.; Mayes, A. M.; Gallagher, P. D.; Satija, S. K. *Phys. Rev. Lett.* **1994**, *72*, 2899-2902.

(28) Kellogg, G. J.; Walton, D. G.; Mayes, A. M.; Lambooy, P.; Russell, T. P.; Gallagher, P. D.; Satija, S. K. *Phys. Rev. Lett.* **1996**, *76*, 2503-2506.

(29) Konrad, M.; Knoll, A.; Krausch, G.; Magerle, R. *Macromol.* **2000**, *33*, 5518-5523.

(30) Xu, T.; Hawker, C. J.; Russell, T. P. *Macromol.* **2005**, *38*, 2802-2805.

(31) Pickett, G. T.; Balazs, A. C. *Macromol.* **1997**, *30*, 3097-3103.

(32) Sommer, J.-U.; Hoffmann, A.; Blumen, A. *J. Chem. Phys.* **1999**, *111*, 3728-3732.

(33) Mansky, P.; Russell, T. P.; Hawker, C. J.; Pitsikalis, M.; Mays, J. *Macromol.* **1997**, *30*, 6810-6813.

(34) Mansky, P.; Russell, T. P.; Hawker, C. J.; Mays, J.; Cook, D. C.; Satija, S. K. *Phys. Rev. Lett.* **1997**, *79*, 237-240.

(35) Ham, S.; Shin, C.; Kim, E.; Ryu, D. Y.; Jeong, U.; Russell, T. P.; Hawker, C. J. *Macromol.* **2008**, *41*, 6431-6437.

(36) Mansky, P.; Liu, Y.; Huang, E.; Russell, T. P.; Hawker, C. *Science* **1997**, *275*, 1458-1460.

(37) Husseman, M.; Malmstroem, E. E.; McNamara, M.; Mate, M.; Mecerreyes, D.; Benoit, D. G.; Hedrick, J. L.; Mansky, P.; Huang, E.; Russell, T. P.; Hawker, C. J. *Macromol.* **1999**, *32*, 1424-1431.

(38) Peters, R. D.; Tang, X. M.; Kim, T. K.; Nealey, P. F. *Langmuir* **2000**, *16*, 9620-9626.

(39) Sohn, B. H.; Yun, S. H. *Polymer* **2002**, *43*, 2507-2512.

(40) Ryu, D. Y.; Shin, K.; Drockenmuller, E.; Hawker, C. J.; Russell, T. P. *Science* **2005**, *308*, 236-239.

(41) Ryu, D. Y.; Wang, J.-Y.; Lavery, K. A.; Drockenmuller, E.; Satija, S. K.; Hawker, C. J.; Russell, T. P. *Macromol.* **2007**, *40*, 4296-4300.

(42) In, I.; La, Y.-H.; Park, S.-M.; Nealey, P. F.; Gopalan, P. *Langmuir* **2006**, *22*, 7855-7860.

(43) Han, E.; Stuen, K. O.; La, Y.-H.; Nealey, P. F.; Gopalan, P. *Macromol.* **2008**, *41*, 9090-9097.

(44) Han, E.; In, I.; Park, S.-M.; La, Y.-H.; Wang, Y.; Nealey, P. F.; Gopalan, P. *Adv. Mater.* **2007**, *19*, 4448-4452.

(45) Ji, S.; Liu, G.; Zheng, F.; Craig, G. S. W.; Himpsel, F. J.; Nealey, P. F. *Adv. Mater.* **2008**, *20*, 3054-3060.

(46) Bang, J.; Bae, J.; Loewenhielm, P.; Spiessberger, C.; Given-Beck, S. A.; Russell, T. P.; Hawker, C. J. *Adv. Mater.* **2007**, *19*, 4552-4557.

(47) Huang, E.; Pruzinsky, S.; Russell, T. P.; Mays, J.; Hawker, C. J. *Macromol.* **1999**, *32*, 5299-5303.

(48) Ji, S.; Liu, C.-C.; Son, J. G.; Gotrik; Craig, G. S. W.; Gopalan, P.; Himpsel, F. J.; Char, K.; Nealey, P. F. *Macromol.* **2008**, *41*, 9098-9103.

(49) Kim, S. H.; Misner, M. J.; Russell, T. P. *Adv. Mater.* **2008**, *20*, 4851-4856.

(50) Shull, K. R. *Macromol.* **1992**, *25*, 2122-2133.

(51) Russell, T. P.; Menelle, A.; Anastasiadis, S. H.; Satija, S. K.; Majkrzak, C. F. *Macromol.* **1991**, *24*, 6263-6269.

(52) Russell, T. P.; Lambooy, P.; Kellogg, G. J.; Mayes, A. M. *Physica B* **1995**, *213-214*, 22-25.

(53) Koneripalli, N.; Singh, N.; Levicky, R.; Bates, F. S.; Gallagher, P. D.; Satija, S. K. *Macromol.* **1995**, *28*, 2897-2904.

(54) Knoll, A.; Tsarkova, L.; Krausch, G. *Nano Letters* **2007**, *7*, 843-846.

(55) Coulon, G.; Collin, B.; Ausserre, D.; Chatenay, D.; Russell, T. P. *J. Phys.* **1990**, *51*, 2801-2811.

(56) Carvalho, B. L.; Thomas, E. L. *Phys Rev Lett* **1994**, *74*, 3321-3324.

(57) Kikuchi, M.; Binder, K. *J. Chem. Phys.* **1994**, *101*, 3367-3377.

(58) Brown, G.; Chakrabarti, A. *J. Chem. Phys.* **1994**, *101*, 3310-3317.

(59) Matsen, M. W. *J. Chem. Phys.* **1997**, *106*, 7781-7791.

(60) Tang, W. H. *Macromol.* **2000**, *33*, 1370-1384.

(61) Suh, K. Y.; Kim, Y. S.; Lee, H. H. *J. Chem. Phys.* **1998**, *108*, 1253-1256.

(62) Wang, Q.; Yan, Q.; Nealey, P. F.; de Pablo, J. J. *J. Chem. Phys.* **2000**, *112*, 450-464.

(63) Koneripalli, N.; Levicky, R.; Bates, F. S. *Langmuir* **1996**, *12*, 6681-6690.

(64) Morkved, T. L.; Jaeger, H. M. *Europhys. Lett.* **1997**, *40*, 643-648.

(65) Fasolka, M. J.; Banerjee, P.; Mayes, A. M.; Pickett, G. T.; Balazs, A. C. *Macromol.* **2000**, *33*, 5702-5712.

(66) Kim, H.-C.; Russell, T. P. *J. Poly. Sci. B* **2001**, *39*, 663-668.

(67) Khanna, V.; Cochran, E. W.; Hexemer, A.; Stein, G. A.; Fredrickson, G. H.; Kramer, E. J.; Li, X.; Wang, J.; Hahn, S. F. *Macromol.* **2006**, *39*, 9346-9356.

(68) Yokoyama, H.; Mates, T. E.; Kramer, E. J. *Macromol.* **2000**, *33*, 1888-1898.

(69) Stein, G. A.; Kramer, E. J.; Li, X.; Wang, J. *Macromol.* **2007**, *40*, 2453-2460.

(70) Stein, G. A.; Cochran, E. W.; Katsov, K.; Fredrickson, G. H.; Kramer, E. J.; Li, X.; Wang, J. *Phys. Rev. Lett.* **2007**, *98*, 158302.

(71) Huinink, H. P.; Brokken-Zijp, J. C. M.; van Dijk, M. A.; Sevink, G. J. A. *J. Chem. Phys.* **2000**, *112*, 2452-2463.

(72) Keddie, J. L.; Jones, R. A. L.; Cory, R. A. *Faraday Discuss.* **1994**, *98*, 219-230.

(73) Grohens, Y.; Brogly, M.; Labbe, C.; David, M.-O.; Schulta, J. *Langmuir* **1998**, *14*, 2929-2931.

(74) Wallace, W. E.; van Zanten, J. H.; Wu, W. L. *Phys. Rev. E* **1995**, *52*, R3329-R3332.

(75) van Zanten, J. H.; Wallace, W. E.; Wu, W.-L. *Phys. Rev. E* **1996**, *53*, R2053-R2056.

(76) Tsui, O. K. C.; Russell, T. P.; Hawker, C. J. *Macromol.* **2001**, *34*, 5535-5539.

(77) Fredrickson, G. H. *Macromol.* **1987**, *20*, 2535-2542.

(78) Milner, S. T.; Morse, D. C. *Phys. Rev. E* **1996**, *54*, 3793-3810.

(79) Foster, M. D.; Sikka, M.; Singh, N.; Bates, F. S.; Satija, S. K.; Majkrzak, C. F. *J. Chem. Phys.* **1992**, *96*, 8605-8615.

(80) Turner, M. S.; Rubenstein, M.; Marques, C. M. *Macromol.* **1994**, *27*, 4986-4992.

(81) Heckmann, M.; Drossel, B. *Macromol.* **2008**, *41*, 7679-7686.

(82) Huinink, H. P.; van Dijk, M. A.; Brokken-Zijp, J. C. M.; Sevink, G. J. A. *Macromol.* **2001**, *34*, 5325-5330.

(83) Yin, Y.; Sun, P.; Jiang, R.; Li, B.; Chen, T.; Jin, Q.; Ding, D.; Shi, A.-C. *J. Chem. Phys.* **2006**, *124*, 184708.

(84) Tsarkova, L.; Knoll, A.; Krausch, G.; Magerle, R. *Macromol.* **2006**, *39*, 3608-3615.

(85) Knoll, A.; Horvat, A.; Lyakhova, K. S.; Krausch, G.; Sevink, G. J. A.; Zvelindovsky, A. V.; Magerle, R. *Phys. Rev. Lett.* **2002**, *89*, 035501.

(86) Horvat, A.; Lyakhova, K. S.; Sevink, G. J. A.; Zvelindovsky, A. V.; Magerle, R. *J. Chem. Phys.* **2004**, *120*, 1117-1126.

(87) Lyakhova, K. S.; Sevink, G. J. A.; Zvelindovsky, A. V.; Horvat, A.; Magerle, R. *J. Chem. Phys.* **2004**, *120*, 1127-1137.

(88) Rehse, N.; Knoll, A.; Magerle, R.; Krausch, G. *Macromol.* **2003**, *36*, 3261-3271.

(89) Yang, Y.; Qiu, F.; Zhang, H.; Yang, Y. *Polymer* **2006**, *47*, 2205-2216.

(90) Templin, M.; Franck, A.; Du Chesne, A.; Leist, H.; Zhang, Y.; Ulrich, R.; Schaedler, V.; Ulrich, W. *Science* **1997**, *278*, 1795-1798.

(91) Jain, A.; Toombes, G. E. S.; Hall, L. M.; Mahajan, S.; Garcia, C. B. W.; Probst, W.; Gruner, S. M.; Wiesner, U. *Angew. Chem. Int. Ed.* **2005**, *44*, 1226-1229.

(92) Lee, J.; Orilall, M. C.; Warren, S. C.; Kamperman, M.; DiSalvo, F. J.; Wiesner, U. *Nature Mater.* **2008**, *7*, 222-228.

(93) Kamperman, M.; Fierke, M. A.; Garcia, C. B. W.; Wiesner, U. *Macromol.* **2008**, *41*, 8745-8752.

(94) Du, P.; Li, M.; Douki, K.; Li, X.; Garcia, C. B. W.; Jain, A.; Smilgies, D.-M.; Fetters, L. J.; Gruner, S. M.; Wiesner, U.; Ober, C. K. *Adv. Mater.* **2004**, *16*, 953-957.

(95) Bockstaller, M. R.; Lapetnikov, Y.; Margel, S.; Thomas, E. L. *J. Am. Chem. Soc.* **2003**, *125*, 5276-5277.

(96) Chiu, J. J.; Kim, B. J.; Yi, G.-R.; Bang, J.; Kramer, E. J.; Pine, D. J. *Macromol.* **2007**, *40*, 3361-3365.

(97) Warren, S. C.; DiSalvo, F. J.; Wiesner, U. *Nature Mater.* **2007**, *6*, 156-161.

(98) Huang, C.-M.; Wei, K.-H.; Jeng, U.-S.; Sheu, H.-S. *Macromol.* **2008**, *41*, 6876-6879.

(99) Warren, S. C.; Messina, L. C.; Slaughter, L. S.; Kamperman, M.; Zhou, Q.; Gruner, S. M.; DiSalvo, F. J.; Wiesner, U. *Science* **2008**, *320*, 1748-1752.

(100) Helfand, E.; Tagami, Y. *J. Chem. Phys.* **1972**, *56*, 3592-3601.

(101) Huang, C.-I.; Lodge, T. P. *Macromol.* **1998**, *31*, 3556-3565.

(102) Noolandi, J.; Hong, K. M. *Ferroelectrics* **1980**, *30*, 117-123.

(103) Whitmore, M. D.; Vavasour, J. D. *Macromol.* **1992**, *25*, 2041-2045.

(104) Hong, K. M.; Noolandi, J. *Macromol.* **1983**, *16*, 1083-1093.

(105) Olvera de la Cruz, M. *J. Chem. Phys.* **1989**, *90*, 1995-2002.

(106) Fredrickson, G. H.; Leibler, L. *Macromol.* **1989**, *22*, 1238-1250.

(107) Lodge, T. P.; Pan, C.; Jin, X.; Liu, Z.; Zhao, D.; Maurer, W. W.; Bates, F. S. *J. Poly. Sci. B* **1995**, *33*, 2289-2293.

(108) Lodge, T. P.; Hamersky, M. W.; Hanley, K. J.; Huang, C.-I. *Macromol.* **1997**, *30*, 6139-6149.

(109) Lodge, T. P.; Hanley, K. J.; Pudil, B.; Alahapperuma, V. *Macromol.* **2003**, *36*, 816-822.

(110) Banaszak, M.; Whitmore, M. D. *Macromol.* **1992**, *25*, 3406-3412.

(111) Lai, C.; Russel, W. B.; Register, R. A. *Macromol.* **2002**, *35*, 841-849.

(112) Hanley, K. J.; Lodge, T. B. *J. Poly. Sci. B* **1998**, *36*, 3101-3113.

(113) Hamley, I. W.; Fairclough, J. P. A.; Ryan, A. J.; Ryu, C. Y.; Lodge, T. B.; Gleeson, A. J.; Pederson, J. S. *Macromol.* **1998**, *31*, 1188-1196.

(114) Hanley, K. J.; Lodge, T. P.; Huange, C.-I. *Macromol.* **2000**, *33*, 5918-5931.

(115) Liu, Y.; Li, M.; Bansil, R.; Steinhart, M. *Macromol.* **2007**, *40*, 9482-9490.

(116) Li, M.; Liu, Y.; Nie, H.; Bansil, R.; Steinhart, M. *Macromol.* **2007**, *40*, 9491-9502.

(117) Holmqvist, P.; Fytas, G.; Pispas, S.; Hadjichristidis, N.; Saijo, K.; Tanaka, H.; Hashimoto, T. *Macromol.* **2004**, *37*, 4909-4916.

(118) Hashimoto, T.; Shibayama, M.; Kawai, H. *Macromol.* **1983**, *16*, 1093-1101.

(119) Shibayama, M.; Hashimoto, T.; Hasegawa, H.; Kawai, H. *Macromol.* **1983**, *16*, 1427-1433.

(120) Shibayama, M.; Hashimoto, T.; Kawai, H. *Macromol.* **1983**, *16*, 1434-1443.

(121) Whitmore, M. D.; Noolandi, J. *J. Chem. Phys.* **1990**, *93*, 2946-2955.

(122) Almdal, K.; J.H., R.; Bates, F. S.; Wignall, G. D.; Fredrickson, G. H. *Phys. Rev. Lett.* **1990**, *65*, 1112-1115.

(123) Lai, C.; Russel, W. B.; Register, R. A. *Macromol.* **2002**, *35*, 4044-4049.

(124) Alexandridis, P.; Olsson, U.; Lindman, B. *Langmuir* **1998**, *14*, 2627-2638.

(125) Huang, C.-I.; Hsu, Y.-C. *Phys. Rev. E* **2006**, *74*, 051802.

(126) Huang, C.-I.; Chiou, Y.-J.; Lan, Y.-K. *Polymer* **2007**, *48*, 877-886.

(127) Zin, W.-C.; Roe, R.-J. *Macromol.* **1984**, *17*, 183-188.

(128) Zin, W.-C.; Roe, R.-J. *Macromol.* **1980**, *17*, 183-188.

(129) Tanaka, H.; Hasegawa, H.; Hashimoto, T. *Macromol.* **1991**, *24*, 240-251.

(130) Hashimoto, T.; Tanaka, H.; Hasegawa, H. *Macromol.* **1990**, *23*, 4378-4386.

(131) Winey, K. I.; Thomas, E. L.; Fetters, L. J. *J. Chem. Phys.* **1991**, *95*, 9367-9375.

(132) Winey, K. I.; Thomas, E. L.; Fetters, L. J. *Macromol.* **1991**, *24*, 6182-6188.

(133) Winey, K. I.; Thomas, E. L.; Fetters, L. J. *Macromol.* **1992**, *25*, 2645-2650.

(134) Mayes, A. M.; Russell, T. P.; Satija, S. K.; Majkrzak, C. F. *Macromol.* **1992**, *25*, 6523-6531.

(135) Torikai, N.; Takabayashi, N.; Noda, I.; Koizumi, S.; Morii, Y.; Matsushita, T. *Macromol.* **1997**, *30*, 5698-5703.

(136) Banaszak, M.; Whitmore, M. D. *Macromol.* **1992**, *25*, 2757-2770.

(137) Urbas, A.; Sharp, R.; Fink, Y.; Thomas, E. L.; Xenidou, M.; Fetters, L. J. *Adv. Mater.* **2000**, *12*, 812-814.

(138) van Krevelen, D. W.; Hoftyzer, P. J. *Properties of Polymers: Their Estimation and Correlation Length With Chemical Structure*; 2nd ed. ed.; Elsevier Scientific Publishing Company: New York, NY, 1976.

(139) Zielinski, J. M.; Duda, J. L. *AIChE Journal* **1992**, *38*, 405-415.

(140) Rauch, J.; Koehler, W. *J. Chem. Phys.* **2003**, *119*, 11977-11988.

(141) Mori, K.; Hasegawa, H.; Hashimoto, T. *Polymer* **1990**, *31*, 2368-2376.

(142) Elbs, H.; Drummer, C.; Abetz, V.; Krausch, G. *Macromol.* **2002**, *35*, 5570-5577.

(143) Kim, G.; Libera, M. *Macromol.* **1998**, *31*, 2569-2577.

(144) Kim, G.; Libera, M. *Macromol.* **1998**, *31*, 2670-2672.

(145) Knoll, A.; Magerle, R.; Krausch, G. *J. Chem. Phys.* **2004**, *120*, 1105-1116.

(146) Horvat, A.; Knoll, A.; Krausch, G.; Tsarkova, L.; Lyakhova, K. S.; Sevink, G. J. A.; Zvelindovsky, A. V.; Magerle, R. *Macromol.* **2007**, *40*, 6930-6939.

(147) Cavicchi, K. A.; Berthiaume, K. J.; Russell, T. P. *Polymer* **2005**, *46*, 11635-11639.

(148) Ludwigs, S.; Schmidt, K.; Stafford, C. M.; Amis, E. J.; Fasolka, M. J.; Karim, A.; Magerle, R.; Krausch, G. *Macromol.* **2005**, *38*, 1850-1858.

(149) Sidorenko, A.; Tokarev, I.; Minko, S.; Stamm, M. *J. Am. Chem. Soc.* **2003**, *125*, 12211–12216.

(150) Tokarev, I.; Krenek, R.; Burkov, Y.; Schmeisser, D.; Sidorenko, A.; Minko, S.; Stamm, M. *Macromol.* **2005**, *38*, 507–516.

(151) Bosworth, J. K.; Paik, M. Y.; Ruiz, R.; Schwartz, E. L.; Huang, J. Q.; Ko, A. W.; Smilgies, D.-M.; Black, C. T.; Ober, C. K. *ACS Nano* **2008**, *2*, 1396-1402.

(152) Niu, S.; Saraf, R. F. *Macromol.* **2003**, *36*, 2428-2440.

(153) Kim, J. K.; Han, C. D. *Macromol.* **1992**, *25*, 271-285.

(154) Schmidt, S. C.; Hillmyer, M. A. *Macromol.* **1999**, *32*, 4794-4801.

(155) Zhang, Q.; Tsui, O. K. C.; Du, B.; Zhang, F.; Tang, T.; He, T. *Macromol.* **2000**, *33*, 9561-9567.

(156) Huang, H.; Zhang, F.; Hu, Z.; Du, B.; He, T.; Lee, F. K.; Wang, Y.; Tsui, O. K. C. *Macromol.* **2003**, *36*, 4084-4092.

(157) Xu, T.; Stevens, J.; Villa, J. A.; Goldbach, J. T.; Guarini, K. W.; Black, C. T.; Hawker, C. J.; Russell, T. P. *Adv. Funct. Mater.* **2003**, *13*, 698-702.

(158) Xu, T.; Goldbach, J. T.; Misner, M. J.; Kim, S. H.; Gibaud, A.; Gang, O.; Ocko, B.; Guarini, K. W.; Black, C. T.; Hawker, C. J.; Russell, T. P. *Macromol.* **2004**, *37*, 2972-2977.

(159) Park, S.; Kim, B.; Wang, J.-Y.; Russell, T. P. *Adv. Mater.* **2008**, *20*, 681-685.

(160) Wang, Y.; Hong, X.; Liu, B.; Ma, C.; Zhang, C. *Macromol.* **2008**, *41*, 5799-5808.

(161) Kim, S. H.; Misner, M. J.; Xu, T.; Kimura, M.; Russell, T. P. *Adv. Mater.* **2004**, *16*, 226-231.

(162) Ho, R.-M.; Tseng, W.-H.; Fan, H.-W.; Chiang, Y.-W.; Lin, C.-C.; Ko, B.-T.; Huang, B.-H. *Polymer* **2005**, *46*, 9362-9377.

(163) Lin, Y.-C.; Mueller, M.; Binder, K. *J. Chem. Phys.* **2004**, *121*, 3816-3828.

(164) Cavicchi, K. A.; Russell, T. P. *Macromol.* **2007**, *40*, 1181-1186.

(165) Park, C.; Yoon, J.; Thomas, E. *Polymer* **2003**, *44*, 6725-6760.

(166) Segalman, R. A. *Mater. Sci. and Eng. R* **2005**, *48*, 191-226.

(167) Stoykovich, M. P.; Nealey, P. F. *Materials Today* **2006**, *9*, 20-29.

(168) Li, M.; Ober, C. K. *Materials Today* **2006**, *9*, 30-39.

(169) Cheng, J. Y.; Ross, C. A.; Smith, H.; Thomas, E. L. *Adv. Mater.* **2006**, *18*, 2505-2521.

(170) Darling, S. B. *Prog. Polym. Sci.* **2007**, *32*, 1152-1204.

(171) Black, C. T. *App. Phys. Lett.* **2005**, *87*, 163116.

(172) Segalman, R. A.; Yokoyama, H.; Kramer, E. J. *Adv. Mater.* **2001**, *13*, 1152-1155.

(173) Segalman, R. A.; Hexemer, A.; Kramer, E. J. *Macromol.* **2003**, *36*, 6831-6839.

(174) Cheng, J. Y.; Ross, C. A.; Thomas, E. L.; Smith, H.; Vancso, G. J. *Adv. Mater.* **2003**, *15*, 1599-1602.

(175) Cheng, J.; Mayes, A. M.; Ross, C. *Nature Materials* **2004**, *3*, 823-828.

(176) Bita, I.; Yang, J. K. W.; Jung, Y. S.; Ross, C. A.; Thomas, E. L.; Berggren, K. K. *Science* **2008**, *321*, 939-943.

(177) Sundrani, D.; Darling, S. B.; Sibener, S. J. *Nano Letters* **2004**, *4*, 273–276.

(178) Sundrani, D.; Darling, S. B.; Sibener, S. J. *Langmuir* **2004**, *20*, 5091–5099.

(179) Black, C. T.; Bezencenet, O. *IEEE Trans. Nanotechnol.* **2004**, *3*, 412-415.

(180) Jung, Y. S.; Jung, W.; Ross, C. A. *Nano Letters* **1008**, *8*, 2975-2981.

(181) Jung, Y. S.; Ross, C. A. *Nano Letters* **2007**, *7*, 2046-2050.

(182) Harrison, C.; Chaikin, P. M.; Huse, D. A.; Register, R. A.; Adamson, D. H.; Daniel, A.; Huang, E.; Mansky, P.; Russell, T. P.; Hawker, C. J.; Egolf, D. A.; Melnikov, I. V.; Bodenschatz, E. *Macromol.* **2000**, *33*, 857-865.

(183) Yang, X.; Xiao, S.; Liu, C.; Pelhos, K.; Minor, K. *J. Vac. Sci. Technol. B* **2004**, *22*, 3331-3334.

(184) Xiao, S.; Yang, X.; Edwards, E.; La, Y.-H.; Nealey, P. *Nanotech.* **2005**, *16*, S324-S329.

(185) Kitano, H.; Akasaka, S.; Inoue, T.; Chen, F.; Takenaka, M.; Hasegawa, H.; Yoshida, H.; Nagano, H. *Langmuir* **2007**, *23*, 6404–6410.

(186) Chen, F.; Akasaka, S.; Inoue, T.; Takenaka, K.; Hasegawa, H.; Yoshida, H. *Macromol. Rapid Commun.* **2007**, *28*, 2137-2144.

(187) Black, C. T.; Ruiz, R. *Proc. of SPIE* **2006**, *6153*, 615302.

(188) Park, S.-M.; Stoykovich, M. P.; Ruiz, R.; Zhang, Y.; Black, C. T.; Nealey, P. F. *Adv. Mater.* **2007**, *19*, 607-611.

(189) Tada, Y.; Akasaka, S.; Yoshida, H.; Hasegawa, H.; Dobisz, E.; Kercher, D. S.; Takenaka, M. *Macromol.* **2008**, *41*, 9267-9276.

(190) Cheng, J. Y.; Rettner, C. T.; Sanders, D. P.; Kim, H.-C.; Hinsberg, W. D. *Adv. Mater.* **2008**, *20*, 3155-3158.

(191) Ruiz, R.; Kang, H.; Detcheverry, F. A.; Dobisz, E.; Kercher, D. S.; Albrecht, T. R.; de Pablo, J. J.; Nealey, P. F. *Science* **2008**, *321*, 936-939.

(192) Rockford, L.; Liu, P.; Mansky, P.; Russell, T. P.; Yoon, M.; Mochrie, S. G. J. *Phys. Rev. Lett.* **1999**, *82*, 2602-2605.

(193) Rockford, L.; Mochrie, S. G. J.; Russell, T. P. *Macromol.* **2001**, *34*, 1487-1492.

(194) Peters, R. D.; Yang, X. M.; Wang, Q.; de Pablo, J. J.; Nealey, P. F. *J. Vac. Sci. Technol. B* **2000**, *18*, 3530-3534.

(195) Kim, S. O.; Solak, H. H.; Stoykovich, M. P.; Ferrier, N. J.; de Pablo, J. J.; Nealey, P. F. *Nature* **2003**, *424*, 411-414.

(196) Stuen, K. O.; In, I.; Han, E.; Streifer, J. A.; Hamers, R. J.; Nealey, P. F.; Gopalan, P. *J. Vac. Sci. Technol. B.* **2007**, *25*, 1958.

(197) Edwards, E. W.; Mueller, M.; Stoykovich, M. P.; Solak, H. H.; de Pablo, J. J.; Nealey, P. F. *Macromol.* **2007**, *40*, 90-96.

(198) Stoykovich, M.; Mueller, M.; Kim, S.; Solak, H.; Edwards, E.; de Pablo, J.; Nealey, P. *Science* **2005**, *308*, 1442-1446.

(199) Park, S. M.; Ravindran, P.; La, Y.-H.; Craig, G. S. W.; Ferrier, N. J.; Nealey, P. F. *Langmuir* **2007**, *23*, 9037-9045.

(200) Ruiz, R.; Sandstrom, R. L.; Black, C. T. *Adv. Mater.* **2007**, *19*, 587-591.

(201) Kim, S. O.; Kim, B. H.; Meng, D.; Shin, D. O.; Chong, M. K.; Solak, H. H.; Wang, Q. W. *Adv. Mater.* **2007**, *19*, 3271-3275.

(202) Edwards, E. W.; Stoykovich, M. P.; Solak, H. H.; Nealey, P. F. *Macromol.* **2006**, *39*, 3598-3607.

(203) Park, S.-M.; Craig, G. S. W.; Liu, C.-C.; La, Y.-H.; Ferrier, N. J.; Nealey, P. F. *Macromol.* **2008**, *41*, 9118-9123.

(204) Park, S. M.; Craig, G. S. W.; La, Y.-H.; Solak, H. H.; Nealey, P. F. *Macromol.* **2007**, *40*, 5084.

(205) La, Y.-H.; Edwards, E. W.; Park, S. M.; Nealey, P. F. *Nano Letters* **2005**, *5*, 1379-1384.

(206) Park, S.-M.; Craig, G. S. W.; La, Y.-H.; Nealey, P. F. *Macromol.* **2008**, *41*, 9124-9129.

(207) Craig, G. S. W.; Nealey, P. F. *J. Vac. Sci. Technol. B* **2007**, *25*, 1969-1975.

(208) Stoykovich, M. P.; Kang, H.; Daoulas, K. C.; Liu, G.; Liu, C.-C.; de Pablo, J. J.; Mueller, M.; Nealey, P. F. *ACS Nano* **2007**, *1*, 168-175.

(209) Kang, H.; Craig, G. S. W.; Nealey, P. F. *J. Vac. Sci. Technol. B.* **2008**, *26*, 2495-2499.

(210) Amundson, K.; Helfland, E.; Davis, D. D.; Quan, X.; Patel, S. S.; Smith, S. D. *Macromol.* **1991**, *24*, 6546-6548.

(211) Amundson, K.; Helfand, E.; Quan, X.; Smith, S. D. *Macromol.* **1993**, *26*, 2698-2703.

(212) Amundson, K.; Helfand, E.; Quan, X.; Hudson, S. D.; Smith, S. D. *Macromol.* **1994**, *27*, 6559-6570.

(213) Boeker, A.; Elbs, H.; Haensel, H.; Knoll, A.; Ludwigs, S.; Zettl, H.; Zvelindovsky, A. V.; Sevink, G. J. A.; Urban, V.; Abetz, V.; Mueller, A. H. E.; Krausch, G. *Macromol.* **2003**, *36*, 8078-8087.

(214) Boeker, A.; Elbs, H.; Haensel, H.; Knoll, A.; Ludwigs, S.; Zettl, H.; Urban, V.; Abetz, C.; Mueller, A. H. E.; Krausch, G. *Phys. Rev. Lett.* **2002**, *89*, 135502.

(215) Schmidt, K.; Boeker, A.; Zettl, H.; Schubert, F.; Haensel, H.; Fischer, F.; Weiss, T. M.; Abetz, V.; Zvelindovsky, A. V.; Sevink, G. J. A.; Krausch, G. *Langmuir* **2005**, *21*, 11974-11980.

(216) Morkved, T. L.; Lu, M.; Urbas, A. M.; Ehrichs, E. E.; Jaeger, H. M.; Mansky, P.; Russell, T. P. *Science* **1996**, *273*, 931-933.

(217) Thurn-Albrecht, T.; DeRouchey, J.; Russell, T. P.; Jaeger, H. M. *Macromol.* **2000**, *33*, 3250-3253.

(218) Elhadj, S.; Woody, J.; Niu, V.; Saraf, R. *App. Phys. Lett.* **2003**, *82*, 871-873.

(219) Xu, T.; Zhu, Y.; Gido, S. P.; Russell, T. P. *Macromol.* **2004**, *37*, 2625–2629.

(220) Tsori, Y.; Andelman, D. *Macromol.* **2002**, *35*, 5161-5170.

(221) Xu, T.; Hawker, C. J.; Russell, T. P. *Macromol.* **2003**, *36*, 6178-6182.

(222) Wang, J.-W.; Xu, T.; Leiston-Belanger, J. M.; Gupta, S.; Russell, T. P. *Phys. Rev. Lett.* **2006**, *96*, 128301.

(223) Xu, T.; Goldbach, J. T.; Leiston-Belanger, J. M.; Russell, T. P. *Colloid Polym Sci* **2004**, *282*, 927-931.

(224) Schmidt, K.; Schoberth, H. G.; Schubert, F.; Haensel, H.; Fischer, F.; Weiss, T. M.; Sevink, G. J. A.; Zvelindovsky, A. V.; Boeker, A.; Krausch, G. *Soft Matter* **2007**, *3*, 448-453.

(225) Wiesner, U. *Macromol. Chem. Phys.* **1997**, *198*, 3319-3352.

(226) Chen, Z.-R.; Kornfield, J. A.; Smith, S. D.; Grothaus, J. T.; Satkowski, M. M. *Science* **1997**, *277*, 1248-1253.

(227) Leist, H.; Maring, D.; Thurn-Albrecht, T.; Wiesner, U. *J. Chem. Phys.* **1999**, *110*, 8225-8228.

(228) Langela, M.; Wiesner, U.; Spiess, H. W.; Wilhelm, M. *Macromol.* **2002**, *35*, 3198-3204.

(229) Lee, H. H.; Register, R. A.; Hajduk, D. A.; Gruner, S. M. *Polymer Engineering and Science* **1996**, *36*, 1414-1424.

(230) Albalak, R. J.; Thomas, E. L.; Capel, M. *Polymer* **1997**, *38*, 3819-3825.

(231) Albalak, R. J.; Capel, M. S.; Thomas, E. L. *Polymer* **1998**, *39*, 1647-1656.

(232) Villar, M. A.; Rueda, D. R.; Ania, F.; Thomas, E. L. *Polymer* **2002**, *43*, 5139-5145.

(233) Cohen, Y.; Albalak, R. J.; Dair, B. J.; Capel, M. S.; Thomas, E. L. *Macromol.* **2000**, *33*, 6502-6516.

(234) Sebastian, J. M.; Graessley, W. W.; Register, R. A. *J. Rheol.* **2002**, *46*, 863-879.

(235) Sebastian, J. M.; Lai, C.; Graessley, W. W.; Register, R. A.; Marchand, G. R. *Macromol.* **2002**, *35*, 2700-2706.

(236) Park, C.; Simmons, S.; Fetters, L. J.; Hsiao, B.; Yeh, F.; Thomas, E. L. *Polymer* **2000**, *41*, 2971-2977.

(237) Zvelindovsky, A. V.; Sevink, G. J. A. *Europhys. Lett.* **2003**, *62*, 370-376.

(238) Anglescu, D. E.; Waller, J. H.; Register, R. A.; Chaikin, P. M. *Adv. Mater.* **2005**, *17*, 1878-1881.

(239) Marencic, A. P.; Wu, M. W.; Register, R. A.; Chaikin, P. *Macromol.* **2007**, *40*, 7299-7305.

(240) Wu, M. W.; Register, R. A.; Chaikin, P. *Phys. Rev. E* **2006**, *74*, 040801 (R).

(241) Vedrine, J.; Hong, Y.-R.; Marencic, A. P.; Register, R. A.; Adamson, D. H.; Chaikin, P. *App. Phys. Lett.* **2007**, *91*, 143110.

(242) Angelescu, D. E.; Waller, J. H.; Adamson, D. H.; Deshpande, P.; Chou, S. Y.; Register, R. A.; Chaikin, P. M. *Adv. Mater.* **2004**, *16*, 1736-1740.

(243) Pelletier, V.; Adamson, D. H.; Register, R. A.; Chaikin, P. *App. Phys. Lett.* **2007**, *90*, 163105.

(244) Hashimoto, T.; Bodycomb, J.; Funaki, Y.; Kimishima, K. *Macromol.* **1999**, *32*, 952-954.

(245) Anglescu, D. E.; Waller, J. H.; Adamson, D. H.; Register, R. A. *Adv. Mater.* **2007**, *19*, 2687-2690.

(246) Mita, K.; Takenaka, M.; Hasegawa, H.; Hashimoto, T. *Macromol.* **2008**, *41*, 8789-8799.

(247) De Rosa, C.; Park, C.; Thomas, E. L.; Lotz, B. *Nature* **2000**, *405*, 433-437.

(248) Park, C.; De Rosa, C.; Thomas, E. L. *Macromol.* **2001**, *34*, 2602-2606.

(249) Tseng, W.-H.; Hsieh, P.-Y.; Ho, R.-M.; Huang, B.-H.; Lin, C.-C.; Lotz, B. *Macromol.* **2006**, *39*, 7071-7077.

(250) Ejima, H.; Itako, J. E.; Ishida, K.; Yoshie, N. *Macromol.* **2007**, *40*, 6445-6447.

(251) Park, C.; Cheng, J.; Fasolka, M.; Mayes, A. M.; Ross, C.; Thomas, E.; De Rosa, C. *App. Phys. Lett.* **2001**, *79*, 848-850.

(252) Deng, T.; Ha, Y.-H.; Cheng, J. Y.; Ross, C. A.; Thomas, E. L. *Langmuir* **2002**, *18*, 6719-6722.

(253) Fichet, G.; Stutzmann, N.; Muir, B. V. O.; Huck, W. T. S. *Adv. Mater.* **2002**, *14*, 47-51.

(254) Li, H.; Huck, W. *Nano Letters* **2004**, *4*, 1633-1636.

(255) Li, L.; Yokoyama, H. *Adv. Mater.* **2005**, *17*, 1432-1436.

(256) Hamley, I. W. *Nanotech.* **2003**, *14*, R39-R54.

(257) Li, M. Q.; Coenjarts, C. A.; Ober, C. K. *Adv. Polym. Sci.* **2005**, *190*, 183-226.

(258) Bockstaller, M. R.; Mickiewicz, R. A.; Thomas, E. L. *Adv. Mater.* **2005**, *17*, 1331-1349.

(259) Reichmanis, E.; Houlihan, F. M.; Nalamasu, O.; Neenan, T. X. *Chem. Mater.* **1991**, *3*, 394-407.

(260) Wallraff, G. M.; Hinsberg, W. D. *Chem Rev* **1999**, *99*, 1801-1821.

(261) Ito, H. *Adv. Polym. Sci.* **2005**, *172*, 37-245.

(262) Ito, H. *Proc. of SPIE* **2008**, *6923*, 692302.

(263) Mansky, P.; Harrison, C.; Chaikin, P. M.; Register, R. A.; Yao, N. *App. Phys. Lett.* **1996**, *68*, 2586-2588.

(264) Harrison, C.; Park, M.; Chaikin, P. M. *J. Vac. Sci. Technol. B.* **1998**, *16*, 544-552.

(265) Thurn-Albrecht, T.; Steiner, R.; DeRouchey, J.; Stafford, C. M.; Huang, E.; Bal, M.; Tuominen, M. T.; Hawker, C. J.; Russell, T. P. *Adv. Mater.* **2000**, *12*, 787-791.

(266) Liu, C.-C.; Nealey, P. F.; Ting, Y.-H.; Wendt, A. E. *J. Vac. Sci. Technol. B* **2007**, *25*, 1963-1968.

(267) Ting, Y.-H.; Park, S.-M.; Liu, C.-C.; Liu, X.; Himpsel, F. J.; Nealey, P. F.; Wendt, A. E. *J. Vac. Sci. Technol. B.* **2008**, *26*, 1684-1689.

(268) Yang, S. Y.; Ryu, I.; Kim, H. Y.; Kim, J. K.; Jang, S. K.; Russell, T. P. *Adv. Mater.* **2006**, *18*, 709-712.

(269) Kim, D. H.; Lau, K. H. A.; Robertson, J. W. F.; Lee, O.-J.; Jeong, U.; Lee, J. I.; Hawker, C. J.; Russell, T. P.; Kim, J. K.; Knoll, W. *Adv. Mater.* **2005**, *17*, 2442-2446.

(270) Zalusky, A. S.; Olayo-Valles, R.; Taylor, C. J.; Hillmyer, M. A. *J. Am. Chem. Soc.* **2001**, *123*, 1519-1520.

(271) Zhang, M.; Yang, L.; Yurt, S.; Misner, M. J.; Chen, J.-T.; Coughlin, E. B.; Venkataraman, D.; Russell, T. P. *Adv. Mater.* **2007**, *19*, 1571-1576.

(272) Fahmi, A.; Stamm, M. *Langmuir* **2005**, *21*, 1062-1066.

(273) Laforgue, A.; Bazuin, C. G.; Prud'homme, R. E. *Macromol.* **2006**, *39*, 6473-6482.

(274) Avgeropoulos, A.; Chan, V. Z.-H.; Lee, V. Y.; Ngo, D.; Miller, R. D.; Hadjichristidis, N.; Thomas, E. L. *Chem. Mater.* **1998**, *10*, 2109-2115.

(275) Chan, V. Z.-H.; Hoffman, J.; Lee, V. Y.; Iatrou, H.; Avgeropoulos, A.; Hadjichristidis, N.; Miller, R. D.; Thomas, E. L. *Science* **1999**, *286*, 1716-1719.

(276) Lammertink, R. G. H.; Hempenius, M. A.; van den Enk, J. E.; Chan, V. Z.-H.; Thomas, E. L.; Vancso, G. J. *Adv. Mater.* **2000**, *12*, 98-103.

(277) Temple, K.; Kulbaba, K.; Power-Billard, K. N.; Manners, I.; Leach, K. A.; Xu, T.; Russell, T. P.; Hawker, C. J. *Adv. Mater.* **2003**, *15*, 297-300.

(278) Rider, D. A.; Cavicchi, K. A.; Power-Billard, K. N.; Russell, T. P.; Manners, I. *Macromol.* **2005**, *38*, 6931-6938.

(279) Eloi, J.-C.; Rider, D. A.; Wang, C.; Russell, T. P.; Manners, I. *Macromol.* **2008**, *41*, 9474-9479.

(280) Kessler, D.; Theato, P. *Macromol.* **2008**, *41*, 5237-5244.

(281) Cheng, J. Y.; Ruiz, R.; Black, C. T.; Kim, H.-C. *App. Phys. Lett.* **2007**, *91*, 143106.

(282) Park, O.-H.; Cheng, J. Y.; Kim, H. S.; Rice, P. M.; Topuria, T.; Miller, R. D.; Kim, H.-C. *App. Phys. Lett.* **2007**, *90*, 233102.

(283) Kim, D. H.; Sun, Z.; Russell, T. P.; Knoll, W.; Gutmann, J. S. *Adv. Funct. Mater.* **2005**, *15*, 1160-1164.

(284) Park, M.; Harrison, C.; Chaikin, P. M.; Register, R. A.; Adamson, D. H. *Science* **1997**, *276*, 1401-1404.

(285) Lammertink, R. G. H.; Hempenius, M. A.; Chan, V. Z.-H.; Thomas, E. L.; Vancso, G. J. *Chem. Mater.* **2001**, *13*, 429-434.

(286) Black, C. T.; Guarini, K. W.; Milkove, K. R.; Baker, S. M.; Russell, T. P.; Tuominen, M. *Applied Physics Letters* **2001**, *79*, 409-411.

(287) Black, C. T.; Guarini, K. W.; Breyta, G.; Colburn, M. C.; Ruiz, R.; Sandstrom, R. L.; Sikorski, E. M.; Zhang, Y. *J. Vac. Sci. Technol. B.* **2006**, *24*, 3188-3191.

(288) Gowrishankar, V.; Miller, N.; McGehee, M. D.; Misner, M. J.; Ryu, D. Y.; Russell, T. P.; Drockenmuller, E.; Hawker, C. J. *Thin Solid Films* **2006**, *513*, 289-294.

(289) Cheng, J. Y.; Ross, C. A.; Chan, V. Z.-H.; Thomas, E. L.; Lammertink, R. G. H.; Vancso, G. J. *Adv. Mater.* **2001**, *13*, 1174-1178.

(290) Lu, J.; Chamberlin, D.; Rider, D. A.; Liu, M.; Manners, I.; Russell, T. P. *Nanotech.* **2006**, *17*, 5792-5797.

(291) Lee, D. H.; Shin, D. O.; Lee, W. J.; Kim, S. O. *Adv. Mater.* **2008**, *20*, 2480-2485.

(292) Ross, C. A.; Jung, Y. S.; Chuang, V. P.; Ilievski, F.; Yang, J. K. W.; Bita, I.; Thomas, E. L.; Smith, H. I.; Berggren, K. K.; Vancso, G. J.; Cheng, J. Y. *J. Vac. Sci. Technol. B.* **2008**, *26*, 2489-2494.

(293) Li, R. R.; Dapkus, P. D.; Thompson, M. E.; Jeong, W. G.; Harrison, C.; Chaikin, P. M.; Register, R. A.; Adamson, D. H. *App. Phys. Lett.* **2000**, *76*, 1689-1691.

(294) Park, J. H.; Khandekar, A. A.; Park, S. M.; Mawst, L. J.; Kuech, T. F.; Nealey, P. F. *J. Cryst. Growth* **2006**, *297*, 283-288.

(295) Thurn-Albrecht, T.; Schotter, J.; Kaestle, G. A.; Emley, N.; Shibauchi, T.; Krusin-Elbaum, L.; Guarini, K.; Black, C. T.; Tuominen, M. T.; Russell, T. P. *Science* **2000**, *290*, 2126-2129.

(296) Bal, M.; Ursache, A.; Tuominen, M. T.; Goldbach, J. T.; Russell, T. P. *App. Phys. Lett.* **2002**, *81*, 3479.

(297) Guarini, K.; Black, C. T.; Milkove, K. R.; Sandstrom, R. L. *J. Vac. Sci. Technol. B* **2001**, *19*, 2784-2788.

(298) Shin, K.; Leach, K. A.; Goldbach, J. T.; Kim, D. H.; Jho, J. Y.; Tuominen, M.; Hawker, C. J.; Russell, T. P. *Nano Letters* **2002**, *2*, 933-936.

(299) Xiao, S.; Yang, X. M.; Edwards, E. W.; La, Y.-H.; Nealey, P. F. *Nanotech.* **2005**, *16*, S324-S329.

(300) Kim, H.-C.; Jia, X.; Stafford, C. M.; Kim, D. H.; McCarthy, T. J.; Thominen, M.; Hawker, C. J.; Russell, T. P. *Adv. Mater.* **2001**, *13*, 795-797.

(301) Misner, M. J.; Skaff, H.; Emrick, T.; Russell, T. P. *Adv. Mater.* **2003**, *15*, 221-224.

(302) Zhang, Q.; Xu, T.; Butterfield, D.; Misner, M. J.; Ryu, D. Y.; Emrick, T.; Russell, T. P. *Nano Letters* **2005**, *5*, 357-361.

(303) Kim, D. H.; Lin, Z.; Kim, H.-C.; Jeong, U.; Russell, T. P. *Adv. Mater.* **2003**, *15*, 811-814.

(304) Seifarth, O.; Schmeisser, D.; Krenek, R.; Sidorenko, A.; Stamm, M. *Progress in Solid State Chemistry* **2006**, *34*, 111-119.

(305) Seifarth, O.; Krenek, R.; Tokarev, I.; Burkov, Y.; Sidorenko, A.; Minko, S.; Stamm, M.; Schmeisser, D. *Thin Solid Films* **2007**, *515*, 6552-6556.

(306) Lee, J. I.; Cho, S. H.; Park, S.-M.; Kim, J. K.; Kim, J. K.; Yu, J.-W.; Kim, Y. C.; Russell, T. P. *Nano Letters* **2008**, *8*, 2315-2320.

(307) Zehner, R. W.; Sita, L. R. *Langmuir* **1999**, *15*, 6139-6141.

(308) Chai, J.; Wang, D.; Fan, X.; Buriak, J. M. *Nature Nanotech.* **2007**, *2*, 500-506.

(309) Chai, J.; Buriak, J. M. *ACS Nano* **2008**, *2*, 489-501.

(310) Kim, D. H.; Kim, S. H.; Lavery, K.; Russell, T. P. *Nano Letters* **2004**, *4*, 1841-1844.

(311) Pai, R. A.; Humayun, R.; Schulberg, M. T.; Sengupta, A.; Sun, J.-N.; Watkins, J. J. *Science* **2004**, *303*, 507-510.

(312) Nagarajan, S.; Bosworth, J. K.; Ober, C. K.; Russell, T. P.; Watkins, J. J. *Chem. Mater.* **2008**, *20*, 604-606.

(313) Hayward, R. C.; Chmelka, B. F.; Kramer, E. J. *Adv. Mater.* **2005**, *17*, 2591-2595.

(314) Bal, M.; Ursache, A.; Tuominen, M.; Goldbach, J. T.; Russell, T. P. *App. Phys. Lett.* **2002**, *81*, 3479-3481.

(315) Spatz, J. P.; Chan, V. Z.-H.; Moessmer, S.; Kamm, F.-M.; Plettl, A.; Zeimann, P.; Moeller, M. *Adv. Mater.* **2002**, *14*, 1827-1832.

(316) Glass, R.; Arnold, M.; Bluemmel, J.; Kueller, A.; Moeller, M.; Spatz, J. P. *Adv. Funct. Mater.* **2003**, *13*, 569-575.

(317) Li, M.; Douki, K.; Goto, K.; Li, X.; Coenjarts, C.; Smilgies, D.-M.; Ober, C. K. *Chem. Mater.* **2004**, *16*, 3800-3808.

(318) Bosworth, J. K.; Black, C. T.; Ober, C. K. *In preparation*.

(319) Vasilopoulou, M.; Boyatzis, S.; Raptis, I.; Dimotikalli, D.; Argitis, P. *J. Mater. Chem.* **2004**, *14*, 3312-3320.

(320) Yang, S.; Ford, J.; Ruengruglikit, C.; Huang, Q.; Aizenberg, J. *J Mater Chem* **2005**, *15*, 4200-4202.

(321) Bosworth, J. K.; Chavis, M. A.; Wang, D. L.; Paik, M. Y.; Schwartz, E. L.; Ober, C. K. *In preparation*.

(322) La, Y.-H.; In, I.; Park, S.-M.; Meagley, R. P.; Leolukman, M.; Gopalan, P.; Nealey, P. F. *J. Vac. Sci. Technol. B* **2007**, *25*, 2508-2513.

(323) Hwang, H. S.; Zakhidov, A. A.; Lee, J. K.; Andre, X.; DeFranco, J. A.; Fong, H. H.; Holmes, A. B.; Malliaras, G. G.; Ober, C. K. *J. Mater. Chem.* **2008**, *18*, 3087-3090.

(324) Lee, J. K.; Chatzichristidi, M.; Zakhidov, A. A.; Taylor, P. G.; DeFranco, J. A.; Hwang, H. S.; Fong, H. H.; Holmes, A. B.; Malliaras, G. G.; Ober, C. K. *J. Am. Chem. Soc.* **2008**, *130*, 11564-11565.

(325) Zakhidov, A. A.; Lee, J. K.; Fong, H. H.; DeFranco, J. A.; Chatzichristidi, M.; Taylor, P. G.; Ober, C. K. *Adv. Mater.* **2008**, *20*, 3481–3484.

CHAPTER 2

CONTROL OF SELF ASSEMBLY OF LITHOGRAPHICALLY-PATTERNABLE BLOCK COPOLYMER FILMS

Joan K. Bosworth,[1,2] Marvin Y. Paik,[2] Ricardo Ruiz[3,†], Evan L. Schwartz,[2] Jenny Q. Huang,[2] Albert W. Ko,[2] Detlef-M. Smilgies,[4] Charles T. Black[2,††], and Christopher K. Ober[2]

1. Department of Chemistry & Chemical Biology, Cornell University, Ithaca, NY 14853

2. Department of Materials Science and Engineering, Cornell University, Ithaca, NY, 14850

3. IBM T. J. Watson Research Center, Yorktown Heights, NY, 10598

4. Cornell High Energy Synchrotron Source, Cornell University, Ithaca, NY, 14853

† Present address: Hitachi Global Storage Technologies, San Jose, CA, 95135

†† Present address: Center for Functional Nanomaterials, Brookhaven National Laboratory, Upton, New York, 11973

Reprinted with permission from *ACS Nano* **2008**, *2*, 1396-1402.

2.1 Abstract

Poly(α-methylstyrene)-*block*-poly(4-hydroxystyrene) acts as both a lithographic deep UV photoresist and a self-assembling material, making it ideal for patterning simultaneously by both top-down and bottom-up fabrication methods. Solvent vapor annealing improves the quality of the self-assembled patterns in this material without compromising its ability to function as a photoresist. The choice of solvent used for annealing allows for control of the self-assembled pattern morphology. Annealing in a nonselective solvent (tetrahydrofuran) results in parallel orientation of cylindrical domains, while a selective solvent (acetone) leads to formation of a trapped spherical morphology. Finally, we have self-assembled both cylindrical and spherical phases within lithographically patterned features, demonstrating the ability to precisely control ordering. Observing the time evolution of switching from cylindrical to spherical morphology within these features provides clues to the mechanism of ordering by selective solvent.

2.2 Introduction

Patterning the nanometer-scale dimensions of microelectronic integrated circuit (IC) elements continues to be a major technological barrier to realizing performance improvements.[1] One proposed pathway to achieving patterning objectives for future IC generations involves designing increased functionality into the polymeric resist patterning materials. For example, a single resist material that is patternable by both conventional deep UV lithography (*i.e.* a top-down method) as well as self assembly techniques (*i.e.* bottom-up methods) provides a vehicle for efficiently implementing both approaches within the technology infrastructure of advanced lithographic patterning.

The diblock copolymer poly(α-methylstyrene)-*block*-poly(4-hydroxystyrene) (PαMS-*b*-PHOST) is a distinctive material because it is patternable by both deep UV lithography and self assembly techniques.[2, 3] This, along with the selective removal of the PαMS minor phase, allows for very precise location of the self-assembled block copolymer pattern that can be used for further patterning applications, especially when coupled with the selective removal of the PαMS minor phase. However, controlling the microphase separation, demonstrated in this work, is key for device applications. PαMS-*b*-PHOST with overall molecular weight 21 kg/mol (M_w/M_n 1.10) and mass fraction of PαMS 33% forms disordered, though perpendicularly oriented, cylindrical domains upon spin casting from a solvent of propylene glycol methyl ether acetate (PGMEA) (Figure 2.1a), regardless of substrate, and for a wide range of film thicknesses. The observed behavior is consistent with reports that a solvent evaporation gradient across the polymer film can promote a perpendicular domain orientation with little hexagonal ordering.[4] For PαMS-*b*-PHOST it is not possible to improve the quality of the self assembly process via a thermal treatment due to the low ceiling temperature[5] and corresponding low decomposition temperature of PαMS, though it is this behavior that allows the selective removal of the PαMS block. We observe thermal degradation of PαMS at a temperature of 150˚C, while we measure the PHOST glass transition temperature of 180-190˚C by differential scanning calorimetry.

Alternatively, solvent annealing has been shown to improve the spatial coherence of patterns in other polymer systems.[6-10] This occurs because the solvent imparts increased polymer chain mobility by acting as a plasticizer, thus effectively lowering the glass transition temperature, T_g, and increasing the mobility of the polymer chains.[11] Additionally, the selectivity of the solvent for the two block allows

further control of the morphology formed by the polymer upon swelling and locked in upon rapid evaporation.

Further control of morphology location is necessary for patterning applications. Additional techniques can be in conjunction with polymer mobility techniques (either thermal or solvent annealing) in order to gain further control of morphology, including electric fields,[12-14] shear,[15-17] chemically-patterned substrates,[18, 19] and graphoepitaxy.[8, 20-23] Graphoepitaxy, or self-aligned self assembly, is particularly interesting because the polymer morphology can subdivide a much larger feature created by traditional photolithographic techniques.

2.3 Methods

2.3.1 Synthesis.

Poly(α-methyl styrene)-*block*-poly(*tert*-butoxystyrene), PαMS-*b*-PtBuOS, was synthesized via sequential anionic polymerization and subsequently deprotected to form PαMS-*b*-PHOST, as described elsewhere.[2] GPC indicates a total number average molecular weight for PαMS-*b*-PtBuOS of 28 kg/mol, 25% by mass PαMS, and with M_w/M_n 1.10. Thus, deprotected PαMS-*b*-PHOST has M_n of 21 kg/mol, 33% PαMS. Complete deprotection was confirmed by FTIR. Polystyrene for surface treatment was synthesized via nitroxide mediated controlled free radical polymerization using TEMPO (2,2,6,6-Tetramethylpiperidine 1-oxyl, Aldrich) and benzoyl peroxide (Aldrich) under nitrogen without hydroxyl termination.[34] While hydroxyl-terminated brushes for surface treatment were found to work even better than non-functionalized PS, the non-functionalized PS was sufficient grafting to the substrate for this purpose. The resulting polymer samples have M_n 12.7 kg/mol and M_w/M_n 1.30 according to GPC.

2.3.2 Film Preparation.

Solutions of 1% and 5% (w/v) PαMS-*b*-PHOST in PGMEA (Aldrich) were spin-coated onto silicon wafers with native oxide or onto silicon oxide substrates with 30 nm deep patterns prepared by lithography and etching techniques. Brush treatment consists of a 1% (w/v) solution of polystyrene spin-coated and baked at 195˚C for 2.5 hours. Immediately before spin coating with PαMS-*b*-PHOST, excess PS was removed by rinsing with toluene. Solvent vapor treatment with THF or acetone was carried out in a closed jar containing a solvent reservoir. Times for solvent annealing leading to the most ordered films were determined for each solvent and for both thick and thin film thicknesses. Films annealed in THF require partial development for both AFM and SEM imaging; this is achieved by treatment with an oxygen plasma etch, for 9 seconds at 50 watts, 100 mTorr, and 30 sccm oxygen using a PlasmaTherm 72 reactive ion etcher. For imaging as-spun and acetone-annealed films by SEM, partial removal of the PαMS block is achieved by heating in a vacuum oven at 165˚C for 30 minutes is sufficient, though the brief oxygen plasma etch is also sufficient; for these films no special treatment is required for AFM imaging.

The photoacid generator triphenyl sulfonium triflate (TPST, Aldrich), and the crosslinker tetramethoxymethyl glycoluril (TMMGU, "Powderlink 1174," Cytec Industries) were added to the 5% polymer solution in amounts of 5% or less (w/w) relative to the polymer. Films were spin-coated and solvent-annealed, and exposures made through a quartz mask using a Hybrid Technology Group system III-HR contact mask aligner with deep UV exposure. A post expose bake of 115˚C

2.3.3 Characterization.

GPC of THF solutions of polymers (1 mg/mL) was carried out using four Waters Styragel HT columns operating at 40 ˚C and Waters 490 ultraviolet (254 nm

wavelength) and Waters 410 refractive index detectors. Scanning electron microscopy is performed on a LEO 1550 FE-SEM, and atomic force microscopy is performed on a Veeco Dimension 3100. Differential scanning calorimetry was performed on a TA Instruments Q1000. Ellipsometry was performed on a Woollam M-2000, and profilometry was performed on scored films using a Tencor P-10 Surface Profiler. The grazing incidence small angle x-ray scattering (GISAXS) image in this paper was taken at the G1 line at the Cornell High Energy Synchrotron Source (CHESS). Additional GISAXS has been performed at the D1 beamline at CHESS and at beamline 8-ID-E of the Advanced Photon Source.

2.4 Results & Discussion

2.4.1 Solvent Swelling Imparts Mobility and Morphology Control.

Because of the difficulties associated with thermal treatments, we have instead used solvent vapor annealing to promote uniform self assembly of PαMS-*b*-PHOST thin films. We observe parallel cylinder domain orientation when polymer chains gain mobility due to swelling in tetrahydrofuran (THF) (Figure 2.1b), a good solvent for both polymer blocks.[24] In this case, preferential surface wetting by the PHOST block drives parallel domain orientation. We measure the cylinder center-to-center distance of 22 nm by atomic force microscopy (AFM) and film thickness of 16 nm by ellipsometry and 14 nm by profilometry; the same annealing behavior is observed for thicker films (127 nm by profilometry) as well. In the case of PαMS-*b*-PHOST annealed in THF, sufficient contrast for AFM imaging is achieved by a brief exposure to a gentle oxygen plasma to remove the top few nm of film; no treatment is necessary for as-spun and acetone-annealed films.[25] The presence of a top uniform polymer surface layer indicates a preferential block affinity for the polymer-air interface.

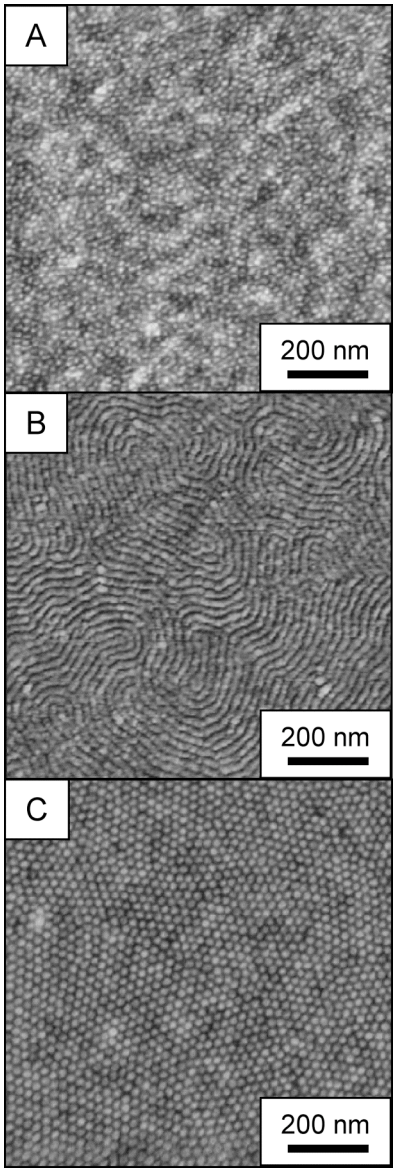

Figure 2.1. Atomic force height micrographs of PαMS-*b*-PHOST films with 16nm thickness. (a) As cast, perpendicularly oriented cylindrical phase. (b) Parallel-oriented cylinders after annealing in THF. (c) Hexagonally packed dot pattern after acetone anneal. In AFM, PαMS appears as the lighter color.

A unique advantage of solvent annealing over thermal treatments is the ability to control block copolymer domain morphology through choice of solvent. Annealing in acetone causes the diblock copolymer film to assemble into a hexagonal array of dots (Figure 2.1c), with improved order as compared to the as-deposited films (Figure 2.1a). These top-down images are consistent with either perpendicularly-oriented cylindrical domains or a spherical morphology. Acetone is not a good solvent for PαMS,[24] though we have found it to be a good solvent for the PHOST homopolymer. Thus, we expect acetone to preferentially swell the PHOST block, inducing an order-order transition from cylindrical to spherical morphology in the swollen state, which may be kinetically trapped in the dried state. It is difficult to distinguish a perpendicular cylinder morphology from a spherical phase in film thicknesses equal to or less than a single morphology period. Thicker films (127 nm) that have been annealed in acetone also display the same ordered arrays of dots in AFM images of the top surface (Figure 2.2a).

2.4.2 Selective Solvent Anneal Yields Spherical Morphology

Grazing incidence small angle X-ray scattering (GISAXS) is a probe well-suited for studying the polymer film interior, used here to determine the interior structure of the dried films after annealing in acetone. The GISAXS image in Figure 2.2b prominently features a sharp Bragg reflection at non-zero wavevector (parallel component $q_{||} = 0.0279$ Å^{-1}, perpendicular component $q_z = 0.0595$ Å^{-1}) indicative of three-dimensional organization inside the film. Additionally, there are two peaks in the Yoneda band between the critical angles of the substrate and film, whose $q_{||}$ values of 0.0327 Å^{-1} and 0.0455 Å^{-1} differ from the first reflection. Moreover, the image does not show the familiar diffuse Bragg rods characteristic of perpendicular cylinders,[2, 3, 26, 27] and thus we conclude that the film does not possess that morphology.

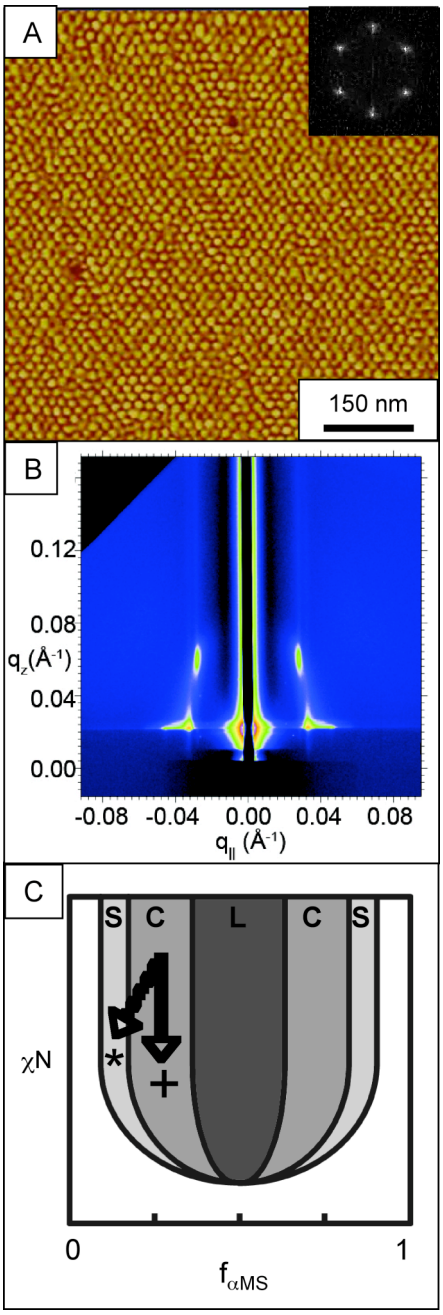

Figure 2.2. (a) AFM phase image of thick PαMS-*b*-PHOST film after annealing in acetone vapor. (b) Corresponding GISAXS image, demonstrating a face-centered orthorhombic (fco) lattice in the dried state. (c) Schematic phase diagram of χN vs. $f_{\alpha MS}$. The solid arrow represents behavior of THF solvent annealing, while the dotted arrow represents acetone annealing. The effective χN parameter of the blocks is modified by the solvent uptake during swelling in both solvents (vertical component of lines). Acetone annealing swells the PHOST block selectively, and thus also shifts the volume ratio $f_{\alpha MS}$, while THF swells both blocks equally.

We expect a (110) oriented body centered cubic (bcc), rather than a hexagonally close-packed lattice of spheres, in the swollen state of these multilayer polymer film samples comprising several layers of spheres.[28] Our data indicates that the rapid evaporation of the solvent from the film upon removal from the chamber kinetically traps the spherical morphology, and the deswelling affects the spacing of the spheres in the direction perpendicular to the surface, resulting in a distorted bcc lattice.

A bcc lattice with the (110) plane parallel to the substrate was used in a first attempt to model the observed peak positions. From the lateral peaks in the Yoneda band we calculate a lattice parameter of 27.5 nm, which corresponds to a spacing of spheres on the top (surface) plane of 24 nm, in reasonable accordance with AFM measurements. However, the observed q_z value of the 3D Bragg reflection suggests film shrinkage in the z-direction. Redefining the (110) oriented bcc lattice to a face-centered orthorhombic (fco) surface lattice allows modeling of the distorted system, while maintaining the highest possible lattice symmetry. The resulting theoretical peak positions agree well with the GISAXS measurements – clear evidence that the film transitioned to a bcc spherical morphology in the swollen state, which was then kinetically trapped and deformed in the vertical direction to an fco spherical morphology upon drying. In the dried state the fco lattice constant perpendicular to the substrate is found to be 16.5 nm, indicating that it has been reduced to 42 % of the original value (38.9 nm) in the bcc phase of the swollen film. Further explanation of the analysis of this data may be found in the supporting information (section 2.6).

The effects of solvent annealing can be visualized in a hypothetical χN vs. $f_{P\alpha MS}$ phase diagram, where χ is the Flory-Huggins interaction parameter, N is the degree of polymerization, and $f_{P\alpha MS}$ is the volume fraction of PαMS in the block copolymer (Figure 2.2c).[9, 10] A good solvent for both copolymer blocks (such as THF)

is uniformly incorporated by the polymer film and imparts chain mobility by acting as a plasticizer. Such behavior is comparable to a downward vertical shift in χN as $f_{P\alpha MS}$ remains constant. Acetone annealing involves the additional variable of preferential solubility PHOST (over PαMS) in the solvent. An affinity of the solvent for one block changes the volume ratio of the two copolymer blocks comprising the film, such that swelling in a selective solvent changes not just the vertical position in the χN vs. $f_{P\alpha MS}$ phase diagram, but the horizontal position as well. In this case, the majority component (PHOST) swells more, causing an order-order transition from cylindrical to spherical morphology as the increased PHOST volume changes the diblock copolymer volume fraction of the swollen state so that it assumes the bcc-packed structure. This state remains trapped in the spherical morphology upon rapid drying, though it changes to an fco lattice when the film shrinks. Previous experiments on other block copolymer systems have reported the collapse of spherical morphology to a perpendicularly-oriented cylindrical phase upon evaporation of a selective solvent[8-10] in contrast to our observations of PαMS-*b*-PHOST via GISAXS. This unidirectional contraction of a bcc lattice into an fco lattice has been observed elsewhere in the case of a Pluronics surfactant upon evaporation of water vapor.[29]

2.4.3 Effect of Solvent on Photoresist Behavior.

The photoresist properties of PαMS-*b*-PHOST do not alter or interfere with the self assembly of PαMS-*b*-PHOST polymer films in solvent vapor. The photoacid generator triphenylsulfonium trifluoromethanesulfonate (TPST) and the crosslinker tetramethoxymethyl glycolunil (TMMGU), in quantities 5% w/w or less, are both necessary for the PαMS-*b*-PHOST to function as a resist.[2] These small quantities have no discernable affect on ordering via solvent annealing, as long as the film is not exposed to solvent vapor (Figure 2.3a). The photopatterns were exposed in both as-

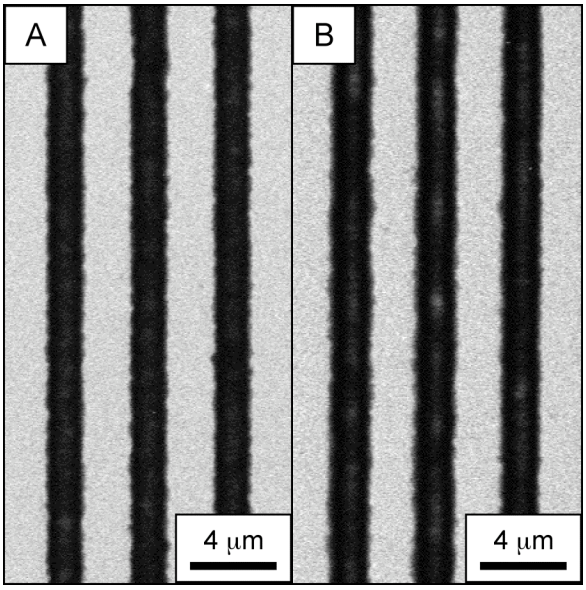

Figure 2.3. Scanning electron micrograph of photolithographic patterns of PαMS-*b*-PHOST. Films containing TPST photoacid generator and TMMGU crosslinker were exposed (a) as spun, and (b) after THF solvent annealing. Dark regions are lines of crosslinked polymer left behind after post-exposure bake and development in solvent.

spun and THF-annealed PαMS-*b*-PHOST films using 248 nm light, a post exposure bake of 115˚C for 60 seconds (insufficient time for significant PαMS damage), and mixed solvent development with cyclohexanone and isopropanol (1:2 v/v), and the pattern resolution is nearly identical. PαMS-*b*-PHOST films annealed in acetone (not shown) have similar lithographic resolution. This indicates that the photoacid generator and crosslinker do not selectively partition into the PαMS phase in either of the solvent annealed films, just as they do not in the as-spun films.

2.4.4 Graphoepitaxy.

High-resolution lithography applications of self-assembled diblock copolymer films would ultimately require both polymer domain registration and ordering, and we have demonstrated registration of PαMS-*b*-PHOST films to topographic features by solvent annealing. For our experiments we prepared 30 nm deep topographic features in silicon dioxide (SiO_2) using conventional deep UV lithography and plasma etching techniques.[30] We pretreat the patterned SiO_2 substrates with a PS brush prior to PαMS-*b*-PHOST deposition in order to achieve preferential wetting by the PαMS minority block,[31, 32] as the minority block must preferentially wet the substrate in order to avoid pinning effects.[33] The same solution and spin speed that formed 16nm thick films on flat substrates were used here. We observe registration of parallel-oriented cylinder domains upon annealing in THF (Figure 2.4a), while films deposited on untreated silicon oxide do not self-align to the patterned substrate upon THF annealing (Figure 2.4b). Sufficient contrast for SEM imaging is achieved by partial development of PαMS for SEM imaging; in the case of THF-annealed films, films are briefly exposed to a gentle oxygen plasma,[25] while acetone-annealed films need only to be heated briefly. Cross-sectional SEM revealed film thicknesses of 20 nm within trenches, consistent with a single-morphology thickness. We have achieved defect-free

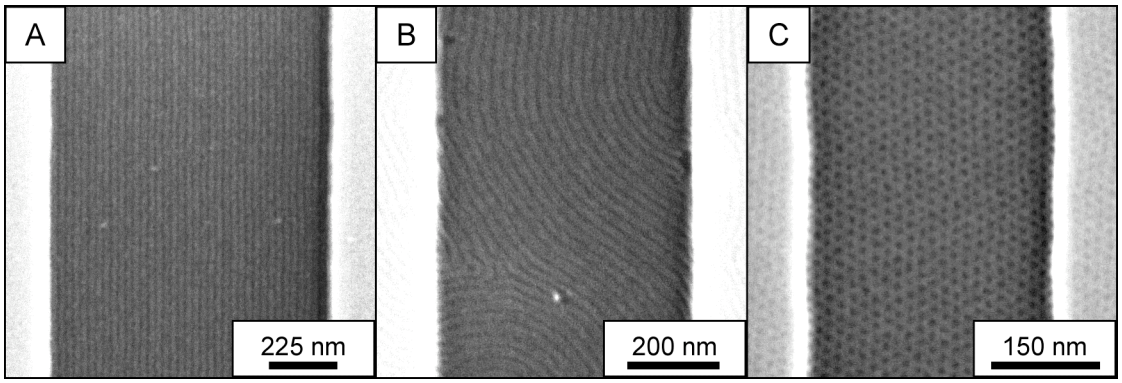

Figure 2.4. Self aligned PαMS -*b*-PHOST patterns on lithographically patterned substrates. (a) On PS brush-treated substrates, annealing in THF leads to self-aligned parallel cylinder domains. (b) On SiO2 substrate without PS brush treatment, annealing in THF does not lead to pattern registration. (c) On SiO2 substrates without PS brush treatment, annealing in acetone leads to aligned hexagonal dot pattern. In SEM images, darker regions are the PαMS phase.

domain alignment of parallel cylinders with 23 nm pitch across trench widths of 840 nm. As the figure shows, the 37 cylindrical domains run distances of over 2 μm without defects.

Solvent annealing PαMS-*b*-PHOST in acetone rather than THF results in aligned hexagonal arrays of dots (Figure 2.4c). We observe this alignment regardless of substrate treatment, *i.e.* for both native SiO_2 (PHOST preferential surface) and for PS-treated (PαMS preferential) substrates. Figure 2.4c shows registration of self-assembled patterns to a lithographically-patterned (and untreated) SiO_2 trench after acetone annealing, and we have observed similar results for patterned substrates treated with PS brushes. We measure the sphere center-to-center spacing to be 23 nm via SEM.

Sequential annealing of aligned PαMS -*b*-PHOST films first in non-preferential (THF) and then preferential (acetone) solvents allows us to switch from parallel cylinder to spherical morphology, a useful experimental lever for observing the process by which the transition takes place. We have observed by SEM the time evolution of the order-order transition to spherical morphology by acetone annealing an aligned film with parallel cylinder orientation. The initial sample contains oriented parallel cylinder domains spanning a 175 nm wide trench treated with a PS brush (Figure 2.5a). At intermediate anneal times during the transition, we observe mixed morphology of lines and dots, further supporting that an order-order transition from, in this case, parallel cylindrical to spherical morphology, occurs in the swollen film. After 3 hours of acetone annealing, independent spheres have begun to form within the trench-aligned pattern (Figure 2.5b). Note that in the thinner film areas outside the lithographic trench, complete morphology changes are already completed. After 3.5 hours of annealing, patches of spheres disrupt the parallel cylinders (Figure 2.5c), and

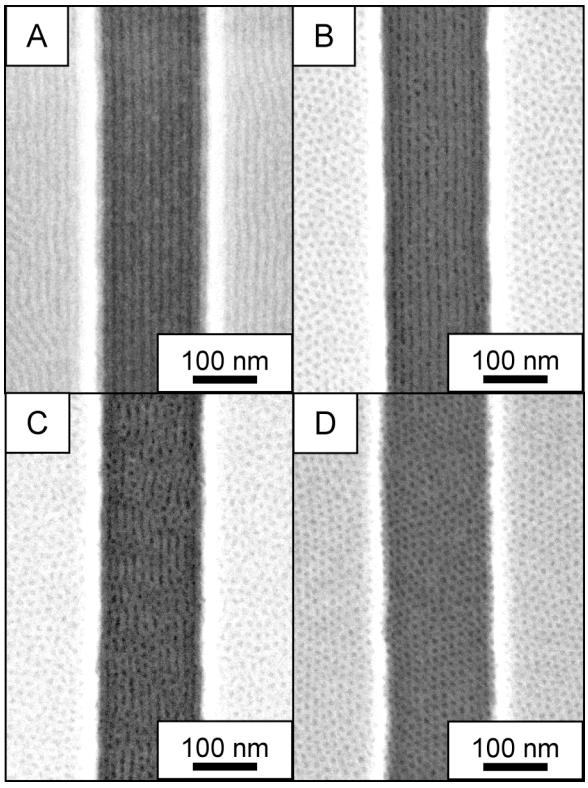

Figure 2.5. Time evolution of acetone anneal of aligned cylinder pattern on PS-treated substrate. (a) Prior to acetone anneal. (b) 3 hour acetone anneal. (c) 3.5 hour acetone anneal. (d) 5 hour acetone anneal.

after 5 hours of annealing, we observe complete hexagonal packing of spheres within the trench region (Figure 2.5d).

2.5 Conclusions

We have demonstrated for the first time control of self assembly in registration with predefined structures and with choice of morphology in PαMS-*b*-PHOST diblock copolymer films, a material well-suited to applications because of its patternability by both lithographic and self assembly approaches. The control provided by reversible solvent annealing processes allows us a window to understanding the fundamental mechanisms of morphology change – in this case a transition from cylindrical to a trapped spherical phase. The demonstration of development of long range ordering and control of morphology by solvent annealing in combination with the precise orientation of grains via graphoepitaxy are the critical steps needed for application to device fabrication.

2.6 Acknowledgements

This work was supported by the National Science Foundation Materials World Network (award DMR 0602821) and the NSF NIRT (award CTS 0304159), and the Semiconductor Research Consortium, and JKB was supported by fellowships from Motorola and IBM. The authors would also like to thank Peter Busch, Cornell, and Xueta Li, Advanced Photon Source, for their help. This work was performed using facilities at the Cornell High Energy Synchrotron Source (CHESS), the Cornell Center for Materials Research (CCMR), and The Cornell NanoScale Facility (CNF). CHESS is supported by the NSF and the National Institutes of Health/National Institute of General Medical Sciences under NSF award DMR-0225180. CCMR is supported by NSF award DMR 0520404, part of the NSF MRSEC Program. CNF, a member of the

National Nanotechnology Infrastructure Network, is supported by NSF award ECS-0335765.

2.7 Supporting Information

The GISAXS image shown in Figure 2.2b was taken slightly above the critical angle of the film at $\alpha_i = 0.125°$. The incident x-ray wavelength was set at 9.97 keV.

In other polymer systems, thin films with spherical morphology display a hexagonally close-packed (HCP) structure. An HCP sphere model is not an accurate model of this polymer thin film system. An HCP sphere system would yield a GISAXS map with a Bragg reflection at a nonzero wavevector stacked vertically above the one of the peaks on the Yoneda band, not seen here.

A bcc lattice was then used to model the thin film since the (110) plane looks very similar to the HCP (001) plane. We defined the real space bcc lattice vectors as:

$$\begin{aligned} \vec{a}_1 &= a\hat{x} \\ \vec{a}_2 &= a\hat{y} \\ \vec{a}_3 &= a\hat{z} \end{aligned} \qquad \text{Eqn. 2.1}$$

giving the following reciprocal lattice vectors:

$$\begin{aligned} \vec{b}_1 &= \frac{2\pi}{a}\hat{x} \\ \vec{b}_2 &= \frac{2\pi}{a}\hat{y} \\ \vec{b}_3 &= \frac{2\pi}{a}\hat{z} \end{aligned} \qquad \text{Eqn. 2.2}$$

We then rotated our coordinate system so that the (110) plane would be parallel to the substrate. Doing this yielded the following rotated reciprocal lattice vectors (assuming $a = 275$ Å^{-1}):

$$\vec{b}_1^{\,*} = -0.0158674\hat{y} + 0.0158674\hat{z}$$
$$\vec{b}_2^{\,*} = 0.0158674\hat{y} + 0.0158674\hat{z} \qquad \text{Eqn. 2.3}$$
$$\vec{b}_3^{\,*} = -0.0224399\hat{x}$$

Using this model, we get scattering from particular planes at the following positions on the GISAXS image:

Table 2.1

Scattering Planes	$q_{\|\|}$	q_z
(1 -1 0)	0.0323119	0.0220456502
(1 0 1)	0.0279829	0.0382015502
(1 -1 2)	0.0456959	0.0220456502

The q_z position of the scattering from the (1 0 1) planes is found to be somewhat altered, after comparing with the experimental GISAXS map. This can be explained using the reasoning that in the swelled state, the polymer thin film morphology is bcc spheres. But after drying, the film shrinks in the z direction.

This changes the morphology from bcc to bct spheres, or face centered orthorhombic. By introducing a convenient surface unit cell, we can model this shrinking in the z direction of the film while maintaining an orthogonal lattice:

$$\vec{a}_1 = \sqrt{2}a\hat{x}$$
$$\vec{a}_2 = a\hat{y} \qquad \text{Eqn. 2.4}$$
$$\vec{a}_3 = 0.6a\hat{z}$$

giving the following reciprocal lattice vectors:

$$\vec{b}_1 = 0.0161559\hat{x}$$
$$\vec{b}_2 = 0.0228479\hat{y} \qquad \text{Eqn. 2.5}$$
$$\vec{b}_3 = 0.0326399\hat{z}$$

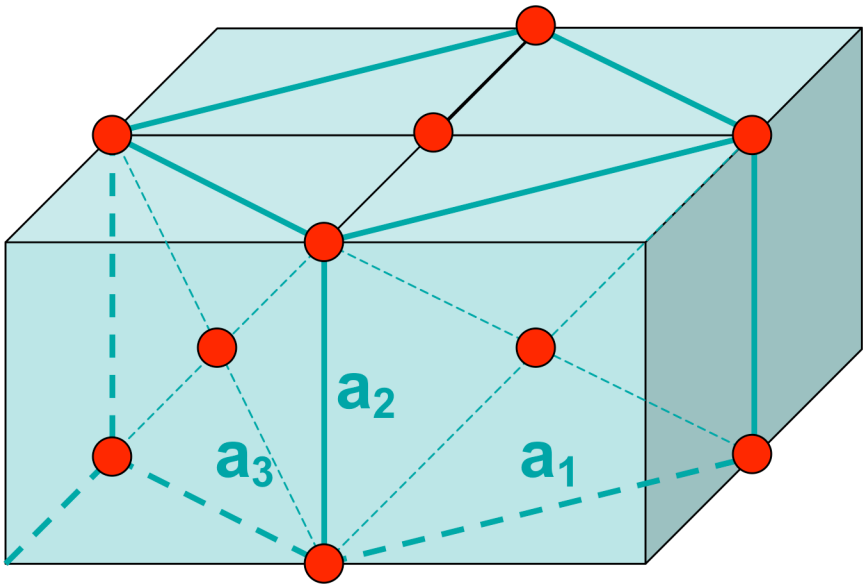

Figure 2.6. The fco lattice derived from the original bcc lattice before shrinkage in the a_3 direction. Note that once the bcc lattice is rotated so the (110) plane is parallel to the surface, the (100) plane of the fco lattice lies parallel to the surface.

Unlike before, it is not necessary that we rotate the coordinate system so that the (110) plane is parallel to the substrate surface. Using this lattice definition, the (100) plane of the fco lattice should lie parallel to the surface as seen in Figure 2.2b.

Since we are using a face centered crystal structure, the allowed peaks should correspond to h,k,l being all even or all odd. With this model, we should get scattering from particular planes at the following positions on the GISAXS image:

Table 2.2

Scattering Planes	$q_{\|\|}$	q_z
(2 0 0)	0.0323119	0.0220456502
(0 2 0)	0.0456959	0.0220456502
(1 1 1)	0.0279829	0.0601255502

The experimental peak positions, shown below, correspond well to the predicted values:

Table 2.3

$q_{\|\|}$	q_z
0.032728	0.021705
0.045519	0.021705
0.027924	0.0594705

Thus, the theoretical model matches the observed GISAXS pattern.

REFERENCES

(1) The International Technology Roadmap for Semiconductors, 2007 Edition. http://www.itrs.net/Links/2007ITRS/Home2007.htm (May 17, 2008).

(2) Li, M.; Douki, K.; Goto, K.; Li, X.; Coenjarts, C.; Smilgies, D. M.; Ober, C. K. *Chem. Mater*. **2004**, 16, 3800-3808.

(3) Du, P.; Li, M.; Douki, K.; Li, X.; Garcia, C. B. W.; Jain, A.; Wiesner, U.; Ober, C. K. *Adv. Mater*. **2004**, 16, 953-957.

(4) Lin, Z.; Kim, D. H.; Wu, X.; Boosahda, L.; Stone, D.; LaRose, L.; Russell, T. P. *Adv. Mater*. **2002**, 14, 1373-1376.

(5) Ivin, K. J.; Leonard, J. *Eur. Poly. J.* **1970**, 6, 331-341.

(6) Fukunaga, K.; Elbs, H.; Magerle, R.; Krausch, G. *Macromol*. **2000**, 33, 947-953.

(7) Cavicchi, K. A.; Berthiaume, K. J.; Russell, T. P. *Polymer* **2005**, 46, 11635-11639.

(8) Kim, S. H.; Misner, M. J.; Xu, T.; Kimura, M.; Russell, T. P. *Adv. Mater*. **2004**, 16, 226-231.

(9) Sidorenko, A.; Tokarev, I.; Minko, S.; Stamm, M. *J. Am. Chem. Soc.* **2003**, 125, 12211-12216.

(10) Tokarev, I.; Krenek, R.; Burkov, Y.; Schmeisser, D.; Sidorenko, A.; Minko, S.; Stamm, M. *Macromol*. **2005**, 38, 507-516.

(11) Mori, K.; Hasegawa, H.; Hashimoto, T. *Polymer* **1990**, *31*, 2368-2376.

(12) Amundson, K.; Helfand, E.; Quan, X.; Hudson, S. D.; Smith, S. D. *Macromol*. **1994**, 27, 6559-6570.

(13) Xu, T.; Zhu, Y.; Gido, S. P.; Russell, T. P. *Macromol*. **2004**, 37, 2625-2629.

(14) Boeker, A.; Elbs, H.; Haensel, H.; Knoll, A.; Ludwigs, S.; Zettl, H.; Zvelindovsky, A. V.; Sevink, G. J. A.; Urban, V.; Abetz, V.; et al.. *Macromol*. **2003**, 36, 8078-8087.

(15) Chen, Z.-R.; Kornfield, J. A.; Smith, S. D.; Grothaus, J. T.; Satkowski, M. M. *Science* **1997**, 277, 1248-1253.

(16) Angelescu, D. E.; Waller, J. H.; Adamson, D. H.; Deshpande, P.; Chou, S. Y.; Register, R. A.; Chaikin, P. M. *Adv. Mater*. **2004**, 16, 1736-1740.

(17) Hamley, I. W. *Curr. Opin. Coll. & Int. Sci*. **2000**, 5, 341-349.

(18) Heier, J.; Genzer, J.; Kramer, E. J.; Bates, F. S.; Walheim, S.; Krausch, G. *J. Chem. Phys.* **1999**, 111, 11101-11110.

(19) Edwards, E. W.; Montague, M. F.; Solak, H. H.; Hawker, C. J.; Nealey, P. F. *Adv. Mater*. **2004**, 16, 1315-1319.

(20) Segalman, R. A.; Yokoyama, H.; Kramer, E. J. *Adv. Mater*. **2001**, 13, 1152-1155.

(21) Cheng, J. Y.; Ross, C. A.; Smith, H. I.; Thomas, E. L. *Adv. Mater*. **2006**, 18, 2505-2521.

(22) Black, C. T. *Appl. Phys. Lett*. **2005**, 87, 163116.

(23) Sundrani, D.; Darling, S. B.; Sibener, S. J. *Langmuir* **2004**, 20, 5091-5099.

(24) Brandrup, J.; Immergut, H.; Grulke, A. *Polymer Handbook*; 4 ed.; John Wiley & Sons.: New York, 2003

(25) Asakawa, K.; Hiraoka, T. *Jpn. J. Appl. Phys*. **2002**, 41, 6112-6118.

(26) Lin, Y.; Boeker, A.; He, J.; Sill, K.; Xiang, H.; Abetz, C.; Li, X.; Wang, J.; Emrick, T.; Long, S.; et al. *Nature* **2005**, 434, 55-59.

(27) Kim, S. H.; Misner, M. J.; Yang, L.; Gang, O.; Ocko, B. M.; Russell, T. P. *Macromol*. **2006**, 39, 8473.

(28) Stein, G. A.; Kramer, E. J.; Li, X.; Wang, J. *Macromol*. **2007**, 40, 2453-2460.

(29) Urade, V. N.; Hillhouse, H. W. *J. Phys. Chem. B*. **2005**, 109, 10538-10541.

(30) Black, C. T.; Bezencenet, O. *IEEE Trans. Nanotechnol*. **2004**, 3, 412-415.

(31) Mansky, P.; Russell, T. P.; Hawker, C. J.; Pitsikalis, M.; Mays, J. *Macromol*. **1997**, 30, 6810-6813.

(32) Mansky, P.; Russell, T. P.; Hawker, C. J.; Mays, J.; Cook, D. C.; Satija, S. K. *Phys. Rev. Lett*. **1997**, 79, 237-240.

(33) Harrison, C.; Chaikin, P. M.; Huse, D. A.; Register, R. A.; Adamson, D. H.; Daniel, A.; Huang, E.; Mansky, P.; Russell, T. P.; Hawker, C. J; et al. *Macromol*. **2000**, 33, 857-865.

(34) Hawker, C. J. *J. Am. Chem. Soc.* **1994**, 116, 11185-11186.

(35) Stein, G.A., Kramer, E.J., Li, X. & Wang, J. *Macromol.* **40**, 2453 (2007)

CHAPTER 3

SELECTIVE AREA CONTROL OF SELF-ASSEMBLED PATTERN ARCHITECTURE USING A LITHOGRAPHICALLY PATTERNABLE BLOCK COPOLYMER

Joan K. Bosworth,[1,2] Charles T. Black,[3] and Christopher K. Ober[*2]

1. Department of Chemistry & Chemical Biology, Cornell University, Ithaca, NY 14853

2. Department of Materials Science & Engineering, Cornell University, Ithaca, NY 14853

3. Center for Functional Nanomaterials, Brookhaven National Laboratory, Upton NY 11973

3.1 Abstract

We leverage distinctive chemical properties of the diblock copolymer poly(α-methylstyrene)-*block*-poly(4-hydroxystyrene) in order to create for the first time high-resolution selective-area regions of two different block copolymer phase morphologies. Exposure of thin films of poly(α-methylstyrene)-*block*-poly(4-hydroxystyrene) to non-selective or block-selective solvent vapors results in polymer phase separation and self assembly of patterns of cylindrical-phase or kinetically trapped spherical-phases, respectively. Poly(4-hydroxystyrene) acts as a high-resolution negative-tone photoresist in the presence of small amounts of a photoacid generator and crosslinker, undergoing radiation-induced crosslinking upon exposure to ultraviolet light or an electron beam. We use lithographic exposure to lock one self-assembled phase morphology in specific sample areas as small as 100 nm in width prior to film exposure to a subsequent solvent vapor in order to form a second self-assembled morphology in unexposed wafer areas.

3.2 Introduction

While block copolymer self assembly holds much promise as a lithography alternative for critical high-resolution patterning of future microelectronic devices,[1] a real limitation of this approach compared to traditional lithography is that self-assembled patterns consist of only a single phase morphology (for example, spheres, cylinders, or lamellae).[2] This is because block copolymer patterns form by phase separation into domain morphologies determined by the constituent polymer block volume fractions, which are constant for a given material.

Here we demonstrate for the first time the ability to selectively pattern the *phase morphology* of a self-assembled block copolymer thin film – an attractive prospect for high-resolution templating applications requiring precise control of the

locations of *more than one type* of self-assembled pattern. Our process is enabled by distinctive properties of the block copolymer poly(α-methylstyrene)-block-poly(4-hydroxystyrene) (PαMS-b-PHOST), which behaves as a chemically-amplified negative-tone photoresist when combined with small amounts of a photoacid generator (e.g., triphenylsulfonium triflate, TPST) and a crosslinker (e.g., tetramethoxymethyl glycoluril, TMMGU).[3, 4]

We have previously demonstrated control of the self-assembled pattern morphology in PαMS-b-PHOST films by exposure to suitable solvent vapor.[5] Exposure of a 33% PαMS polymer film to tetrahydrofuran (THF), a good solvent for both PαMS and PHOST blocks, results in phase separation into a cylindrical film morphology. Annealing in acetone, a solvent selective for the PHOST majority component, causes an order-order transition in the swollen state to spherical morphology, which is kinetically trapped upon drying.

We can use sequential solvent vapor treatments to reversibly switch between PαMS-b-PHOST film phase morphologies. However, crosslinked PHOST domains remain fixed and do not change morphology upon exposure to subsequent solvent, allowing the selective formation of regions of two different morphologies within a single PαMS-b-PHOST film. A different self-assembling block copolymer system with photoresist behavior, polystyrene-block-poly(*tert*-butylacrylate), was shown to behave as a positive-tone photoresist with ~400 nm resolution upon inclusion of a photoacid generator, in which the acid formed upon UV exposure catalyzes deprotection of the poly(*tert*-butyl acrylate) block.[6] The mass loss from block deprotection can also cause an order-order transition in polymer films, inducing a shift from cylindrical polystyrene-block-poly(*tert*-butyl acrylate) to spherical polystyrene-block-poly(acrylic acid), although there have been no attempts to achieve multiple phase morphologies in a single polymer film using this approach.[7] Here, we have

demonstrated the resolution of our selective-area PαMS-b-PHOST patterning approach to be less than 100 nanometers.

Although until now there have been no demonstrations of selective-area patterning of two self-assembled phase morphologies within a single block copolymer film, there have been several demonstrations showing control of two domain *orientations* within a block copolymer film composed of a *single phase morphology*. Surface-neutralizing techniques have been used extensively to gain perpendicular orientation of both cylindrical and lamellar morphologies of polystyrene-block-poly(methyl methacrylate) (PS-b-PMMA).[8-14] Patternable surface neutralization materials have been demonstrated to form perpendicular orientations on within neutral surface patterns and parallel orientations on untreated areas, although the patterned regions are limited to micrometer-scale resolution.[11-14] Alternatively, chemical epitaxy, in which chemical patterns on a substrate having a length scale similar to the block copolymer can induce alignment in block copolymer film, both by aligning the morphology and controlling the orientation of cylindrical and lamellar domains in films of PS-b-PMMA in select wafer areas.[15-19] An advantage to the crosslinking-induced patterning of PαMS-b-PHOST demonstrated here is the ability to directly-write the high-resolution morphology pattern. Using the selective-crosslinking method demonstrated here, large defect-free patterns can in principle be achieved by combining lithographic exposure with established methods of inducing order in block copolymer films, including not only chemical epitaxy, but also graphopitaxy,[5, 20-23] electric fields,[24-27] and shear forces.[28-31]

3.3 Methods

The PαMS-b-PHOST block copolymer material used here has total M_n 21 kg/mol, 33% PαMS by mass, and distribution 1.10, as described previously;[5] synthesis

by sequential anionic polymerization of poly(α-methylstyrene)-block-poly(*tert*-butoxystyrene) and subsequent deprotection to PαMS-b-PHOST have also been described previously.[3] Films were spin coated from propylene glycol methyl ether acetate (Aldrich, 1% w/v) with spin speed previously determined to yield single morphology thickness films, measured here to be 20 nm by ellipsometry.[5] Spinning solution also contained 1.5% (w/w relative to PαMS-b-PHOST) triphenylsulfonium triflate (TPST, Aldrich) photoacid generator and 4% (w/w relative to PαMS-b-PHOST) tetramethoxymethyl glycoluril (TMMGU, "Powderlink 1174," Cytec Industries) crosslinker. These small quantities of TPST and TMMGU do not to affect the self assembly of the PαMS-b-PHOST, as long as films are not exposed to UV.

Spin coating and solvent vapor annealing with acetone (Aldrich) and tetrahydrofuran (THF, Aldrich) (in a sealed 1L jar with solvent reservoir, 6 mL for THF and 4 mL for acetone) are performed under yellow light conditions to prevent photoacid generator exposure. Atomic force microscopy (AFM) is performed on a Veeco Dimension 3100 in tapping mode. In Figure 3.6, partial removal of the PαMS was achieved by heating films on a hotplate at 115˚C for 15 minutes in air, aiding AFM imaging.

In the case of UV-exposed films, an HTG mask aligner with 254 nm exposure was used to blanket-expose films; output was measured to be 2.6 mW/cm^2. Post exposure bake in all cases was 115˚C for 60 seconds. Solvent develop conditions determined previously[3] were used again here, involving 1:2 cyclohexanone and isopropanol (v/v) mixture for 1 minute, followed by 1 minute in isopropanol, and nitrogen dry. Electron beam lithography was written using an NPGS on a Helios Nanolab (FEI) with exposures at 30 kV. Films used for e-beam patterning contain TPST and TMMGU, but no post-expose bake step is applied after e-beam patterning. Film thicknesses were measured with a Nanofilm EP3 imaging ellipsometer.

3.4 Results & Discussion

The key to using PαMS-b-PHOST for this combined patterning method is that the presence of the photoacid generator TPST and crosslinker TMMGU (necessary for the material to act as a negative-tone photoresist) do not interfere with the solvent vapor-induced self assembly processes. Sequential exposure of 20nm thick PαMS-b-PHOST films containing 1.5% w/w TPST and 4% w/w TMMGU to different solvent vapor environments results in self-assembled patterns corresponding to the final solvent vapor treatment (Figure 3.1). The pattern self assembly process is not only unaffected by inclusion of small quantities of photoactive compounds, but the solvent anneal history does not play a role in the pattern morphology. PαMS-b-PHOST films annealed in non-selective THF form the fingerprint pattern consistent with parallel-oriented cylindrical phase morphology (Figure 3.1a), while films exposed to acetone vapor (selective for the PHOST block) form spherical-phase patterns of hexagonally-arranged dots (Figure 3.1b). Subsequent exposure of the cylindrical-phase morphology (Figure 3.1a) to acetone converts the fingerprint pattern to hexagonal dots (Figure 3.1c) that are indistinguishable from films annealed singly in acetone (Figure 3.1b). As well, spherical dot patterns are completely converted to cylindrical morphology by further annealing in THF (Figure 1d). We have avoided possible film crosslinking from ambient light exposure by performing all experiments entirely under yellow light conditions.

We can prevent phase-separated PαMS-b-PHOST films from switching morphology upon subsequent solvent vapor annealing by inducing a sufficient crosslink density in the film through controlled exposure to ultraviolet (UV) light (Figure 3.2). In traditional photolithography, film crosslinking further prevents

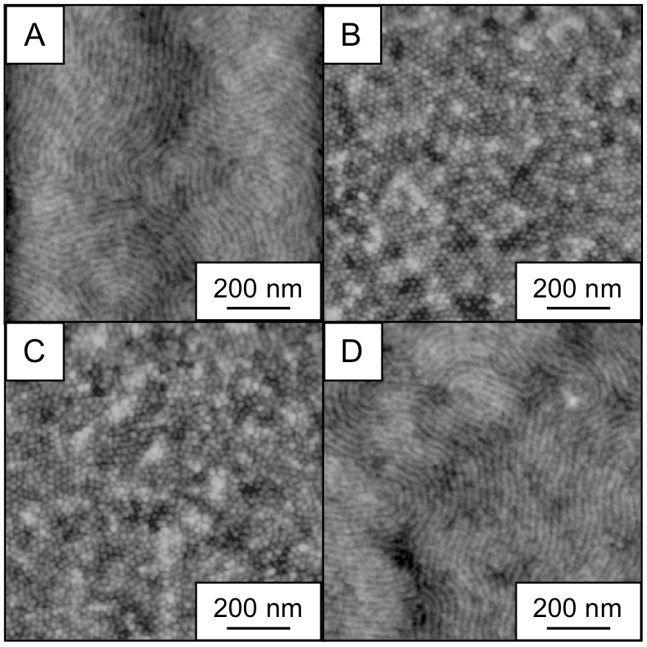

Figure 3.1. AFM height images of self-assembled PαMS-b-PHOST films annealed in different solvent vapor environments. (a) Annealed in THF (b) Annealed in acetone. (c) Annealed first in THF and then annealed for a second time in acetone (d) Annealed in acetone followed by THF. The height scale for all images is 10 nm.

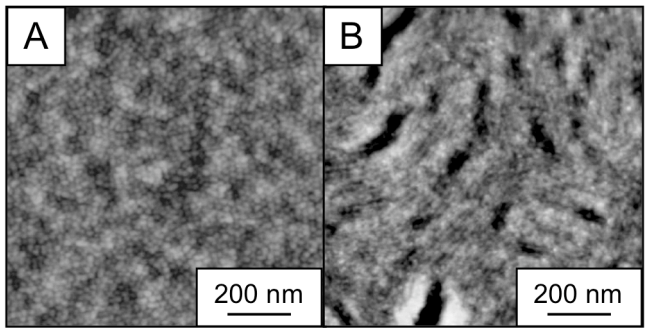

Figure 3.2 AFM height images of self-assembled PαMS-b-PHOST films exposed to UV followed by a post-exposure bake prior to the second solvent vapor treatment. (a) A PαMS-b-PHOST film annealed in acetone, UV exposed and annealed in THF remains in a spherical morphology; (b) a film annealed first in THF and exposed to UV, then annealed in acetone maintains the cylindrical morphology of a THF anneal. The height scale for both images is 10 nm.

dissolution of the polymer upon developing in a solvent or aqueous base. PαMS-b-PHOST films annealed in a first solvent (in the dark) and subsequently exposed to a sufficient dose of UV light and post-exposure baked (115˚C, 60 seconds) before exposure to a second solvent vapor all maintain the phase morphology from their *first anneal*, demonstrating that film crosslinking prevents morphology switching. Films annealed first in acetone before UV exposure and then THF solvent vapor remain locked in a spherical-phase dot pattern (Figure 3.2a), while films annealed first in THF, crosslinked with UV light, and then exposed to acetone vapor show the cylindrical pattern morphology of the fingerprint pattern (Figure 3.2b). We observe significant pattern degradation only in films first annealed in THF prior to crosslinking and subsequent acetone exposure (Figure 3.2b).

We have measured the UV exposure dose required to lock a self-assembled morphology and prevent switching during subsequent exposure to a second solvent vapor; the exposure dosage necessary to lock a spherical morphology is shown in Figure 3.3. Films initially annealed in acetone form a spherical morphology (Figure 3.1b), and UV exposure of at least 10.4 mJ/cm^2 is enough to preserve the hexagonal dot pattern structure upon further annealing in THF (Figure 3.3d; also the dotted exposure range in Figure 3a), indicating the introduction of sufficient crosslink density to lock the spherical morphology. Films exposed to lower doses show either a complete switch to cylindrical phase (diagonal striped range in Figure 3.3a) or a mixed cylinder/sphere morphology (Figure 3.3c; also the grey range in Figure 3.3a) after a similar second THF treatment.

We can similarly lock a self-assembled cylindrical phase morphology by exposure to sufficient UV light (Figure 3.4), although this case requires a larger minimum exposure dose (increased from 10.4 mJ/cm^2 to 15.6 mJ/cm^2) necessary to prevent switching to a cylindrical phase upon a second anneal in acetone (Figure 3.4d;

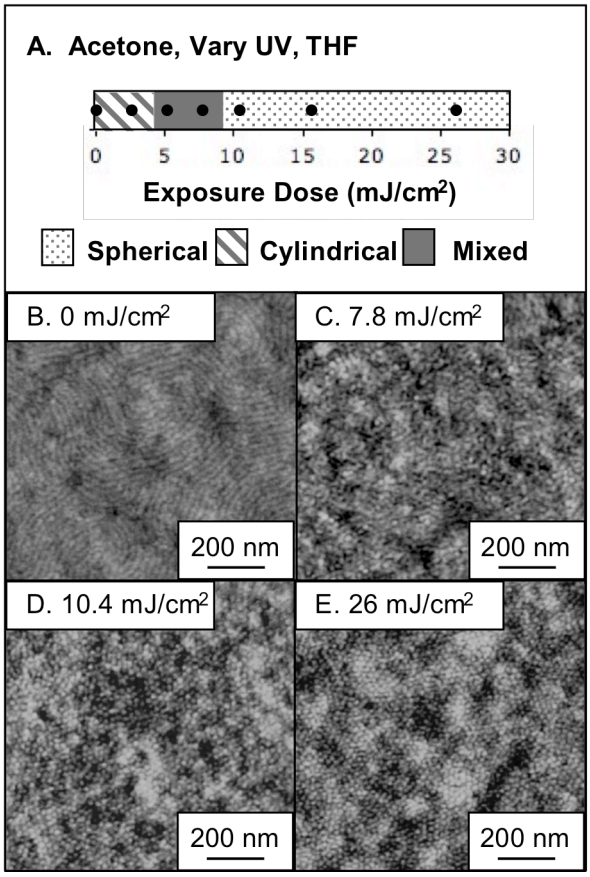

Figure 3.3. UV exposure dose required to lock the spherical film morphology. (a) UV dose range and resulting block copolymer film morphology after subsequent solvent vapor treatment in THF. The black dots correspond to exposures tested, and the background indicates morphology observed; the interfaces between the morphologies are not known, but for clarity is indicated at the midpoints. AFM height images of PαMS-b-PHOST films having UV exposure doses of (b) 0 mJ/cm^2, (c) 7.8 mJ/cm^2, (d) 10.4 mJ/cm^2, and (e) 26 mJ/cm^2. The height scale for (b) is 10 nm, and the scale is 5 nm for (c-e).

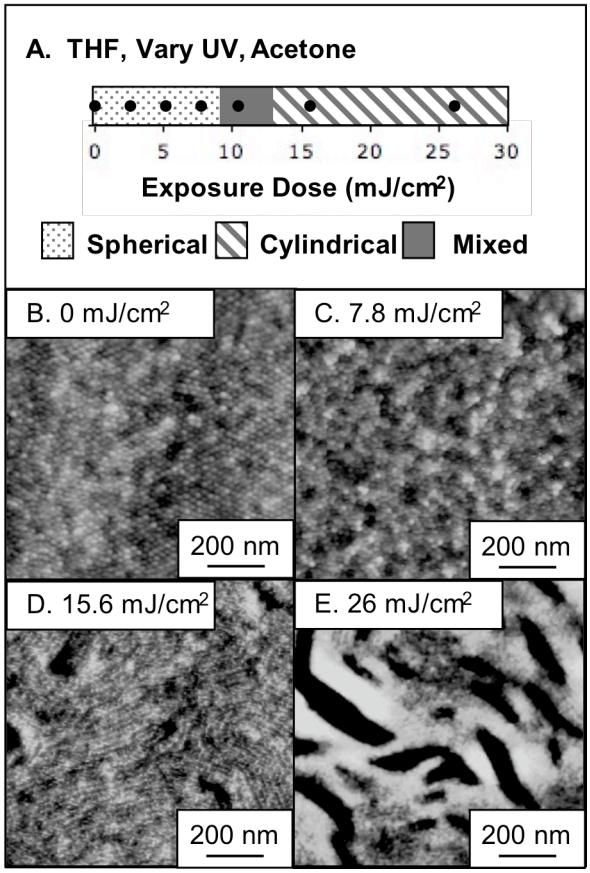

Figure 3.4. UV exposure dose required to lock the cylindrical film morphology. (a) UV dose range and resulting block copolymer film morphology after subsequent solvent vapor treatment in acetone. AFM height images of PαMS-b-PHOST films having UV exposure doses of (b) 0 mJ/cm^2, (c) 7.8 mJ/cm^2, (d) 15.6 mJ/cm^2, and (e) 26 mJ/cm^2. The height scale for images (b-e) is 10 nm.

also the diagonal stripe range in Figure 3.4a). Cylindrical patterns receiving lower UV exposure doses either switch to spherical morphology upon annealing in acetone (the dotted range in Figure 3.4a) or form a mixed cylinder sphere pattern (Figure 3.4c; also the grey range in Figure 3.4a). Our observations are consistent with PαMS-b-PHOST films requiring a higher degree of swelling in acetone (compared to THF) in order to gain sufficient mobility for pattern formation. Because acetone is a selective solvent for PHOST, the less-soluble PαMS block crosses the swelling threshold for polymer mobility, and thus self assembly, at a larger overall swell ratio than in the case of annealing in a nonselective solvent such as THF. We believe that the higher film swelling condition required for pattern formation in acetone interferes with the morphology of the crosslinked film, thereby resulting in a higher exposure dose required to prevent morphology switching (Figure 3.4a) as well as larger film roughness (Figure 3.4d-e) for PαMS-b-PHOST films annealed in acetone after crosslinking.

We have also measured the PαMS-b-PHOST photoresist sensitivity by UV exposure to a range of doses, followed by a post-exposure bake and immersion in a solvent developer (1:2 cyclohexanone/isopropanol). The resulting contrast curve shows the normalized remaining film thickness after development versus the UV exposure dose (Figure 3.5). For a negative-tone photoresist material, the sensitivity is defined by the dose at which 50% of original film thickness remains in the UV exposed regions – in this case, ~6mJ/cm^2, though typically the exposure dose for patterning is chosen between this value and the exposure dose that gives nearly 100% of the original PαMS-b-PHOST resist thickness (here approximately 10.4 mJ/cm^2), thereby limiting the line broadening that occurs upon overexposure.[32] The required exposure dose to prevent film dissolution (10.4 mJ/cm^2) (Figure 3.5) is the same as the

dose to prevent morphology switching in an acetone-to-THF annealing sequence (Figure 3), indicating that the overall resolution for this order of solvent vapor

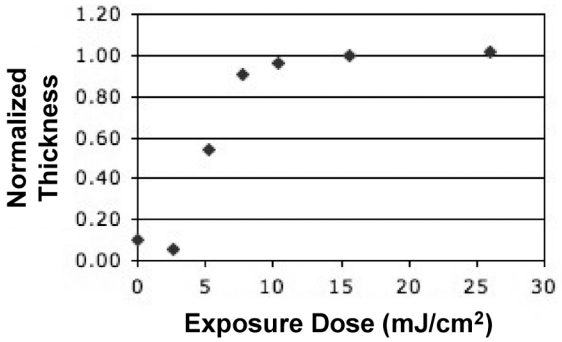

Figure 5. Normalized PαMS-b-PHOST film thickness after UV exposure and solvent develop versus UV exposure dose.

exposures will have a higher resolution than a THF-to-acetone sequence (Figure 3.4), which has a minimum exposure dose to lock in phase morphology of 15.6 mJ/cm^2.

We combine the UV sensitivity of PαMS-b-PHOST together with its solvent vapor processability in order to form high-resolution patterns of *two different block copolymer phases* within select wafer areas. We have employed electron-beam (e-beam) lithography in order to investigate the smallest achievable length scales, even though this exposure method requires recalibrating the resist sensitivity for electron-beam doses because there is no direct correlation between UV and e-beam sensitivity. We focus on the solvent vapor sequence of first forming a spherical morphology by annealing in acetone and then annealing in THF after e-beam exposure in order to maximize the patterned film spatial resolution.

Film exposure to a range of e-beam doses reveals optimal high-resolution patterns of spherical morphology within a field of cylindrical-phase morphology (Figure 3.6). PαMS-b-PHOST films containing the photoacid generator TPST and the crosslinker TMMGU are annealed first in acetone to form a spherical-phase dot pattern (Figure 3.1b), and next patterned by e-beam exposure of a series of lines having 1:4 spacing, leading to crosslinking in the exposed regions. The exposed films are next annealed in THF to switch the unexposed regions to a cylindrical morphology. Unlike photolithography, e-beam-exposed PαMS-b-PHOST films do not require a post-expose bake prior to solvent annealing, as this was found to increase line broadening. Even without a resist post-expose bake, the optimal exposure dose needed to lock the self-assembled morphology is 5 times smaller for films containing TPST and TMMGU (100 μC/cm^2 for films containing TPST and TMMGU, and 500 μC/cm^2 for neat PαMS-b-PHOST films - not shown).

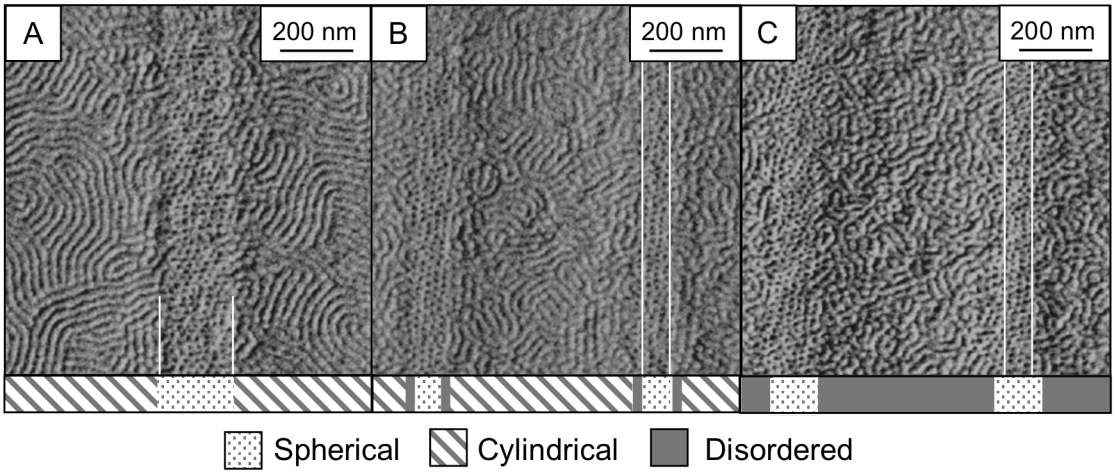

Figure 3.6. AFM phase images demonstrate a single PαMS-b-PHOST film having both regions of spherical morphology and regions of cylindrical morphology. The electron-beam exposure doses used are a) 100 μC/cm^2, b) 200 μC/cm^2, c) 400 μC/cm^2. White overlaid lines indicate where e-beam exposed lines were written, and the scale underneath indicates the morphology observed. The phase scale for all images is 6°.

PαMS-PHOST films patterned with a 100 μC/cm^2 e-beam exposure dose showed 200 nm wide lines having spherical morphology within a field of cylindrical morphology without significant line broadening (Figure 3.6a). Written line widths smaller than 200 nm failed to sufficiently crosslink in order to prevent switching in exposed regions. Unexposed film regions switch to cylindrical morphology during the second solvent vapor treatment, while the exposed regions show a mixed cylinder/sphere morphology, albeit one with minimal line broadening.

Writing a series of 75nm wide lines with 1:4 spacing using the optimal electron-beam dose of 200 μC/cm^2 locks the spherical morphology in regions approximately 4 spheres wide (or ~95nm, based on the measured 24nm sphere repeat distance), meaning that this dose produces ~20nm of line broadening (Figure 3.6b). We measure a film thickness decrease of ~5 nm in the exposed regions (from an original film thickness of 20 nm) by atomic force microscopy (images not shown).

Higher electron-beam exposure doses (Figure 3.6c) leave the exposed spherical-phase areas unaffected although we observe a significant increase in line broadening. Over-exposure also negatively affects self assembly of cylindrical phase regions in nominally unexposed areas as crosslinks are introduced into these film areas from proximity effects. With lower exposure doses (100 μC/cm^2), we observe virtually no line broadening, but the ultimate achievable resolution for the spherical-morphology crosslinked region is worse (Figure 3.6a, 200 nm lines). The optimum dose is achieved with 200 μC/cm^2 exposure (Figure 3.6b): little crosslinking occurs outside of the exposed region and we observe only a narrow band of mixed-phase morphology (less than a single 24 nm domain repeat-unit in width) between exposed and unexposed areas, demonstrating high-resolution and high-contrast patterning of block copolymer film morphologies.

We have demonstrated here that PαMS-b-PHOST film morphology can be switched by sequential annealing in solvent vapors having different block selectivities, enabling formation of either spherical or cylindrical morphologies. We can prevent morphology switching in select wafer regions by selective radiation-induced crosslinking using either UV light or an electron-beam prior to film exposure to a second solvent vapor environment. By combining electron-beam-induced crosslinking and solvent induced morphology switching, we have shown for the first time selective high-resolution patterning of a single block copolymer film into ~100nm regions of two different self-assembled phase morphologies.

3.5 Acknowledgements

This work was supported by the National Science Foundation Materials World Network (award DMR 0602821), the NSF NIRT (award CTS 0304159), and the Semiconductor Research Consortium, and J.K.B. was supported by fellowships from Motorola and IBM. Research was carried out in part at the Center for Functional Nanomaterials (CFN) at Brookhaven National Laboratory, which is supported by the U.S. Department of Energy, Division of Materials Sciences and Division of Chemical Sciences, under Contract No. DE-AC02-98CH10886. This work was also performed using facilities at the Cornell NanoScale Facility, (CNF), the Cornell Center for Materials Research (CCMR) and the Cornell Nanobiotechnology Center (NBTC). CNF is a member of the NNIN, supported by NSF award ECS-0335765, CCMR is supported by NSF award DMR 0520404, part of the NSF MRSEC program, and the NBTC is supported by the STC Program of the NSF, award ECS-9876771. The authors thank Aaron Stein of the CFN as well as Drew Forman and Jing Sha of Cornell for assistance with electron beam patterning.

REFERENCES

(1) Black, C. T., Polymer Self Assembly as a Novel Extension to Optical Lithography. *ACS Nano* **2007,** 1, 147-150.

(2) Bates, F. S.; Fredrickson, G. H., Block Copolymers - Designer Soft Materials. *Phys. Today* **1999,** 52, (February), 32-38.

(3) Li, M.; Douki, K.; Goto, K.; Li, X.; Coenjarts, C.; Smilgies, D.-M.; Ober, C. K., Spatially Controlled Fabrication of Nanoporous Clock Copolymers. *Chem. Mater.* **2004,** 16, 3800-3808.

(4) Du, P.; Li, M.; Douki, K.; Li, X.; Garcia, C. B. W.; Jain, A.; Smilgies, D.-M.; Fetters, L. J.; Gruner, S. M.; Wiesner, U.; Ober, C. K., Additive-driven phase-selective chemistry in block copolymer thin films: The Convergence of Top-Down and Bottom-Up Approaches. *Adv. Mater.* **2004,** 16, 953-957.

(5) Bosworth, J. K.; Paik, M. Y.; Ruiz, R.; Schwartz, E. L.; Huang, J. Q.; Ko, A. W.; Smilgies, D.-M.; Black, C. T.; Ober, C. K., Control of Self Assembly of Lithographically Patternable Block Copolymer Films. *ACS Nano* **2008,** 2, 1396-1402.

(6) La, Y.-H.; In, I.; Park, S.-M.; Meagley, R. P.; Leolukman, M.; Gopalan, P.; Nealey, P. F., Pixelated Chemically Amplified Resists: Investigation of Material Structure in the Spatial Distribution of Photoacids and Line Edge Roughness. *J. Vac. Sci. Technol. B* **2007,** 25, 2508-2513.

(7) La, Y.-H.; Edwards, E. W.; Park, S. M.; Nealey, P. F., Directed Assembly of Cylinder-Forming Block Copolymer Films and Thermochemically Induced Cylinder to Sphere Transition: A Heirarchical Route to Linear Arrays of Nanodots. *Nano Letters* **2005,** 5, 1379-1384.

(8) Mansky, P.; Liu, Y.; Huang, E.; Russell, T. P.; Hawker, C., Controlling Polymer-Surface Interactions With Random Copolymer Brushes. *Science* **1997,** 275, 1458-1460.

(9) Mansky, P.; Russell, T. P.; Hawker, C. J.; Pitsikalis, M.; Mays, J., Ordered Diblock Copolymer Films on Random Copolymer Brushes. *Macromol.* **1997,** 30, 6810-6813.

(10) Huang, E.; Pruzinsky, S.; Russell, T. P.; Mays, J.; Hawker, C. J., Neutrality Conditions for Block Copolymer Systems on Random Copolymer Brush Surfaces. *Macromol.* **1999,** 32, 5299-5303.

(11) Ryu, D. Y.; Shin, K.; Drockenmuller, E.; Hawker, C. J.; Russell, T. P., A Generalized Approach to the Modification of Solid Surfaces. *Science* **2005,** 308, 236-239.

(12) Bang, J.; Bae, J.; Loewenhielm, P.; Spiessberger, C.; Given-Beck, S. A.; Russell, T. P.; Hawker, C. J., Facile Routes to Patterned Surface Neutralization Layers for Block Copolymer lithogrpahy. *Adv. Mater.* **2007,** 19, 4552-4557.

(13) Han, E.; In, I.; Park, S.-M.; La, Y.-H.; Wang, Y.; Nealey, P. F.; Gopalan, P., Photopatternable Imaging Layers for Controlling Block Copolymer Microdomain Orientation. *Adv. Mater.* **2007,** 19, 4448-4452.

(14) Han, E.; Stuen, K. O.; La, Y.-H.; Nealey, P. F.; Gopalan, P., Effect of Composition of Substrate-Modifying Random Copolymers on the Orientation of Symmetric and Asymmetric Diblock Copolymer Domains. *Macromol.* **2008,** 41, 9090-9097.

(15) Stoykovich, M.; Mueller, M.; Kim, S.; Solak, H.; Edwards, E.; de Pablo, J.; Nealey, P., Directed Assembly of Block Copolymer Blends Into Nonregular Device-Oriented Structures. *Science* **2005,** 308, 1442-1446.

(16) Kim, S. O.; Kim, B. H.; Meng, D.; Shin, D. O.; Chong, M. K.; Solak, H. H.; Wang, Q. W., Novel Complex Nanostructure From Directed Assembly of Block Copolymers on Incommensurate Surface Patterns. *Adv. Mater.* **2007,** 19, 3271-3275.

(17) Park, S.-M.; Craig, G. S. W.; Liu, C.-C.; La, Y.-H.; Ferrier, N. J.; Nealey, P. F., Characterization of Cylinder-Forming Block Copolymers Directed to Assemble on Spotted Chemical Patterns. *Macromol.* **2008,** 41, 9118-9123.

(18) Cheng, J. Y.; Rettner, C. T.; Sanders, D. P.; Kim, H.-C.; Hinsberg, W. D., Dense Self Assembly on Sparse Chemical Patterns: Rectifying and Multiplying Lithographic Patterns Using Block Copolymers. *Adv. Mater.* **2008,** 20, 3155-3158.

(19) Ruiz, R.; Kang, H.; Detcheverry, F. A.; Dobisz, E.; Kercher, D. S.; Albrecht, T. R.; de Pablo, J. J.; Nealey, P. F., Density Multiplication and Improved Lithography by Directed Block Copolymer Assembly. *Science* **2008,** 321, 936-939.

(20) Segalman, R. A.; Yokoyama, H.; Kramer, E. J., Graphoepitaxy of Spherical Domain Block Copolymer Films. *Adv. Mater.* **2001,** 13, 1152-1155.

(21) Cheng, J. Y.; Ross, C. A.; Smith, H.; Thomas, E. L., Templated Self Assembly of Block Copolymers: Top-Down Helps Bottom-Up. *Adv. Mater.* **2006,** 18, 2505-2521.

(22) Black, C. T., Self-Aligned Self Assembly of Multi-Nanowire Silicon Field Effect Transistors. *App. Phys. Lett.* **2005,** 87, 163116.

(23) Park, S.; Kim, B.; Yavuzcetin, O.; Tuominen, M. T.; Russell, T. P., Ordering of PS-P4VP on Patterned Silicon Substrates. *ACS Nano* **2008,** 2, 1363-1370.

(24) Amundson, K.; Helfand, E.; Quan, X.; Hudson, S. D.; Smith, S. D., Alignment of Lamellar Block Copolymer Microstructures in an Electric Field. 2. Mechanisms of Alignment. *Macromol.* **1994,** 27, 6559-6570.

(25) Xu, T.; Zhu, Y.; Gido, S. P.; Russell, T. P., Electric Field Alignment of Symmetric Diblock Copolymer Thin Films. *Macromol.* **2004,** 37, 2625–2629.

(26) Boeker, A.; Elbs, H.; Haensel, H.; Knoll, A.; Ludwigs, S.; Zettl, H.; Zvelindovsky, A. V.; Sevink, G. J. A.; Urban, V.; Abetz, V.; Mueller, A. H. E.; Krausch, G., Electric Field Induced Aligment of Concentrated Block Copolymer Solutions. *Macromol.* **2003,** 36, 8078-8087.

(27) Olszowka, V.; Kuntermann, V.; Boeker, A., Control of Orientational Order in Block Copolymer Thin Films by Electric Fields: A Combinatorial Approach. *Macromol.* **2008,** 41, 5155-5518.

(28) Chen, Z.-R.; Kornfield, J. A.; Smith, S. D.; Grothaus, J. T.; Satkowski, M. M., Pathways to Macroscale Order in Nanostructured Block Copolymers. *Science* **1997,** 277, 1248-1253.

(29) Angelescu, D. E.; Waller, J. H.; Adamson, D. H.; Deshpande, P.; Chou, S. Y.; Register, R. A.; Chaikin, P. M., Macroscopic Orientation of Block Copolymer Cylinders in Single-Layer Films by Shearing. *Adv. Mater.* **2004,** 16, 1736-1740.

(30) Hamley, I. W., The Effect of Shear on Ordered Block Copolymer Solutions. *Curr. Opin. Coll. & Int. Sci.* **2000,** 5, 341-349.

(31) Sebastian, J. M.; Lai, C.; Graessley, W. W.; Register, R. A., Steady-Shear Rheology of Block Copolymer Melts and Concentrated Solutions: Disordering Stress in Body-Centered-Cubic Systems. *Macromol.* **2002,** 35, 2707-2713.

(32) Ito, H., Chemical Amplification Resists for Microlithography. *Adv. Polym. Sci.* **2005,** 172, 37-245.

CHAPTER 4

SOLVENT ANNEALING FOR SELF ASSEMBLY IN AN ALTERNATIVE COMBINED TOP-DOWN/BOTTOM-UP PATTERNABLE BLOCK COPOLYMER

Joan K. Bosworth,[1,2] Michelle A. Chavis,[2] Diana L. Wang,[2] Marvin Y. Paik,[2] Evan L. Schwartz,[2] and Christopher K. Ober[2]

1. Department of Chemistry & Chemical Biology, Cornell University, Ithaca, NY 14853

2. Department of Materials Science & Engineering, Cornell University, Ithaca, NY 14853

4.1 Abstract

A combined top-down/bottom up patternable block copolymer, poly(methyl methacrylate)-*block*-poly(hydroxyethyl methacrylate), or PMMA-*b*-PHEMA, is presented. The majority component, PHEMA, can act as a negative-tone photoresist upon addition of a photoacid generator and crosslinker. Control of self assembly has been demonstrated by annealing in a vapor of 2-methoxyethanol. Morphology tuning is possible by controlling the degree of swelling: annealing for moderate times leads to formation of hexagonally packed parallel cylinders, and we observe a transition to spherical morphology upon further swelling.

4.2 Introduction

As photolithography approaches limitations for achieving small resolution requirements for patterning, block copolymer self assembly has received attention for future patterning applications. Block copolymer self assembly holds promise for patterning length scales in the sub-30 nm region, smaller than is possible today by high volume photolithography. Block copolymers self-assemble into a variety of morphologies, typically including spherical, cylindrical, and lamellar morphologies[1] each of which offers new possibilities for high-resolution patterning. Utility for applications requires long-range ordering combined with secondary ordering techniques to gain long-range ordering and to further control orientation of anisotropic morphologies, and good progress is being made in these areas.

We have previously demonstrated combined top-down/bottom-up patterning with the block copolymer poly(α-methylstyrene)-*block*-poly(4-hydroxystyrene), or PαMS-*b*-PHOST, with 33% PαMS minor phase.[2,3] PHOST is a well known deep-UV negative-tone photoresist when combined with small quantities of a photoacid

generator and crosslinker and in block copolymer form has a resolution of 450 nm. This combined system allows not only self assembly of sub-50 nm features but also the very precise placement of the self-assembled block copolymer itself in an arbitrary pattern.

Here we introduce a new block copolymer capable of patterning by combined top-down/bottom-up techniques, poly(methyl methacrylate)-*block*-poly(hydroxyethyl methacrylate), or PMMA-*b*-PHEMA. Like PHOST, PHEMA can be photocrosslinked upon addition of a photoacid generator and crosslinker.[4,5] PMMA is an easily synthesized and easily removed block, even more readily removed than poly(α-methylstyrene). For example, in the commonly used polystyrene-*block*-poly(methyl methacrylate) system, the PMMA block has proven easy to remove by UV exposure followed by selective solvent washing.[6] An earlier attempt to use poly(4-hydroxystyrene)-*block*-poly(methyl methacrylate) for combined patterning was unsuccessful, as the PMMA and PHOST blocks were found to be miscible even with large molecular weight.[7] In contrast, PMMA-*b*-PHEMA has been found here to phase separate cleanly in addition to being photopatternable, making it a good candidate for combined patterning.

Patterning applications require a high degree of precision; block copolymers used for these applications must self-assemble with a high degree of order, often requiring control of both the size and the orientation of self-assembled domains as well as orientation control. Secondary ordering techniques have been used to further control ordering of thin films, including use of neutral substrates,[8-11] graphoepitaxy,[12-17] chemical epitaxy,[18-22] electric fields,[23-26] and shear forces.[27-29] However, these secondary techniques must be used in tandem with processes that allow self assembly to occur, all of which enable enhanced polymer chain mobility.

Formation of long-range ordering of self-assembled patterns in block copolymers is made possible by providing polymer chain mobility. Many common block copolymer components have glass transition temperatures (T_g) well above room temperature, and the most common method for achieving self assembly is to heat the block copolymer above the T_g of the blocks. Alternatively, mobility of the block copolymer is achieved by swelling the block copolymer in a solvent vapor and lowering the effective T_g,[30-32] providing another method of gaining long-range ordering in thin films.[33-37] For example, in the case of PαMS-*b*-PHOST, solvent swelling provides sufficient mobility for long range ordering to occur, and solvent selectivity dictates the morphology formed.[37] Annealing in tetrahydrofuran (THF), a nonselective good solvent for both blocks, leads to parallel cylinders of PαMS, an expected morphology given the PαMS mass fraction of 33%. Thus solvent annealing is particularly useful for gaining self assembly in block copolymers that undergo thermal degradation at temperatures below the T_g of the blocks, as is the case for PαMS-*b*-PHOST. Another advantage is the ability to tune morphology in the swollen state. Annealing in a selective solvent, can cause order-order transitions in the swollen state.[33,34] In PαMS-*b*-PHOST we observe this when annealing in acetone, selective for the PHOST majority component, which leads to a formation of spherical morphology in the swollen state, and the spherical morphology is then kinetically trapped in the dried state.[37]

Observation of the order-order transition upon selective solvent swelling reminds us that not only does the solvent afford polymer mobility, but it also has an effect on the phase behavior in the swollen state. Bulk studies of the blending of a block copolymer that is completely selective for one block – that is, a solvent for one block and a nonsolvent for the other – leads to order-order transitions to other

morphologies.[38-40] This can be visualized as a horizontal shift in the phase diagram of the neat polymer, as demonstrated in Scheme 4.1.

Alteration of the phase behavior is also observed in bulk studies of block copolymers blended with nonselective good solvents.[41-43] The dilution approximation states that an effective Flory-Huggins interaction parameter, χ_{EFF}, for the swollen diblock copolymer is found to be lower than that of the neat block copolymer, χ_{AB}. This occurs because the solvent selectively segregates at the interface of the two blocks in the assembled polymer, decreasing the interaction between the two blocks. The degree of this depression, χ_{EFF}, is given by $\chi_{EFF} = \chi_{AB}\phi_P^{\alpha}$, where χ_{AB} is the interaction parameter for the diblock copolymer, ϕ_P is the concentration of polymer in the blended material, and α is an exponent to reflect non-ideal behavior observed in experiments (the dilution theory states that $\alpha = 1$). Experimentally, values of α are typically 1.0 for order-order transitions and 1.3 to 1.6 for the order-disorder transition, and the values vary depending on the solvent and block copolymer system.[42] This overall behavior can be visualized as a downward vertical shift in the phase diagram (Scheme 4.1).

In the case of solvent annealing thin films, plasticization by the swelling solvent leads to depression of the T_g below room temperature;[32] phase behavior effects are secondary. In bulk studies of the phase behavior of block copolymers blended with either selective or nonselective solvents, mobility in both blocks is still achieved by thermal annealing. In the case of thin films processed using solvent annealing, however, mobility must be achieved by plasticization in both blocks for self assembly to occur, and thus both blocks must be swollen sufficiently to decrease their respective glass transition temperatures below room temperature. This is easily achieved when swelling in a nonselective good solvent, but becomes more complicated in the case of a selective solvent. If a block copolymer film is subjected to a solvent that is selective

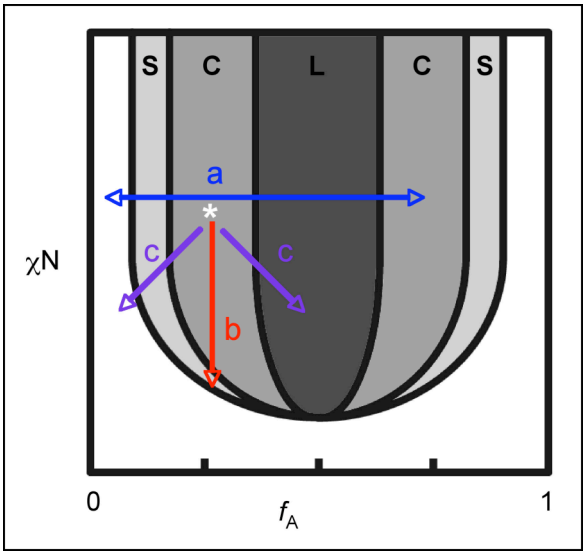

Scheme 4.1. Block copolymer morphology behavior upon blending with a solvent, as understood in a hypothetical phase diagram. The location of the white asterisk indicates the position in the phase diagram of an unswollen block copolymer alone. a) Adding a solvent completely selective for one block (and a nonsolvent for the other) can cause a shift in the relative volume fraction of the blocks, corresponding to horizontal shifts (blue arrow). b) Blending a nonselective good solvent for both blocks depresses the Flory-Huggins interaction parameter χ, visualized as a downward shift in the phase diagram (red arrow). This can also cause morphological transitions if the volume fraction of the initial block copolymer is asymmetric. c) In the case of solvent annealing a glassy block polymer, both blocks must be swollen in order to depress the T_g of each block to allow mobility. Thus, in the case of solvent annealing with a selective block, the two components of annealing (horizontal shift due to solvent preference, vertical shift due to alteration of χ) visualized as a diagonal movement (purple arrows)

for only one block, no annealing effects are observed in the unswollen block. Immersion into such a solvent can lead to partial pore formation in the dissolved block, especially if the undissolved block is the majority component and anchors the material to the substrate.[44] Thus, in order to gain long range order when annealing with a selective solvent, even the less soluble block must be somewhat soluble in order for its T_g to be depressed. If we visualize a shift in the phase diagram upon annealing in a selective solvent, we expect there to be a selective volume shift in the polymer (horizontal component to shift) as well as alteration of the Flory-Huggins interaction parameter (downward vertical component to shift): the overall effect is a diagonal shift in the phase diagram (Scheme 4.1).[37]

The evaporation of solvent from films has been demonstrated in other systems to control orientation of cylindrical morphologies. Stamm et al. observed different behavior upon evaporation of a bulk-cylinder forming block copolymer swollen to spherical morphology: collapse to perpendicular orientation is observed.[33,34] Formation of perpendicular orientations under controlled evaporation conditions has been demonstrated for other block copolymer systems as well.[45-48] Thus, in the case of solvent annealed films in particular, it is very important to distinguish perpendicular cylindrical morphologies from spherical, which can appear the same in surface techniques. This requires observation of morphology throughout the films.

Solvent annealing has proven useful for enabling long range ordering in PMMA-*b*-PHEMA and is reported here. This polymer has demonstrated interesting solvent behavior upon annealing in a vapor of 2-methoxyethanol (2MOE), chosen because of its nonselectivity for the two blocks.[49] Sufficient mobility for self assembly is demonstrated for moderate swelling, in which parallel cylinders of PMMA are formed in agreement with the volume fraction of the block copolymer. At higher swelling ratios, however, an order-order transition to spherical morphology is

observed. This provides a method for tuning morphology formed using degree of solvent swelling, proving again that solvent annealing has advantages over thermal annealing. In contrast, thermal crosslinking of PMMA-*b*-PHEMA occurs upon heating above the T_g for the blocks, rendering thermal annealing incapable of producing such long range ordering.

4.3 Methods

The synthesis of PMMA-*b*-PHEMA follows previously published procedures.[50-52]

4.3.1 Materials.

Chemicals were obtained from Aldrich and used without further purification, unless otherwise noted. Methyl methacrylate (MMA) and 2-(trimethylsilyloxy)ethyl methacrylate (TMS-HEMA) monomers were each placed in a flamed flask outfitted with outfitted with a Rotoflo valve and were degassed repeatedly (freeze, pump, thaw). Trioctylaluminum (25% in hexanes) was added dropwise until a faint yellow color persisted. The monomers were then distilled under high vacuum prior to use. 1,1-Diphenylethylene was purified in the same manner, using *n*-butyl lithium (2.5 M in hexanes) instead of trioctylaluminum.

Tetrahydrofuran was refluxed under nitrogen for 3 days with calcium hydride, and then distilled under vacuum to a flask containing sodium and benzophenone. The THF was degassed repeatedly until a purple color persisted. Lithium chloride (LiCl, anhydrous, ≥98%, Fluka) was dried in high vacuum at 300 ˚C for 3 days and stored under nitrogen. A 10x molar excess (with respect to the initiator) of dry LiCl (240 mg) was added to the reaction vessel outfitted with a Rotoflo valve and attached to the vacuum line. The flask containing LiCl was flamed and then left under vacuum

overnight until ready for use. Immediately before polymerization, THF was distilled into the flask containing dry LiCl.

4.3.2 Polymer Synthesis.

The synthesis strategy of PMMA-*b*-PHEMA is shown in Scheme 4.2. Poly(methyl methacrylate)-*block*-poly(2-(trimethylsilyloxy)ethyl methacrylate) was synthesized by sequential living anionic polymerization in THF (600 mL) at -78˚C. 1,1-diphenyl-3-methylpentyllithium (DPHLi) was used as an initiator for the anionic polymerization and was generated in situ by the reaction of *sec*-butyllithium (1.4M solution in cyclohexane) with an excess of 1,1-diphenylethylene (0.4 mL, 10x excess to initiator) in THF at -78 °C. MMA (5 mL) was polymerized first for 65 min and a small aliquot of PMMA was terminated with degassed methanol. 18 mL of TMS-HEMA was introduced to the reactor and the reaction was terminated with degassed methanol after 85 min. An aliquot of was precipitated into cold water and dried overnight under vacuum for molecular weight characterization by GPC in THF. The transparent solution of the PMMA-*b*-P(TMS-HEMA) diblock copolymer in THF became opalescent by addition of 10 mL of concentrated hydrochloric acid and changed to a white emulsion when the reaction was completed. The PMMA-*b*-PHEMA was precipitated into a large excess of cold water, filtered and dried under vacuum until constant mass.

4.3.3 Polymer Purification & Characterization

Three dissolve/precipitate cycles further purified the polymer using a 1:1 mixture of methanol and THF to dissolve the polymer and diethyl ether to precipitate the polymer. Complete deprotection was confirmed using FTIR. Gel permeation chromatography indicated the number average molecular weight of PMMA to be 11

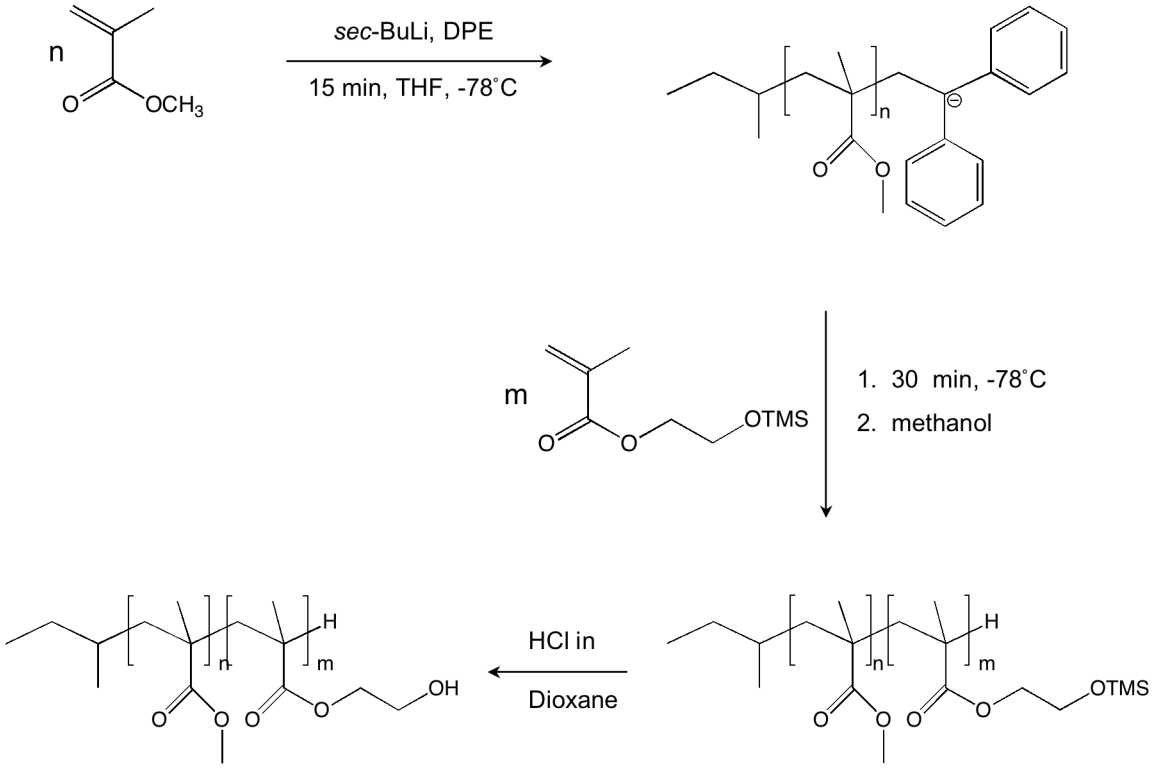

Scheme 4.2. Synthesis of PMMA-*b*-PHEMA.

kg/mol, molecular weight distribution (D) 1.06; the M_n of the PMMA-*b*-PHEMA diblock copolymer is 34 kg/mol with D 1.15 indicating the PHEMA block M_n is 23 kg/mol. The density of PMMA is known to be 1.17 g/cm^3, and the PHEMA density was calculated to be 1.43 g/cm^3.[53] This corresponds to a PMMA volume fraction of f_{PMMA} 0.37. While the accuracy of the additive Fedor estimation of PHEMA density is unknown, the volume fraction suggests formation of either cylindrical or lamellar morphology.

4.3.4 Film Preparation & Solvent Annealing

Three film thickness ranges were prepared. A 5% PMMA-*b*-PHEMA solution in pyridine spin coated at 2000 RPM yielded thickness 257 nm. 5% solutions in ethyl lactate yielded thickness of 132 nm after spin coating at 1750 RPM; 2% in ethyl lactate, 42 nm at 1750 RPM. 2-methoxyethanol was chosen as a nonselective solvent for annealing. Annealing takes place in a closed container containing a monomer reservoir.

4.3.5 Photopatterning

To a 2% (w/v) solution of PMMA-*b*-PHEMA in ethyl lactate, 1.5% triphenylsulfonium triflate (TPST) and 4% tetramethoxymethyl glycoluril (TMMGU, "Powderlink 1174," Cytec Industries) relative to the block copolymer (w/w); the solution is filtered through 0.2 μm nylon syringe prior to spin coating at 1750 RPM. After spin coating, an ABM High Resolution Mask Aligner with 254 nm exposure is used for photopatterning. A post expose bake of 115˚C for 60 seconds is followed by development for 5 minutes in THF. The optimum exposure time is 6 seconds, corresponding to an exposure dose of approximately 39 J/cm^2.

4.3.6 Characterization.

Complete deprotection to PMMA-*b*-PHEMA was confirmed using FTIR. Gel permeation chromatography of THF solutions of polymers (1 mg/mL) was carried out using four Waters Styragel HT columns operating at 40 ˚C and Waters 410 refractive index detector. Thermogravimetric analysis (TGA) was carried out on a TA Instruments Q500 and differential scanning calorimetry (DSC) was carried out on a TA instruments Q1000, both using 10˚C scan rates. Grazing incidence small-angle X-ray scattering (GISAXS) experiments were carried out at the Cornell High Energy Synchrotron Source (CHESS) G1 line, and collected images were processed using the FIT2D program. Polymer film self assembly was observed using scanning electron microscopy (SEM, LEO 1550 FESEM) and atomic force microscopy (AFM, Veeco Dimension 3100). The spatial period was calculated using the power spectral density feature in Veeco Nanoscope version 5.3, with results accurate within ~5%. Alternatively, spatial period calculated by analysis of GISAXS is more precise. Film thickness was measured using a Filmetrics F20 reflectometer for films thicker than 100 nm (accuracy better than 5% for thickness greater than 50 nm), and a Nanofilm EP3 imaging ellipsometer for films 100 nm or less gives very high accuracy (± 1 nm or less).

4.4 Results & Discussion

PMMA-*b*-PHEMA is of interest for its ability to produce both self-assembled block copolymer films and its ability to undergo photopatterning, which enables precise location control of self-assembled structures. Here we discuss both characteristics of this polymer and focus initially on the use of solvent annealing to produce a self-assembled structure.

Long-range order formation of PMMA-*b*-PHEMA was observed after annealing in 2-methoxyethanol vapor (2MOE). We chose 2MOE because it has been demonstrated to be largely nonselective for PMMA-*b*-PHEMA.[49] Calculation of its selectivity for PMMA-*b*-PHEMA was unsuccessful due to the wide range of solubility parameters determined experimentally for PMMA (see supporting information 4.7.1). In this case, we have chosen films with thickness of 257 nm, well above the periodicity of the polymer in order to clearly distinguish perpendicular cylindrical morphologies from spherical ones.

PMMA-*b*-PHEMA annealing was carried out in a sealed jar containing a small monomer reservoir. As the solvent vapor increased concentration within the jar and reached equilibration, the degree of swelling increased. Thus, a longer period of time in the jar corresponds with a larger swelling ratio. We observed the development of morphology over time in films annealing in 2MOE, as seen in by atomic force microscopy images in Figure 4.1. Upon spin coating from 2MOE, films are largely featureless. After annealing for 5 hours, films clearly display some phase separation, but no long range ordering is observed; spatial period of 25 nm is observed. After 45 hours, we observe a fingerprint pattern consistent with parallel cylinder formation; periodicity of 26 nm is observed. After 72 hours, we see near-complete transformation from the fingerprint pattern to a hexagonal array of dots; spacing has decreased to 20 nm. This pattern could be consistent with transformation to perpendicular cylinders or to spherical morphology.

Grazing incidence small angle X-ray scattering, GISAXS, was used to probe the interior of the films (Figure 4.2), and results are found to be in strong agreement with the observation of the surface structures by AFM. The angle of incidence was chosen slightly above the critical angle of the films not only to maximize the signal, but also to probe the entire thickness of the film; the critical angle is 0.145, and the

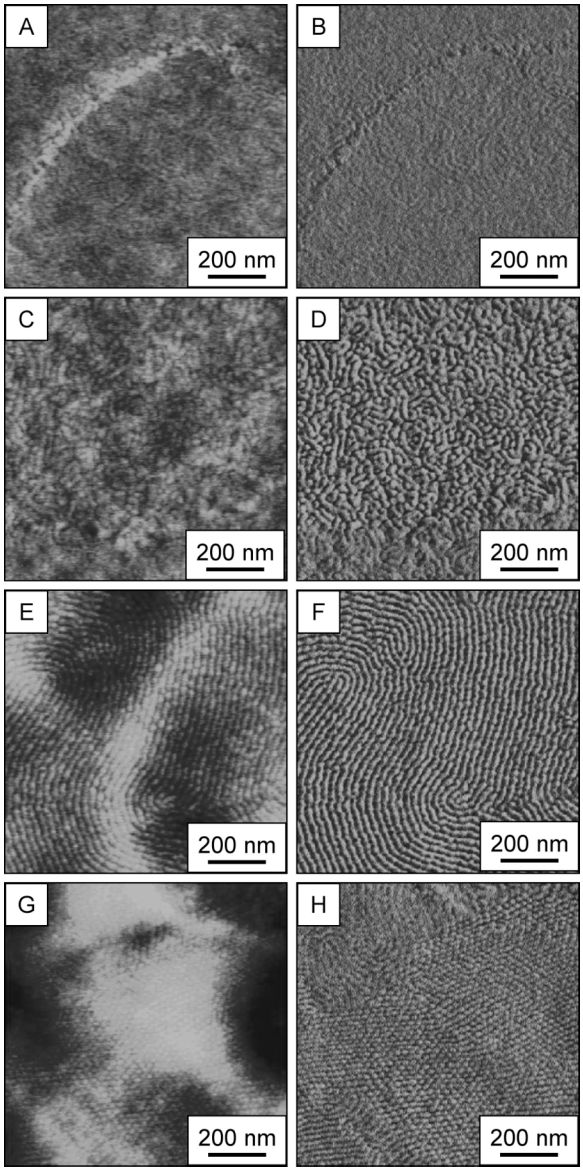

Figure 4.1. PMMA-*b*-PHEMA films 257 nm thick after spin coating (a-b), and after annealing in 2MOE for 5 hours (c-d), 45 hours (e-f), and 72 hours (g-h). Left column of images are atomic force microscopy height images; right column are the corresponding phase images.

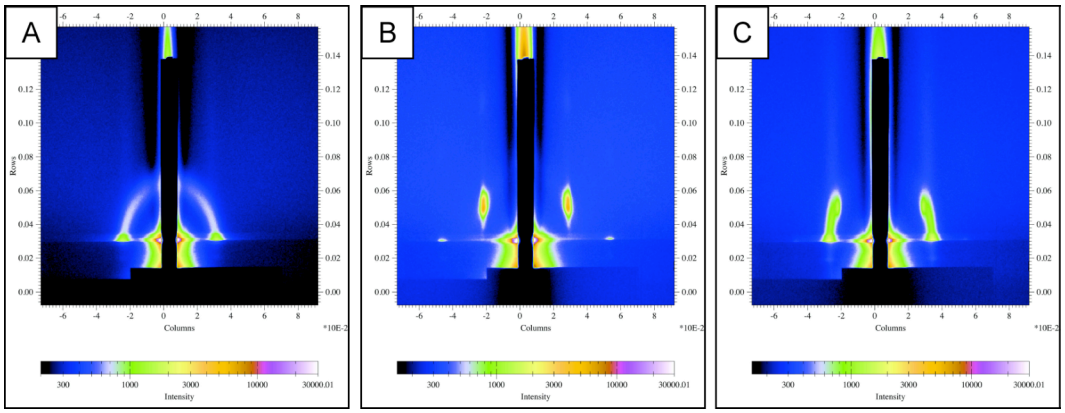

Figure 4.2. GISAXS images of PMMA-*b*-PHEMA after annealing in 2MOE for a) 5 hours, (disordered morphology), b) 45 hours (parallel cylinders), and c) 72 hours (mixed parallel cylinders and spheres).

incident angle used here is 0.150. Films annealed for 5 hours possessed a ring structure in the GISAXS image (Figure 4.2a). The ring structure indicates a disordered morphology, consistent with AFM in Figure 4.2b. We used the peaks along the Yoneda band to characterize the spacing of this sample. The Yoneda band is defined as the bright horizontal band appearing near the bottom of the image; it results from an enhancement of scattered intensity due to the Vineyard effect when the exit angle of the scattered beam is between the critical angles of the sample film and the substrate.[54] In Figure 4.2a, the appearance of Bragg rods perpendicular to the surface indicates a standing cylinder morphology. However, no higher order Bragg rods are seen – this indicates that there is only short range order in the packing of the cylinders. In order to calculate the nearest-neighbor spacing of the cylinders we model the system as hexagonally-packed cylinders. The resulting spacing of 26 nm is in good agreement with the 25 nm spacing observed in the AFM.

The elongation of the ring in the vertical direction, compared to a perfect hemisphere, is consistent with a contraction in the morphology due to evaporation of the solvent, and a 14.5% contraction from the swollen film value is calculated. Contraction of film morphology perpendicular to the plane of the film has been observed in other solvent annealed systems as well.[37,45]

According to the GISAXS results, films annealed for 45 hours display parallel cylindrical morphology with hexagonal packing, indicated by the off-specular first order peak and the second order peak located at the Yoneda band (Figure 4.2b). By modeling the system as hexagonally packed parallel cylinders, the peak positions correlate to a nearest neighbor period of 25 nm, in agreement with the 26 nm from the AFM image. The off-specular location of the first order peaks again are located in a different position than expected for perfect hexagonal packing of cylinders; thus contraction effects due to evaporation again seem to have occurred. A contraction of

32% of the swollen film value was calculated for this sample, consistent with a higher swelling ratio after the longer anneal time.

After annealing for 72 hours, the peaks from the 45 hour GISAXS image are maintained, but an additional peak at the Yoneda band and first-order Bragg rods appear. The additional peak at the Yoneda band is consistent with a face-centered orthorhombic (fco) spherical morphology. The two peaks for hexagonally-packed parallel cylindrical morphology, observed to a small degree in the AFM, overlap with the fco peaks and cannot be distinguished. The observed mixed morphology indicates that we are very near the solvent-induced order-order transition for this system. Further swelling would be expected to allow full transformation to spherical morphology. The spatial period of the lateral spacing is found to be 21 nm, in agreement with the 20 nm spacing observed in the AFM.

The weak Bragg rod above this peak is consistent with partial collapse of the spherical morphology to a perpendicular cylindrical morphology, observed in several other block copolymer systems due to gradient solvent evaporation effects.[33,34,45] The weakness of the Bragg rods indicate that this is only observed to a small degree here.

To summarize these results: we gain mobility with sufficient swelling (45 hours), which allows the cylindrical morphology, a likely bulk structure of PMMA-*b*-PHEMA, to form. At longer anneal times, an order-order transition to spherical morphology is observed. The decrease in periodicity from 26 nm (5 hours) to 25 nm (45 hours) and 21 nm (72 hours) is consistent with literature indicating a decrease of block copolymer periodicity with increased blending of a nonselective solvent,[55,56] indicating that polymer films swell more at longer anneal times. Larger swelling at longer anneal times is also observed in the increased contraction of films at 45 hours of annealing than for 5 hours of annealing. Thus we conclude that the order-order

transition observed in films swelled for longer period of time is due to more solvent in the swollen film.

We can understand this behavior in terms of a hypothetical phase diagram, Scheme 4.3. Due to the mass fraction composition of the studied PMMA-*b*-PHEMA block copolymer, we would expect a cylindrical or lamellar morphology to form in the bulk, given sufficient mobility. Two different scenarios can explain the behavior of the order-order transition demonstrated using GISAXS. If 2MOE is completely nonselective for the two blocks, we would observe a downward vertical shift in the location in the phase diagram upon swelling, forming cylinders in 2MOE and then transitioning to spherical morphology in the weak-field regime. Alternatively, even a small degree of selectivity can lead to a shift in relative volume fractions at very high swell ratios, leading to an order-order transition in a more strongly-segregating region of the phase diagram. The estimation of Flory-Huggins interaction parameters of the solvent with PMMA and PHEMA are demonstrated in the supporting information (section 4.7), though they cannot be estimated with any degree of accuracy due to the wide range of solubility parameters demonstrated for PMMA. They do indicate, however, that 2MOE may be nonselective to PMMA and PHEMA or it may be selective for PHEMA, supporting both of these scenarios.

We chose thick films for initial solvent annealing tests, but this behavior has also been observed for thinner films as well (Figure 4.3). Here we demonstrate cylindrical morphology of 132 nm and 42 nm thickness films by AFM. Similar morphology transition behavior from cylindrical to spherical morphology is also observed using AFM, but is not demonstrated here.

An important aspect of our selection of PMMA-*b*-PHEMA is its ability to undergo lithographic patterning. A photopattern of a film of PMMA-*b*-PHEMA with trace quantities of TPST photoacid generator and TMMGU crosslinker can be

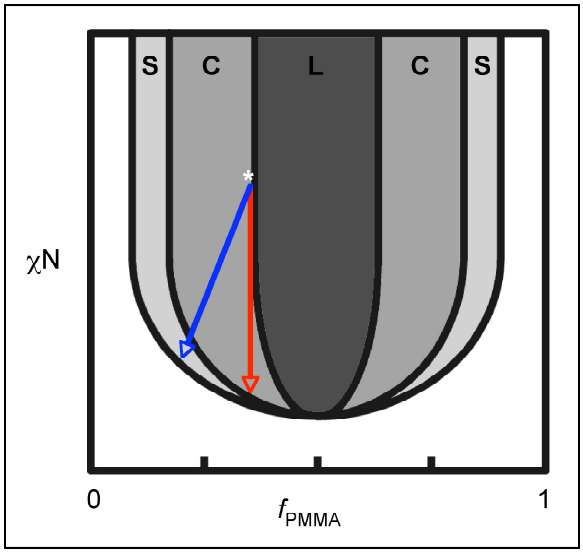

Scheme 4.3. A hypothetical phase diagram indicating two scenarios to explain the shift in morphology due to solvent swelling of PMMA-*b*-PHEMA with 2MOE. The white star indicates a possible position of the neat PMMA-*b*-PHEMA in the phase diagram. It is placed in agreement with f_{PMMA} of 0.37 calculated for this sample; the χN value cannot be calculated with accuracy, and so the placement of * is arbitrary in the y axis. The transition from cylindrical to spherical morphology could occur both for nonselective (red, vertical) and selective swelling (blue, diagonal).

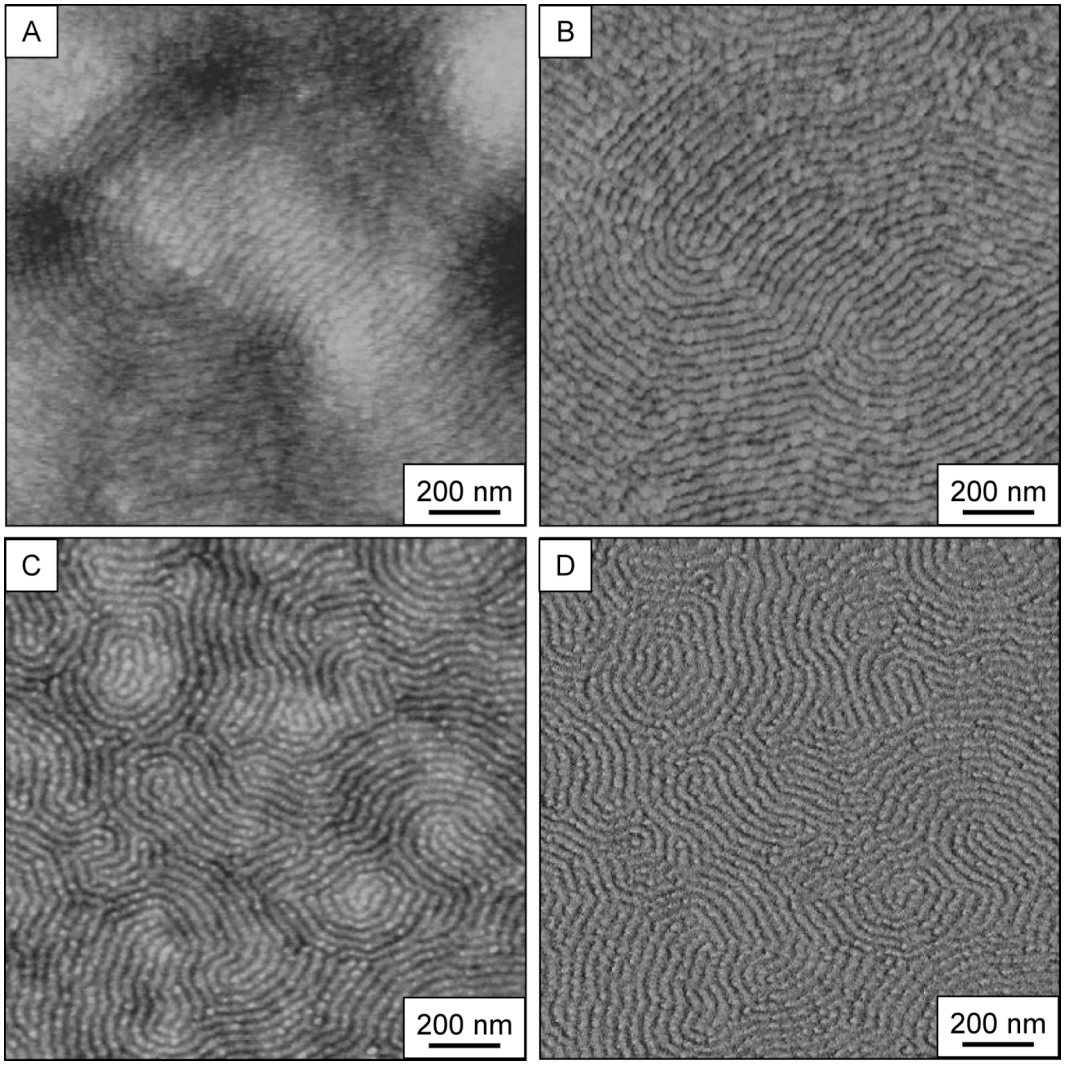

Figure 4.3. AFM images of thinner films with different thickness display cylindrical morphology upon annealing. Films 132 nm thick (a-b) and 42 nm thick (c-d) display fingerprint pattern, though grain sizes differ. Height images are shown on the left, phase images are shown on the right.

produced after exposure and development in THF. As shown in Figure 4.4, patterns with resolution of 1 μm have been demonstrated. This resolution is consistent with our use of a mask aligner. A higher resolution would be expected for patterning with a DUV stepper or another high-resolution patterning technique. Use of a mask aligner demonstrates proof of patternability of the diblock copolymer has been demonstrated.

Two important considerations are the impact of the photoacid generator and crosslinker inclusion on the self assembly and the effect that solvent annealing has on subsequent photopatterning. These films were not solvent annealed prior to photopatterning, but we have previously demonstrated little impact on photopatterning after solvent annealing in other block copolymers.[37] We have also shown here that small quantities (less than 5% w/w relative to block copolymer) of photoacid generator triphenylsulfonium triflate (TPST) and crosslinker tetramethoxymethylglycoluril (TMMGU) do not interfere with self assembly of other polymer systems, as long as solvent annealing occurs under dark conditions.

PHEMA-*b*-PMMA was originally intended to be used as a thermally stable block copolymer capable of gaining long range ordering via thermal annealing. We now believe this is not the case. The T_g of the block copolymer was found to be 119˚C by DSC (Figure 4.5); the observation of only a single T_g for the system is most likely due to the very similar glass transition temperatures of PMMA and PHEMA.

We also observe the onset of decomposition at approximately 300˚C by thermogravimetric analysis, indicating that thermal decomposition occurs well above the T_g of the block copolymer. Films thermally annealed in a vacuum oven for 24 hours at 180˚C are featureless in the AFM (Figure 4.6a). There are several possible explanations for why we do not observe morphology in thermally annealed films. The first possibility is that a parallel lamellar morphology forms upon annealing, which

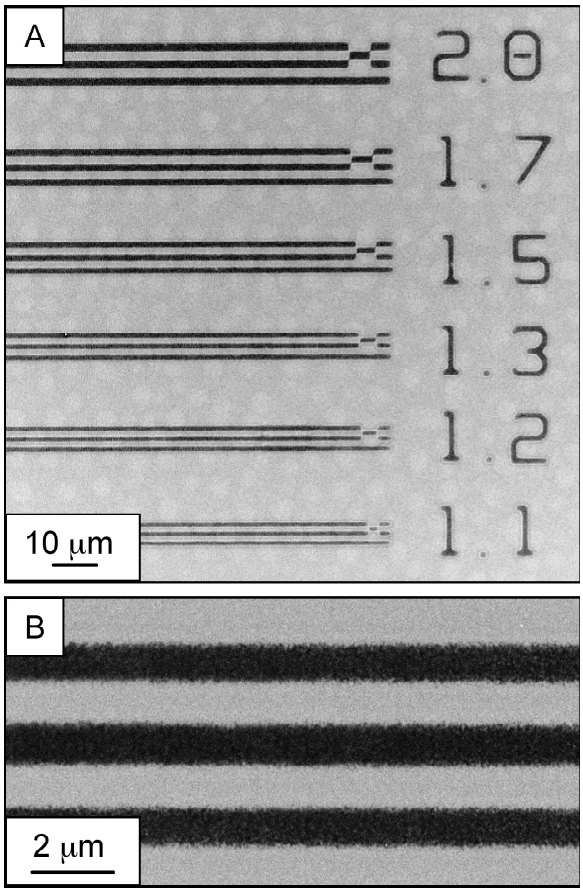

Figure 4.4. The dark lines seen in SEM are crosslinked PMMA-*b*-PHEMA photopatterns after development in THF. A) Numbers represent the line width in μm; B) 1 μm line width are near the resolution limit for patterning with a mask aligner.

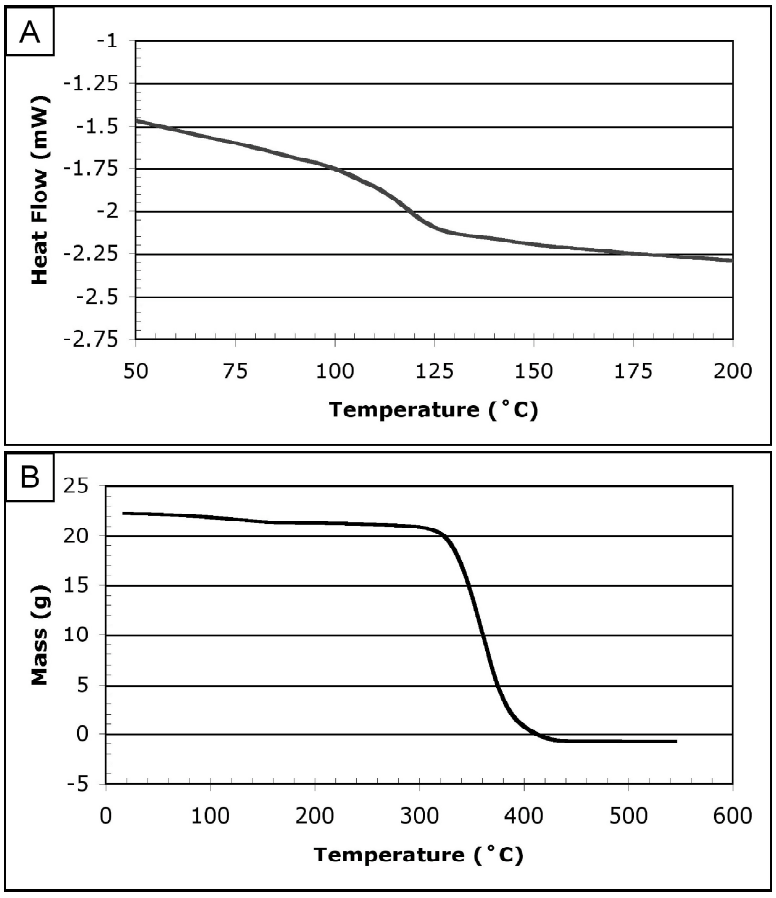

Figure 4.5. Thermal analysis of PMMA-*b*-PHEMA. A) Differential scanning calorimetry (DSC) indicating a glass transition 119˚C, according to midpoint of second heat scan. B) Thermogravimetric analysis (TGA) showing decomposition onset near 300˚C

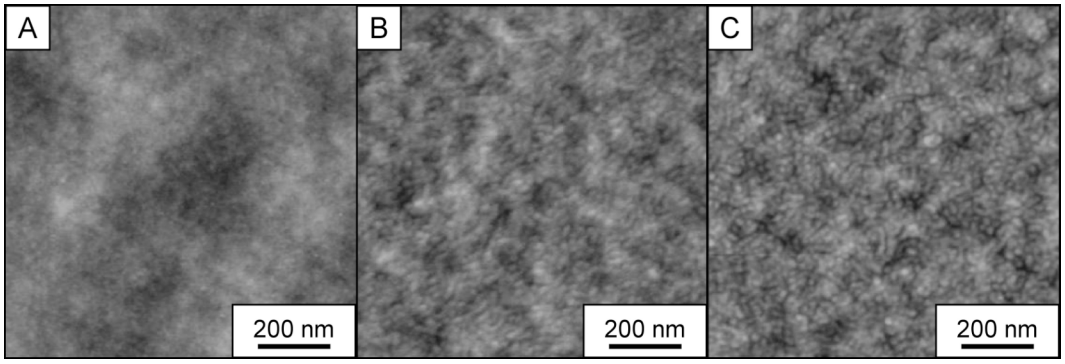

Figure 4.6. AFM height images of thermally annealed films. a) After annealing for 24 hours at 180˚C, the film displays no visible morphology. b) A film thermally annealed at 180˚C for 24 hours, followed by solvent annealing in 2MOE for 20 hours (a condition that would form parallel cylinders in unheated films) shows roughness indicating some phase separation, though no fingerprint pattern consistent with parallel cylinders. c) A film thermally annealed at 125˚C, near the T_g of the polymer, and then annealed in 2MOE for 20 hours possesses the same disordered morphology. Switching tests (b, c) indicate that thermal annealing damages the films, and thus is not an option for gaining long range ordering.

would appear featureless on the surface. The second possibility is that cylindrical morphology exists in the film, but a surface wetting layer prevents observation of the morphology by AFM. Typically, though, AFM can detect morphologies located below a wetting layer, making this unlikely. A third possibility is that the morphology undergoes a thermoreversible transition to disordered state upon heating. Estimation of the interaction parameter for the diblock is inconclusive for this possibility (see supporting information, section 4.7.2). The film in Figure 4.6a was quenched quickly from 180˚C, trapping any morphology present in the heated state. However, films that were cooled very slowly displayed the same lack of morphology (not shown), indicating that the lack of features in the AFM is not because the film is disordered at 180˚C.

A final possibility is that PMMA-*b*-PHEMA films undergo thermal degradation upon heating. We used the switching ability of solvent annealing to investigate if films are thermally degraded. We have previously demonstrated the ability of solvent annealing in different solvents to change morphology[37]. With PαMS-*b*-PHOST, annealing in nonselective solvent THF leads to parallel cylinder formation, while annealing in majority-selective acetone leads to an order-order transition to spherical morphology. Switching orientation by sequential solvent anneal sessions indicates that the morphology formed upon solvent annealing is independent of annealing history, so long as film degradation does not occur.[57]

In the case of PMMA-*b*-PHEMA, if films are degraded upon thermal annealing, we should observe different solvent annealing behavior in films heated prior to solvent annealing (Figure 4.6b-c). Two 42 nm films are spin coated, and one was annealed for 24 hours at 180˚C, the other 125˚C for 24 hours. The films were then solvent annealed under conditions that provided parallel cylinders in as spun films (compare with Figure 4.3c-d). No fingerprint pattern was observed for films

thermally treated prior to solvent annealing, strongly supporting the hypothesis that degradation occurs during thermal annealing, even when films are heated to temperatures near the glass transition of the polymer.

If thermal decomposition of one block occurred, we would expect a large decrease in the film mass and thickness, while a small contraction of the thickness would result from thermal crosslinking. TGA indicates spontaneous decomposition of the material beginning at approximately 300˚C (Figure 4.5b), far above the thermal anneal temperatures, though this does not address decomposition over a longer period of time at lower temperatures. The thicknesses of the films from Figure 4.6 were compared with that of an untreated spin coated film in Table 4.1. Since we observe only a small contraction in the thickness upon thermal annealing, we conclude that thermal crosslinking, not thermal decomposition, prevents development of long range ordering.

Table 4.1.

Anneal Treatment, 24 hour	Film Thickness
Room Temperature, air	42 nm
125˚C, vacuum	41 nm
180˚C, vacuum	38 nm

While we have observed that it is not possible to gain long range ordering in PMMA-*b*-PHEMA films by thermal annealing, solvent annealing successfully provides a method for gaining long range ordering in this photopatternable block copolymer. Furthermore, the ability to tune the morphology from a cylindrical morphology to a spherical one with higher degree of swelling provides a method for tuning the morphology formed in the film, an advantage over thermal annealing.

4.5 Future Work

We propose that the solvent annealing behavior of PMMA-*b*-PHEMA in 2MOE be investigated further. First, correlation of morphology formed (as well as the kinetics of long range ordering for particular swell ratios) to the swell ratio would be helpful. This would be possible with a solvent annealing chamber in which film thickness of swollen film can be measured while swelling is controlled by a gas counter-flow.

Further study of different morphologies swollen with 2MOE would allow determination of degree of selectivity. If the solvent were completely nonselective, a symmetric block copolymer would not undergo any order-order transition, but would instead transition directly to the disordered state. If the solvent were slightly selective, transition to other morphologies would be observed. If tests to determine the Flory-Huggins interaction parameter for the neat block copolymer system were done, then an effective Flory-Huggins interaction parameter due to solvent swelling could also be calculated

Demonstration of the selective removal of PMMA from self-assembled PMMA-*b*-PHEMA films has proven difficult using UV exposure and selective solvent washing. The similarity of structure of PMMA and PHEMA leads to degradation of both blocks. We are confident that PHEMA can be made stable given sufficient crosslinking density, allowing selective removal of only the PMMA block. Another method to investigate is selective plasma etching.[58,59]

However, not all patterning techniques require the selective removal of one block. For example, the Wiesner group has investigated the selective segregation of oxide precursors into a variety of block copolymers to yield hybrid materials with altered self assembly; porous monolithic oxides are possible after polymer removal.[3,60-62] Studies of PMMA-*b*-PHEMA films blended with both metal oxide

precursors and photoacid generators and crosslinkers could also be investigated to allow lithographically patternable porous oxide films.

Now that self assembly of PMMA-*b*-PHEMA has been demonstrated, application of secondary ordering techniques can be investigated. One intriguing idea is to use random copolymers composed of PMMA and PHEMA (PMMA-*ran*-PHEMA) grafted to the substrate to achieve neutral wetting conditions for perpendicular orientation of morphologies. Perpendicular orientation of cylindrical and lamellar morphologies are appealing for high aspect ratio patterning methods.

Neutral substrate wetting has been extensively used to gain perpendicular morphologies of with polystyrene-*block*-poly(methyl methacrylate), PS-*b*-PMMA.[8] This is primarily achieved by grafting random copolymers of hydroxyl-terminated PS-*ran*-PMMA to the silicon oxide substrate, though the synthesis of these hydroxyl-terminated random copolymers is a multi-step process.[63] The Gopalan group recently demonstrated substrate neutralization for PS-*b*-PMMA using random copolymers synthesized from styrene, methyl methacrylate, and a small amount (1-2%) of hydroxyethyl methacrylate, PS-*ran*-PMMA-*ran*-PHEMA.[9] The preparation of this material is simpler, and the hydroxyl moieties from the HEMA component allow grafting of the material to the substrate. In the case of PMMA-*b*-PHEMA, random copolymers of PMMA-*ran*-PHEMA contain hydroxyl moieties for easy grafting the substrates.

However, neutral substrate techniques often only work for monolayer-thickness films – in more than a single layer, preferential attraction of one block to the air interface overcomes the neutralization condition at the surface, leading to parallel morphologies. In some solvent annealing systems block copolymers, solvent annealing lowers the surface tension, leading to neutral wetting at the air interface.[35,64,65] The use of PMMA-*ran*-PHEMA neutral substrates combined with solvent annealing

conditions that lead to neutral air interfaces could lead to perpendicular morphologies in very thick films.

4.6 Acknowledgements

This work was supported by the National Science Foundation Materials World Network (award DMR 0602821) and the NSF NIRT (award CTS 0304159), and the Semiconductor Research Consortium. JKB was supported by fellowships from Motorola and IBM. This work was performed using facilities at the Cornell High Energy Synchrotron Source (CHESS), the Cornell Center for Materials Research (CCMR), and The Cornell NanoScale Facility (CNF). CHESS is supported by the NSF and the National Institutes of Health/National Institute of General Medical Sciences under NSF award DMR-0225180. CCMR is supported by NSF award DMR 0520404, part of the NSF MRSEC Program. CNF, a member of the National Nanotechnology Infrastructure Network, is supported by NSF award ECS-0335765. Dr. Detlef-M. Smilgies of CHESS assisted with the collection and interpretation of GISAXS data.

4.7 Supporting Information

4.7.1 Estimation of Polymer-Solvent Interaction Parameter

The Flory-Huggins interaction parameter χ for a polymer-solvent interaction has both enthalpic and entropic components.[66]

$$\chi = \chi_H + \chi_S \qquad \text{Eqn. 4.1}$$

The criterion for complete polymer miscibility is $\chi<0.5$. The entropic component is typically between 0.3 and 0.4 for nonpolar systems, and $\chi_S = 0.34$ is often used. The entalpic contribution may be estimated from the Hildebrand solubility

parameters for the solvent and the polymer dissolved, respectively δ_1 and δ_2, as well as the molar volume of the solvent, V_1.

$$\chi_H = \frac{V_1}{RT}(\delta_1 - \delta_2)^2 \qquad \text{Eqn. 4.2}$$

Here, T is the temperature and R is the universal gas constant (R = 8.314 J K^{-1} mol^{-1}). If the solvent molar volume V is not available, it may be calculated from the density (a more commonly available value), ρ, and the molecular weight *m* of the material.

$$V = \frac{m}{\rho} \qquad \text{Eqn. 4.3}$$

Thus, the combination of estimates for χ_H and χ_S can be combined to form[66]

$$\chi = \frac{V_1}{RT}(\delta_1 - \delta_2)^2 + 0.34 \qquad \text{Eqn. 4.4}$$

We can use these equations to estimate the interaction of 2-methoxyethanol (2MOE) for each of the blocks of poly(methyl methacrylate)-*block*-poly(hydroxyethyl methacrylate). The solubility parameter of 2MOE, δ_{2MOE}, is 24.7 $MPa^{1/2}$, and its molar volume V_{2MOE} is 78.8 cm^3/mol.[53] An experimentally-determined solubility parameter for PHEMA, δ_{PHEMA}, is 26.93 $MPa^{1/2}$.[67] A wide range of solubility parameters have been measured for PMMA. Van Krevelen lists values 18.6 to 26.4 $MPa^{1/2}$,[53] while the Polymer Handbook lists 22.69 $MPa^{1/2}$.[66] We use temperature of 298K (room temperature). We estimate $\chi s = 0.34$ here, though this may be a poor estimate due to the polarity of the system.

The results of these calculations may be found in Table 4.2. Given the wide range of experimentally-observed values for PMMA, we cannot make a definite conclusion about solvent selectivity. However, the ranges do indicate that 2MOE is

either nearly nonselective for PMMA and PHEMA or it is selective for PHEMA. Selectivity for PHEMA would be expected to cause increased PHEMA swelling, and thus a shift from PMMA cylinders to PMMA spheres as more 2MOE is added.

Table 4.2

Block	**δ_{block}, MPa$^{1/2}$**	**Source of δ_{block}**	**χ_H**	**$\chi_H+\chi_S$**
PHEMA	26.93	Van Krevelen	0.16	0.50
PMMA	18.6	Van Krevelen	1.18	1.52
PMMA	26.2	Van Krevelen	0.07	0.41
PMMA	22.69	Polymer Handbook	0.13	0.47

4.7.2 Estimation of Interaction Parameter of PMMA-b-PHEMA

Estimation of the interaction parameter of a block copolymer (the enthalpic term) may be achieved using the same equation

$$\chi_H = \frac{V(\delta_A - \delta_B)^2}{RT} \qquad \text{Eqn. 4.5}$$

except that an overall molar volume V is calculated from that of the two blocks, V_A and V_B:

$$V = \sqrt{V_A \times V_B} \qquad \text{Eqn. 4.6}$$

Calculation of the interaction parameter for PMMA-*b*-PHEMA requires a molar volume for each of the two blocks. Van Krevelen lists the molar volume of PMMA, V_{PMMA}, as 85.6 cm^3/mol.[53] An estimation of the PHEMA molar volume V_{PHEMA} yields 90.6 cm^3/mol using the additive Fedors method; likewise, an estimation of V_{PMMA} gives 81.9 cm^3/mol, relatively close to its observed value indicates that the additive method gives a fairly good estimate.[53] The degree of polymerization N is

calculated from the molecular weight of PMMA-*b*-PHEMA determined by GPC, PMMA block 11 kg/mol and PHEMA block 23 kg/mol, giving total $N = N_{PMMA} + N_{PHEMA} = 287$. We use the solubility parameters listed above for PMMA and PHEMA, calculating χ for the range of solubility parameters reported for PMMA. We also calculate the parameter using both room temperature (T = 298K) and the temperature at which samples were thermally annealed (T = 180˚C = 453K). The entropic component of the interaction parameter (χs) is ignored in the estimation of χN.

Table 4.3

δ_{PMMA}, $MPa^{1/2}$	Source of δ_{PMMA}	Temperature, K	χ_H	$\chi_H N$
18.6	Van Krevelen	298	2.47	708
26.2	Van Krevelen	298	0.02	5
22.69	Polymer Handbook	298	0.64	183
18.6	Van Krevelen	453	1.62	466
26.2	Van Krevelen	453	0.01	4
22.69	Polymer Handbook	453	0.42	121

The results are found in Table 4.3, using both room temperature and thermal anneal temperature of 180˚C (453 K). The results of the values are fully inconclusive due to the wide range of solubility parameters for PMMA: the polymer could be disordered or strongly segregating at both room temperature and at 180˚C. Based on our solvent annealing results, the real behavior lies somewhere between these extremes.

REFERENCES

(1) Bates, F. S.; Fredrickson, G. H. *Phys. Today* **1999**, *52*, 32-38.

(2) Li, M.; Douki, K.; Goto, K.; Li, X.; Coenjarts, C.; Smilgies, D.-M.; Ober, C. K. *Chem. Mater.* **2004**, *16*, 3800-3808.

(3) Du, P.; Li, M.; Douki, K.; Li, X.; Garcia, C. B. W.; Jain, A.; Smilgies, D.-M.; Fetters, L. J.; Gruner, S. M.; Wiesner, U.; Ober, C. K. *Adv. Mater.* **2004**, *16*, 953-957.

(4) Vasilopoulou, M.; Boyatzis, S.; Raptis, I.; Dimotikalli, D.; Argitis, P. *J. Mater. Chem.* **2004**, *14*, 3312-3320.

(5) Yang, S.; Ford, J.; Ruengruglikit, C.; Huang, Q.; Aizenberg, J. *J Mater Chem* **2005**, *15*, 4200-4202.

(6) Thurn-Albrecht, T.; Steiner, R.; DeRouchey, J.; Stafford, C. M.; Huang, E.; Bal, M.; Tuominen, M. T.; Hawker, C. J.; Russell, T. P. *Adv. Mater.* **2000**, *12*, 787-791.

(7) Chao, C.-Y., Cornell University, 2003.

(8) Mansky, P.; Russell, T. P.; Hawker, C. J.; Pitsikalis, M.; Mays, J. *Macromol.* **1997**, *30*, 6810-6813.

(9) Han, E.; Stuen, K. O.; La, Y.-H.; Nealey, P. F.; Gopalan, P. *Macromol.* **2008**, *41*, 9090-9097.

(10) Ham, S.; Shin, C.; Kim, E.; Ryu, D. Y.; Jeong, U.; Russell, T. P.; Hawker, C. J. *Macromol.* **2008**, *41*, 6431-6437.

(11) Mansky, P.; Russell, T. P.; Hawker, C. J.; Mays, J.; Cook, D. C.; Satija, S. K. *Phys. Rev. Lett.* **1997**, *79*, 237-240.

(12) Segalman, R. A.; Yokoyama, H.; Kramer, E. J. *Adv. Mater.* **2001**, *13*, 1152-1155.

(13) Cheng, J.; Mayes, A. M.; Ross, C. *Nature Materials* **2004**, *3*, 823-828.

(14) Bita, I.; Yang, J. K. W.; Jung, Y. S.; Ross, C. A.; Thomas, E. L.; Berggren, K. K. *Science* **2008**, *321*, 939-943.

(15) Jung, Y. S.; Ross, C. A. *Nano Letters* **2007**, *7*, 2046-2050.

(16) Xiao, S.; Yang, X.; Edwards, E.; La, Y.-H.; Nealey, P. *Nanotech.* **2005**, *16*, S324-S329.

(17) Park, S.-M.; Stoykovich, M. P.; Ruiz, R.; Zhang, Y.; Black, C. T.; Nealey, P. F. *Adv. Mater.* **2007**, *19*, 607-611.

(18) Kim, S. O.; Solak, H. H.; Stoykovich, M. P.; Ferrier, N. J.; de Pablo, J. J.; Nealey, P. F. *Nature* **2003**, *424*, 411-414.

(19) Kim, S. O.; Kim, B. H.; Meng, D.; Shin, D. O.; Chong, M. K.; Solak, H. H.; Wang, Q. W. *Adv. Mater.* **2007**, *19*, 3271-3275.

(20) Park, S.-M.; Craig, G. S. W.; Liu, C.-C.; La, Y.-H.; Ferrier, N. J.; Nealey, P. F. *Macromol.* **2008**, *41*, 9118-9123.

(21) Cheng, J. Y.; Rettner, C. T.; Sanders, D. P.; Kim, H.-C.; Hinsberg, W. D. *Adv. Mater.* **2008**, *20*, 3155-3158.

(22) Ruiz, R.; Kang, H.; Detcheverry, F. A.; Dobisz, E.; Kercher, D. S.; Albrecht, T. R.; de Pablo, J. J.; Nealey, P. F. *Science* **2008**, *321*, 936-939.

(23) Amundson, K.; Helfland, E.; Davis, D. D.; Quan, X.; Patel, S. S.; Smith, S. D. *Macromol.* **1991**, *24*, 6546-6548.

(24) Boeker, A.; Elbs, H.; Haensel, H.; Knoll, A.; Ludwigs, S.; Zettl, H.; Zvelindovsky, A. V.; Sevink, G. J. A.; Urban, V.; Abetz, V.; Mueller, A. H. E.; Krausch, G. *Macromol.* **2003**, *36*, 8078-8087.

(25) Morkved, T. L.; Lu, M.; Urbas, A. M.; Ehrichs, E. E.; Jaeger, H. M.; Mansky, P.; Russell, T. P. *Science* **1996**, *273*, 931-933.

(26) Thurn-Albrecht, T.; DeRouchey, J.; Russell, T. P.; Jaeger, H. M. *Macromol.* **2000**, *33*, 3250-3253.

(27) Angelescu, D. E.; Waller, J. H.; Adamson, D. H.; Deshpande, P.; Chou, S. Y.; Register, R. A.; Chaikin, P. M. *Adv. Mater.* **2004**, *16*, 1736-1740.

(28) Anglescu, D. E.; Waller, J. H.; Register, R. A.; Chaikin, P. M. *Adv. Mater.* **2005**, *17*, 1878-1881.

(29) Pelletier, V.; Adamson, D. H.; Register, R. A.; Chaikin, P. *App. Phys. Lett.* **2007**, *90*, 163105.

(30) Zielinski, J. M.; Duda, J. L. *AIChE Journal* **1992**, *38*, 405-415.

(31) Rauch, J.; Koehler, W. *J. Chem. Phys.* **2003**, *119*, 11977-11988.

(32) Mori, K.; Hasegawa, H.; Hashimoto, T. *Polymer* **1990**, *31*, 2368-2376.

(33) Sidorenko, A.; Tokarev, I.; Minko, S.; Stamm, M. *J. Am. Chem. Soc.* **2003**, *125*, 12211–12216.

(34) Tokarev, I.; Krenek, R.; Burkov, Y.; Schmeisser, D.; Sidorenko, A.; Minko, S.; Stamm, M. *Macromol.* **2005**, *38*, 507–516.

(35) Cavicchi, K. A.; Berthiaume, K. J.; Russell, T. P. *Polymer* **2005**, *46*, 11635-11639.

(36) Ludwigs, S.; Schmidt, K.; Stafford, C. M.; Amis, E. J.; Fasolka, M. J.; Karim, A.; Magerle, R.; Krausch, G. *Macromol.* **2005**, *38*, 1850-1858.

(37) Bosworth, J. K.; Paik, M. Y.; Ruiz, R.; Schwartz, E. L.; Huang, J. Q.; Ko, A. W.; Smilgies, D.-M.; Black, C. T.; Ober, C. K. *ACS Nano* **2008**, *2*, 1396-1402.

(38) Huang, C.-I.; Lodge, T. P. *Macromol.* **1998**, *31*, 3556-3565.

(39) Hanley, K. J.; Lodge, T. P.; Huange, C.-I. *Macromol.* **2000**, *33*, 5918-5931.

(40) Lai, C.; Russel, W. B.; Register, R. A. *Macromol.* **2002**, *35*, 841-849.

(41) Whitmore, M. D.; Vavasour, J. D. *Macromol.* **1992**, *25*, 2041-2045.

(42) Lodge, T. P.; Hanley, K. J.; Pudil, B.; Alahapperuma, V. *Macromol.* **2003**, *36*, 816-822.

(43) Lodge, T. P.; Pan, C.; Jin, X.; Liu, Z.; Zhao, D.; Maurer, W. W.; Bates, F. S. *J. Poly. Sci. B* **1995**, *33*, 2289-2293.

(44) Xu, T.; Goldbach, J. T.; Misner, M. J.; Kim, S. H.; Gibaud, A.; Gang, O.; Ocko, B.; Guarini, K. W.; Black, C. T.; Hawker, C. J.; Russell, T. P. *Macromol.* **2004**, *37*, 2972-2977.

(45) Kim, G.; Libera, M. *Macromol.* **1998**, *31*, 2569-2577.

(46) Kim, G.; Libera, M. *Macromol.* **1998**, *31*, 2670-2672.

(47) Kim, S. H.; Misner, M. J.; Xu, T.; Kimura, M.; Russell, T. P. *Adv. Mater.* **2004**, *16*, 226-231.

(48) Ho, R.-M.; Tseng, W.-H.; Fan, H.-W.; Chiang, Y.-W.; Lin, C.-C.; Ko, B.-T.; Huang, B.-H. *Polymer* **2005**, *46*, 9362-9377.

(49) Yin, D.; Horiuchi, S.; Masuoka, T. *Chem. Mater.* **2005**, *17*, 463-469.

(50) Boeker, A.; Mueller, A. H. E.; Krausch, G. *Macromol.* **2001**, *34*, 7477-7488.

(51) Mori, H.; Wakisaka; Hirao, A.; Nakahama, S. *Macromol. Chem Phys* **1994**, *195*, 3213-3224.

(52) Hirao, A.; Kato, H.; Yamaguchi, K.; Nakahama, S. *Macromol.* **1986**, *19*, 1294-1299.

(53) van Krevelen, D. W.; Hoftyzer, P. J. *Properties of Polymers: Their Estimation and Correlation Length With Chemical Structure*; 2nd ed. ed.; Elsevier Scientific Publishing Company: New York, NY, 1976.

(54) Busch, P.; Rauscher, M.; Smilgies, D.-M.; Posselt, D.; Papadakis, C. M. *J. Appl. Cryst.* **2006**, *39*, 433-442.

(55) Whitmore, M. D.; Noolandi, J. *J. Chem. Phys.* **1990**, *93*, 2946-2955.

(56) Lai, C.; Russel, W. B.; Register, R. A. *Macromol.* **2002**, *35*, 4044-4049.

(57) Bosworth, J. K., Cornell University, Chapter 3, 2009.

(58) Liu, C.-C.; Nealey, P. F.; Ting, Y.-H.; Wendt, A. E. *J. Vac. Sci. Technol. B* **2007**, *25*, 1963-1968.

(59) Ting, Y.-H.; Park, S.-M.; Liu, C.-C.; Liu, X.; Himpsel, F. J.; Nealey, P. F.; Wendt, A. E. *J. Vac. Sci. Technol. B*. **2008**, *26*, 1684-1689.

(60) Templin, M.; Franck, A.; Du Chesne, A.; Leist, H.; Zhang, Y.; Ulrich, R.; Schaedler, V.; Ulrich, W. *Science* **1997**, *278*, 1795-1798.

(61) Jain, A.; Toombes, G. E. S.; Hall, L. M.; Mahajan, S.; Garcia, C. B. W.; Probst, W.; Gruner, S. M.; Wiesner, U. *Angew. Chem. Int. Ed.* **2005**, *44*, 1226-1229.

(62) Kamperman, M.; Fierke, M. A.; Garcia, C. B. W.; Wiesner, U. *Macromol.* **2008**, *41*, 8745-8752.

(63) Mansky, P.; Liu, Y.; Huang, E.; Russell, T. P.; Hawker, C. *Science* **1997**, *275*, 1458-1460.

(64) Lin, Y.-C.; Mueller, M.; Binder, K. *J. Chem. Phys.* **2004**, *121*, 3816-3828.

(65) Cavicchi, K. A.; Russell, T. P. *Macromol.* **2007**, *40*, 1181-1186.

(66) *Polymer Handbook*; 4th ed.; Brandrup, J., Immergut, E. H., Grulke, E. A., Eds.; John Wiley & Sons.: New York, 2003.

(67) Caykara, T.; Oezyuerek, C.; Kantoglu, O.; Gueven, O. *J. Poly. Sci. B* **2002**, *40*, 1995-2003.

CHAPTER 5

CONTROL OF SELF-ASSEMBLED BLOCK COPOLYMER FILM MORPHOLOGY, DIMENSIONS, AND PACKING THROUGH COMBINED SELECTIVE MOLECULE BLENDING AND SOLVENT VAPOR ANNEALING

Joan K. Bosworth,[1,2] Christopher K. Ober,[2] and Charles T. Black[3]

1. Department of Chemistry & Chemical Biology, Cornell University, Ithaca, NY 14853

2. Department of Materials Science & Engineering, Cornell University, Ithaca, NY 14853

3. Center for Functional Nanomaterials, Brookhaven National Laboratory, Upton NY 11973

5.1 Abstract

We combine the incorporation of small molecule additives with solvent vapor annealing to influence the self assembly of films of polystyrene-*block*-poly(2-vinylpyridine) diblock copolymers. Choosing a non-selective or selective solvent vapor controls the resulting pattern morphology, while blending increasing amounts of the poly(2-vinylpyridine)-miscible small molecule 2-(4-hydroxyphenylazo)benzoic acid provides precise nanometer-scale control of the resulting pattern dimensions. We have observed for the first time that combined small molecule blends and selective solvent annealing can be useful in controlling the film pattern packing. Spherical morphologies can be tuned between hexagonal and face-centered orthorhombic packing through choice of material film thickness. We also explore benefits of this combined processing approach for applications in templating inorganic materials.

5.2 Introduction

Block copolymer self assembly requires both a free energy benefit from phase separation and sufficient polymer chain mobility for the system in order to reach an equilibrium phase-separated morphology. The assembly process can be promoted by either thermal annealing[1], where the polymer material is heated above its glass transition temperature, or by annealing in solvent vapor, [2-7] where polymer chain mobility is induced by swelling the film with solvent. The vapor acts as a plasticizer within the film, effectively lowering the glass transition of the swollen film to below room temperature.[8-10]

Solvent vapor annealing also affects the *phase behavior* of a self-assembled polymer – an additional experimental lever not available with a thermal annealing

process. For a diblock copolymer film swollen with a nonselective solvent (that is, a solvent that equally dissolves both polymer blocks), the interaction between polymer blocks (χ_{AB}) is modified according to the dilution approximation:

$$\chi_{EFF} = \chi_{AB}\phi_p \qquad \text{Eqn. 5.1}$$

where ϕ_p is the volume fraction of the block copolymer in the solvent-polymer blend.[11] In experiments, ϕ_p is found to posses an exponent α, such that $\phi_p{}^{\alpha}$ typically ranging between 1.3 and 1.6, depending on the solvent and polymer system.[12] The overall effect of swelling in a nonselective solvent is a net reduction in block interaction strength (χ_{EFF}) and a vertical shift of the phase diagram with minimal change in shape of transition locations. For a symmetric diblock copolymer swollen in a nonselective solvent, the minimum condition for phase separation is given by:

$$\chi_{EFF}N = (\chi_{AB}\phi_p{}^{\alpha})N = 10.5 \qquad \text{Eqn. 5.2}$$

which demonstrates that swelling a given material in a solvent vapor ($\phi_p<1$) *increases* the minimum degree of polymerization (N) required for self assembly.

Annealing a diblock copolymer material in a selective solvent – a good solvent for one polymer block and complete non-solvent for the other block – has the additional consequence of changing the relative block volume fractions due to uneven swelling of the two blocks. We understand this effect as a horizontal shift in the phase diagram to a different diblock copolymer volume fraction (*f*), without an accompanying vertical change in the minimum condition for self assembly (Equation 5.1).[13-15] A self-assembled block copolymer film may be immersed into a solvent that is completely selective for one block (and a nonsolvent for the other block) without any effect on the film ordering, especially if the insoluble block is the majority

component such that the film is anchored to the surface.[16] Swelling of only a single block can result in partial pore formation in the polymer film.[20,21]

Effective block copolymer self assembly by solvent annealing requires mobility in *both* constituent polymer blocks – a condition easily achieved by annealing in non-selective good solvents. Selective solvents must at least *slightly* swell the less-soluble block in order to achieve polymer chain mobility and subsequent film self assembly. In this case, the selective solvent annealing causes *both* a horizontal shift in the phase diagram due to the change in relative block volume fraction (*f*) and a vertical shift due to dilution (Equation 5.1).[7]

We have previously experimentally studied the effects of solvent selectivity on thin film self assembly of poly(α-methylstyrene)-*block*-poly(4-hydroxystyrene) (PαMS-*b*-PHOST). Annealing films of these materials in tetrahydrofuran (THF), a good solvent for both blocks, results in assembly of parallel-oriented cylinder domains as expected from the constituent block volume fraction (*f*~33%).[7] A solvent selective for the PHOST majority component (acetone), changes the assembled pattern to a spherical morphology in the swollen state, which is kinetically trapped upon fast solvent evaporation.

Other groups have experimentally observed similar behaviors in thin films of different block copolymer materials.[5,6] For example, blends of polystyrene-*block*-poly(4-vinylpyridine) (PS-*b*-P4VP) and 2-(4-hydroxyphenylazo)benzoic acid (HABA) self-assemble into fingerprint patterns characteristic of a parallel-oriented cylindrical phase when annealed in dioxane, a good solvent for the three blend components (PS, P4VP, and HABA). In this system, HABA selectively segregates to the polar P4VP block due to hydrogen bonding [5,6] such that the total mass fraction of the polar phase (P4VP+ HABA) is approximately *f*~25%. Annealing in solvents that are selective for the polystyrene block (either chloroform or toluene) results in formation of spherical

morphology in the swollen state, which then collapses to a perpendicular-oriented cylindrical phase upon solvent evaporation.

In this work we experimentally understand the effects of combined solvent vapor annealing and blending a small molecule additive (HABA) on the self assembly of thin films of cylindrical-phase polystyrene-*block*-poly(2-vinylpyridine) (PS-*b*-P2VP). Annealing in non-selective or selective solvent vapor environments controls film morphology and therefore the type of self-assembled pattern. We demonstrate that blending increasing amounts of the small molecule HABA to the material system provides precise nanometer-scale control of the pattern dimensions, and we quantitatively understand this effect using an effective blend molecular weight and volume fraction. In principle there are many materials capable of hydrogen bonding with P2VP and thereby selectively localizing in the P2VP domain of a self-assembled PS-*b*-P2VP film. In this work we have used HABA because of its previously demonstrated use.[5,6] However, future work may involve comparing additives of crystalline versus amorphous materials such as molecular glasses.[22,23] We have observed for the first time that annealing a blended PS-*b*-P2VP/HABA material in a selective solvent vapor also controls pattern packing for a spherical morphology and we can tune between a hexagonal arrangement and square packing via choice of material film thickness. Using the blend material in combination with solvent vapor annealing also provides benefits for templating applications as selective HABA removal leaves increased exposed P2VP surface area and an improved geometry for loading with metal precursors from solution.

5.2 Methods

PS-*b*-P2VP was purchased from Polymer Source, Inc. with PS block 32500 kg/mol and P2VP block 12000 kg/mol and molecular weight distribution 1.05. Blends

with 2-(4-hydroxyphenylazo)benzoic acid ("HABA," Aldrich) are formed by mixing differing amounts of 1% PS-*b*-P2VP (w/v) and 1% HABA (w/v), both dissolved in dioxane (Aldrich). No special treatment of the HABA – PS-*b*-P2VP blend solution was found necessary in order to gain selective partitioning of HABA into the P2VP phase. Thicker films (79-88 nm thick, depending on HABA content) are achieved by spin coating 1% (total mass/volume) blends at 2000 RPM, and are used for cross-sectional imaging. Prior to cleaving for cross-sectional SEM, a thin layer of gold is sputtered on films using a Cressington 208HR High Resolution Sputter Coater. Films with terracing displaying single and double morphology thickness are achieved by diluting the solution with further dioxane, either to 0.75 or 0.5%, and varying spin coating speed. Films possess film thickness of 25 – 30 nm in the dried state, near or slightly less than the spatial period for the polymers (Figure 5.5), though this is consistent with single morphology or double morphology thickness in the swollen state as shrinkage occurs upon evaporation of the annealing solvent. Film thicknesses are measured using a J.A. Woollam M-2000 spectroscopic ellipsometer.

Solvent annealing takes place in a closed container with a solvent reservoir, either dioxane or toluene (Aldrich). Annealing time is determined as the minimum time needed to gain long range ordering for the particular annealing conditions. Overall times are also dependent on anneal chamber volume, reservoir size and solvent volatility. Anneal times reported here compare to other data in this work with the same solvent, but cannot be used as standardized times. In the case of thermally annealed films, films spin coated on silicon are placed in a vacuum oven for 4 hours at 190˚C.

After annealing, films are immersed in methanol (Aldrich) for 5 minutes and then blown dry in a stream of nitrogen. The methanol serves to selectively extract any HABA present and to selectively swell the P2VP block.

Aqueous germanium oxide solution ("GeO_2," Aldrich, 100 mMol in Millipore water) is mixed immediately prior to use and filtered through a 0.2 μM nylon syringe filter. Methanol-treated films are soaked in GeO_2 solution for 10 minutes and then blown dry in a stream of nitrogen. Removal of polymeric material is achieved by treatment in a UV/ozone cleaner (UVOCS T10X10/OES) for 60 minutes.

Gold solution is made from gold chloride trihydrate (Aldrich, 100 mMol) dissolved in 2% hydrochloric acid (concentrated hydrochloric acid, Baker, diluted to 2% with Millipore water). Methanol-treated PS-*b*-P2VP films are soaked in the gold solution for 60 minutes, rinsed by a brief immersion in Millipore water, and blown dry in a stream of nitrogen. An oxygen reactive ion etch (March Plasma CS1701F, 100 mTorr, O_2 20 sccm, 100 W, 60 seconds) removes the PS-*b*-P2VP and reduces the gold.

A Hitachi S-4800 Scanning Electron Microscope and Veeco Dimension 3100 Atomic Force Microscopy are used for surface imaging. Spatial period is determined from AFM images using the 2D power spectral density feature in Veeco Nanoscope v. 5.3 software; accuracy of this technique is typically ±2nm.

5.3 Results & Discussion

5.3.1 Solvent Annealing in Nonselective & Selective Solvents

Annealing both neat PS-*b*-P2VP and HABA-blended PS-*b*-P2VP (PS-*b*-P2VP/HABA) films in non-selective (dioxane) and selective (toluene) solvents facilitates both material phase segregation and self-organization. We have defined the film anneal time as that required to achieve large defect-free ordered domains (Table 5.1). PS-*b*-P2VP films (without HABA) annealed in non-selective dioxane form fingerprint patterns, consistent with a cylindrical morphology (Figure 5.1a) and similar

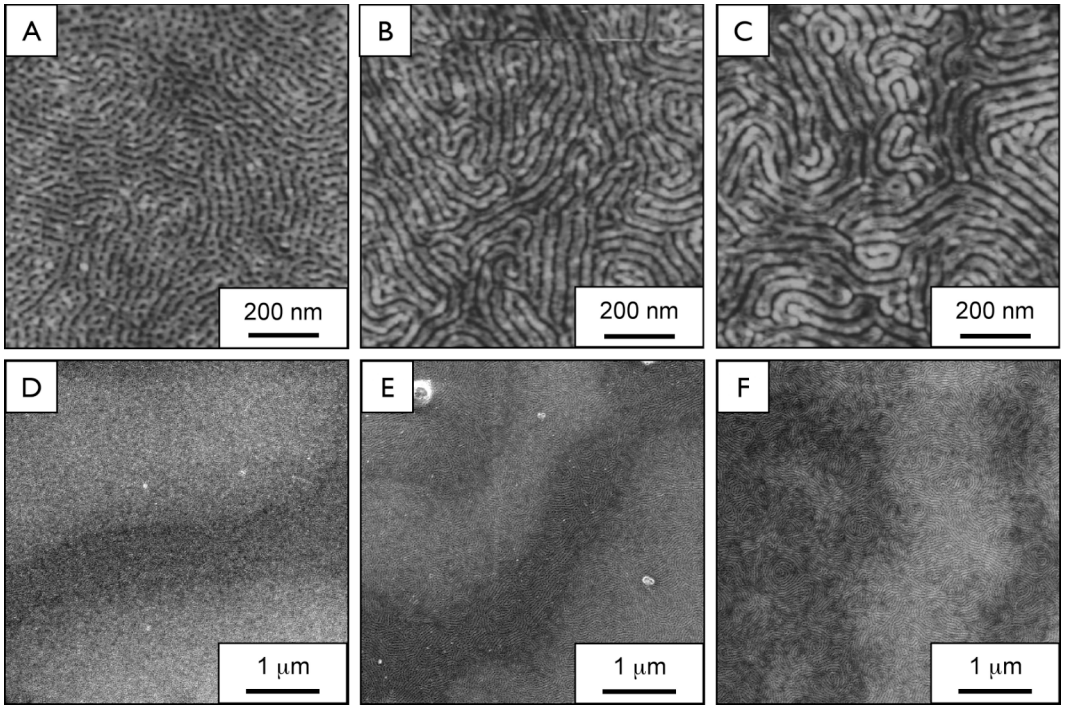

Figure 5.1. Dioxane-annealed films of PS-*b*-P2VP with 0% HABA (a, d), 10% HABA (b, e), and 20% HABA (c, f). Atomic Force Microscopy height images demonstrating fingerprint pattern are seen on the top (a-c), while scanning electron micrographs on the bottom show terracing present in nearly-single layer films (d-f). The observed fingerprint pattern combined with the terracing indicate formation of parallel cylinders for all samples.

Table 5.1

% HABA	Mass Fraction				Anneal Time, hours	
	HABA	PS	P2VP	Total Polar: PVP + HABA	Dioxane	Toluene
0	0.00	**0.73**	**0.27**	0.27	4	5
5	0.05	0.69	0.26	0.31	4	10
10	0.10	0.66	0.24	0.34	5	12
15	0.15	0.62	0.23	0.38	5	25
20	0.20	0.58	0.22	0.42	5	---

to the morphology observed in thermally-annealed PS-*b*-P2VP films (Figure 5.2). Observed film terraces also support our conclusion of a cylindrical morphology (Figure 5.1d). Parallel-oriented cylindrical domains formed below a surface-wetting layer are partially exposed to the surface as a series of uneven holes after rinsing in PVP-selective methanol to swell P2VP domains below a wetting layer at the surface. The parallel cylinder domain orientation is likely driven by both preferential substrate wetting of the polar P2VP minor phase and preferential wetting of one block to the air interface.

PS-*b*-P2VP blends with 10% and 20% HABA (w/w) annealed in dioxane assemble into similar fingerprint patterns (Figure 5.1b-c) with film terraces (Figure 5.1e-f) indicating parallel cylinder formation. After solvent annealing, films are rinsed with methanol to swell the P2VP domains as well as to extract the HABA. (Table 5.1 displays the relative mass fractions of PS, P2VP, and HABA in the blend materials. The blend volume fractions are difficult to calculate because of unknown HABA density.) The required dioxane anneal time (4-5 hours) does not increase with added HABA amounts. A 20% added HABA mass fraction results in a 42% polar mass (P2VP+HABA) (Table 5.1) which could in principle move the blend to a lamellar morphology; however, the presence of film terraces combined with the observed

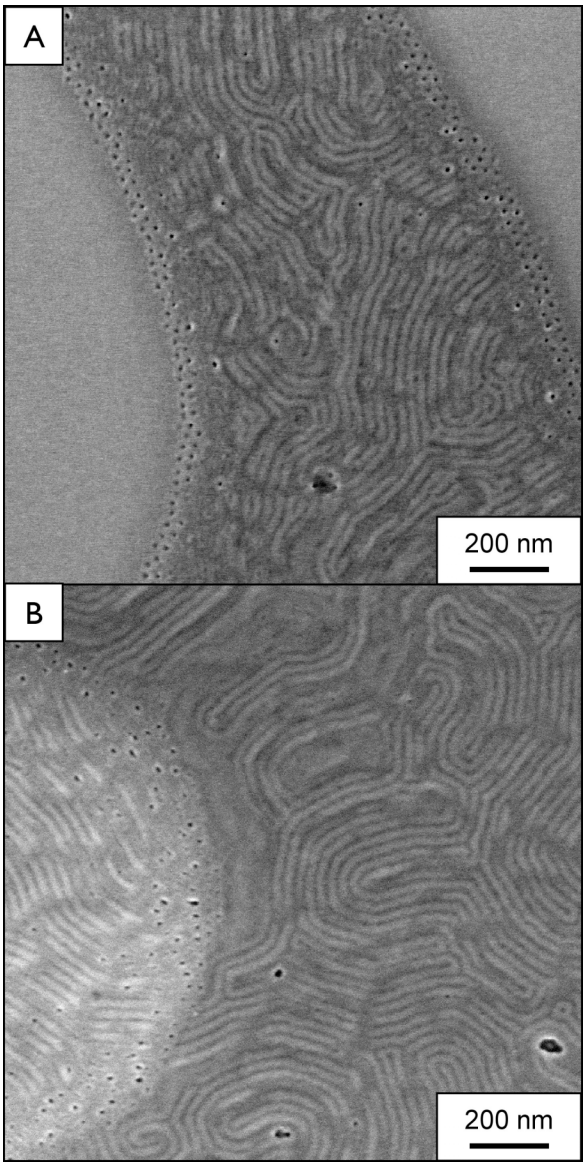

Figure 5.2. Parallel orientation of PS-*b*-P2VP (without HABA) after thermal annealing 190˚C for 4 hours demonstrates island and hole formation with two film thicknesses : a) below single layer thickness and b) above single layer thickness. Repeat spacing is measured to be 28 - 29 nm. A) thinner film (top) shows single thickness terrace next to area with too thin of film to form morphology, while B) thicker film shows an island with two integer thicknesses. Note the formation of dots at terrace interface, consisitent with perpendicular cylinder formation at incommensurate film thicknesses

fingerprint pattern strongly suggests parallel-oriented cylinder domains rather than lamellae.

Solvent vapor annealing allows control of film morphology by choosing preferential solvents for the constituent polymer blocks. Annealing PS-*b*-P2VP/HABA films in toluene (a selective solvent for PS) leads to formation of ordered dot patterns (Figure 5.3a-c) and film terraces (Figure 5.3d-e) for added HABA amounts less than 10%. We expect that selective toluene incorporation into the majority PS block results in a film with spherical morphology in the swollen state. Previous experiments with PS-*b*-P4VP/HABA have reported cylinder-forming block copolymer films transitioning to a spherical morphology in the swollen state and collapsing to a perpendicular cylinder morphologies upon drying,[5,6] while in PαMS-*b*-PHOST cylinder-forming systems the spherical morphology is maintained upon solvent removal.[7] Cross-sectional SEM images of toluene-annealed PS-*b*-P2VP/HABA films containing 5% HABA after solvent removal and HABA extraction (by methanol) indicate that these materials maintain a spherical morphology (Figure 5.4). The 79 nm thick film contains half-sphere divots in the top surface rather than being fully penetrated by perpendicularly-oriented cylindrical pores. We observe similar morphology in 10% HABA blend films, and it is difficult to observe the morphology of neat PS-*b*-P2VP films after toluene annealing because P2VP cannot be selectively removed.

Films containing increasing HABA concentration require longer toluene anneal times for self assembly, in contrast to films annealed in non-selective solvents (Table 5.1). Blend films containing 20% HABA are not fully self-assembled even after 24 hours in toluene vapor (Figure 5.3f). Visual observation of the film color change upon annealing for longer times indicates that films swell more when annealed

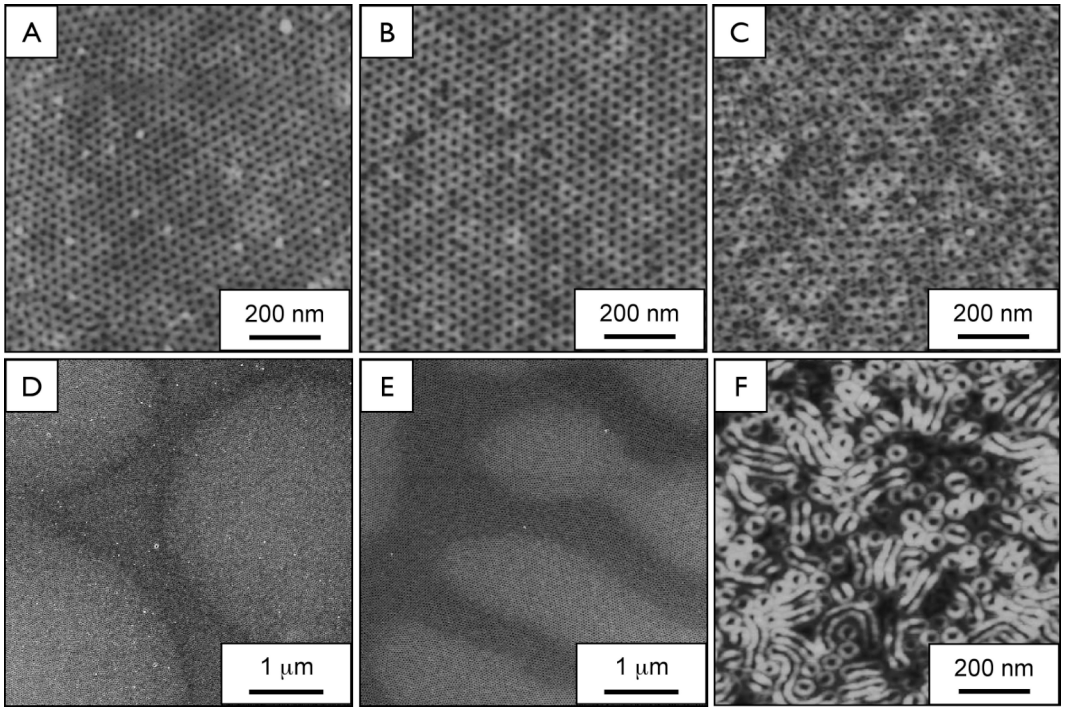

Figure 5.3. Toluene-annealed films of PS-*b*-P2VP with 0% HABA (a, d), 5% HABA (b), 10% HABA (c, e), and 20% HABA (f). Atomic Force Microscopy height images demonstrating hexagonal dot are seen at the top (a, c, e), while scanning electron micrographs show terracing present in nearly-single layer films (d, e). The observed hexagonal pattern combined with the terracing indicate formation of sperical morphology for 0 - 10% HABA. Films with 20% HABA cannot gain sufficient mobility for long range ordering to occur, as observed in the AFM image (f).

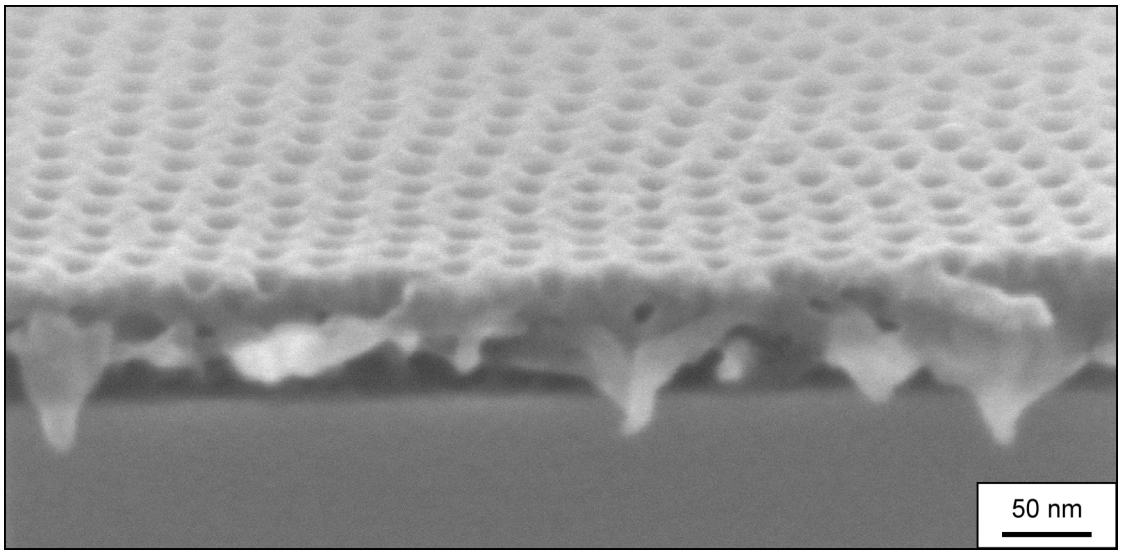

Figure 5.4. Cross-sectional SEM of PS-*b*-P2VP + 5% HABA after annealing in toluene. Film thickness of 79 nm is chosen in order to distinguish spherical from perpendicular morphology. Divots of top layer of spheres are observed at the top, indicating a spherical morphology is trapped in the dried state.

for longer times. Therefore, longer anneal time required for self assembly indicates a higher swell ratio in the blended films is needed to obtain sufficient mobility. We attribute this behavior to the poor solubility of HABA (and thus the PVP + HABA block) in toluene.

5.3.2 Blended HABA Changes Domain Period (d_0)

The spatial period of the PS-*b*-P2VP domains (d_0) increases when blended with increasing amounts of HABA (seen visually in the SEM images of Figures 5.1, 5.3 and graphically in Figure 5.5). Dioxane is a good solvent for all three blend components (PS and P2VP blocks, and HABA), and we observe similar film anneal times of 4-5 hours for all blend compositions. We measure a domain period d_0 ~31 nm in neat PS-*b*-P2VP films annealed in dioxane, a value slightly larger than that measured for thermally annealed films of the same molecular weight (d_0 ~28 nm, measured from the SEM image in Figure 5.2), though these numbers are difficult to compare because of the different imaging methods used to calculate them. The spatial period of polymers annealed in a nonselective solvent are known to decrease with added solvent.[24] Because the blend film annealing time (and thus polymer swelling ratio) remains constant for all amounts of added HABA, we can attribute increases in d_0 beyond 31 nm to the presence of HABA in the film.

We can quantitatively understand the effect of added HABA on the film domain periodicity d_0 using a simple model for the PS-*b*-P2VP/HABA blend. For each blend composition, we calculate the mass of added HABA per PS-*b*-P2VP polymer chain and estimate a polar molecular weight (P2VP+HABA) by assuming the P2VP/HABA material behaves as a single P2VP block with larger molecular weight.

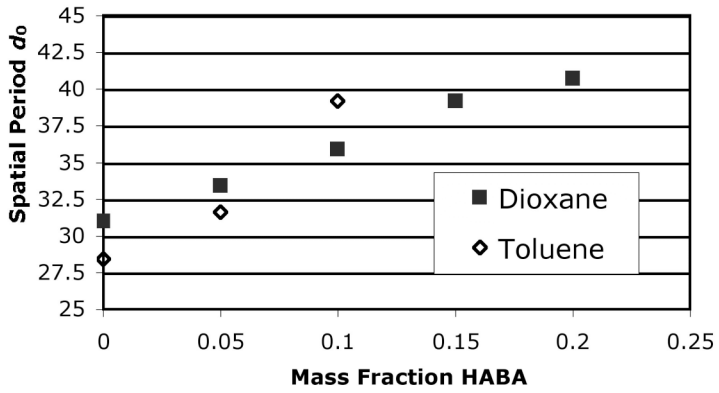

Figure 5.5. Spatial period d_0 increases as the HABA content increases, both for dioxane-annealed and toluene-annealed films. Slope of toluene annealed films is higher than that of dioxane annealed film, indicating incorporation of both HABA and toluene solvent contributes to spacing after toluene annealing.

This rough approximation assumes: completely nonselective solvent swelling; small amounts of added HABA do not affect the film swelling ratio; strong blend material phase segregation; and negligible solvent effect on the domain spacing (experimental data shows this to be small). Despite these assumptions, the data are well fit by $d_0 \sim N_{eff}^{2/3}$ (Figure 5.5), where N_{eff} is the total degree of polymerization calculated from the PS-*b*-P2VP/HABA blend effective molecular weight (Table 5.2).

Table 5.2. Effective molecular weight of (PS-*b*-P2VP + HABA) blend, with a hypothetical block copolymer composed of PS-*b*-P(2VP/HABA). This is useful for assessing the increase of spatial period d_0 as HABA content increases when swollen with a nonselective good solvent. The effective total M_n is transformed to total degree of polymerization N, and the plot is found to follow $d_0 \sim N^{2/3}$.

% HABA	# HABA / polymer chain	kg HABA / mole PS-b-P2VP	Effective Polar Mn (HABA + P2VP)	**Effective total Mn, kg/mol**
0	0	0.0	12.0	**47.5**
0.05	10	2.3	14.3	**49.8**
0.1	20	5.0	17.0	**52.5**
0.15	32	7.9	19.9	**55.4**
0.2	46	11.2	23.2	**58.7**

The PS-*b*-P2VP domain period (d_0) increases significantly faster in HABA blend films annealed in toluene (Figure 5.5), a selective solvent for PS. Linear fits to the data for added HABA blend amounts less than 10% show that toluene annealing changes the periodicity $d_0 \sim 2$ times faster than dioxane. The different behavior may be attributed to the increase of solvent in the films as the HABA content increases. Toluene annealing requires significantly longer times as the blend HABA content increases (Table 5.1), meaning that films require higher swelling ratios to achieve polymer mobility in both blocks, (and in particular, the P2VP/HABA domain). Lai et al. observed that the degree of selectivity of a swelling solvent has a strong effect on the change in periodicity of the blended material: as the solvent becomes more

selective, the periodicity can actually increase.[25] We are unable to distinguish d_0 increases due to incorporated HABA or toluene from solvent contributions in toluene annealed films, but the increase in periodicity may be attributed to both increased HABA and increased toluene content in the films, two related parameters.

5.3.3 Cubic Lattice in Toluene-Annealed PS-b-P2VP/HABA Films

Blended PS-*b*-P2VP/HABA films annealed in a selective solvent (toluene) show regions of cubically-arranged dot patterns as well as hexagonally-packed equilateral triangle orientations (Figures 5.6a-d), indicating two different lattice alignments in the film. These packings are only possible for spherical morphology. We have observed square-packing behavior in both 5% and 10% HABA blend films (the 10% blend is shown in Figures 5.6a-d), although never in films of neat PS-*b*-P2VP films without HABA.

Hexagonal or square dot domain packing occurs for specific blend film thickness. A monolayer of P2VP/HABA domains packs hexagonally (Figure 5.6b), while a second sphere layer results in square packing (Figures 5.6c-d) of both the lower and upper layers. High-resolution SEM images of square-packed dot regions reveal small indentations at center points indicating a first layer with a similar packing arrangement. Thicker PS-*b*-P2VP/HABA blend films show only hexagonal domain packing (e.g., the 80nm thick film in Figure 5.4). The key observation is that film thickness controls the resulting pattern domain packing, providing a method to further expand possibilities for templating applications.[26-28]

Previous experiments with multilayer spherical-phase PS-*b*-P2VP films have demonstrated body-centered-cubic (bcc) packing with the (110) crystallographic direction oriented perpendicular to the substrate.[17-19] This particular crystal orientation

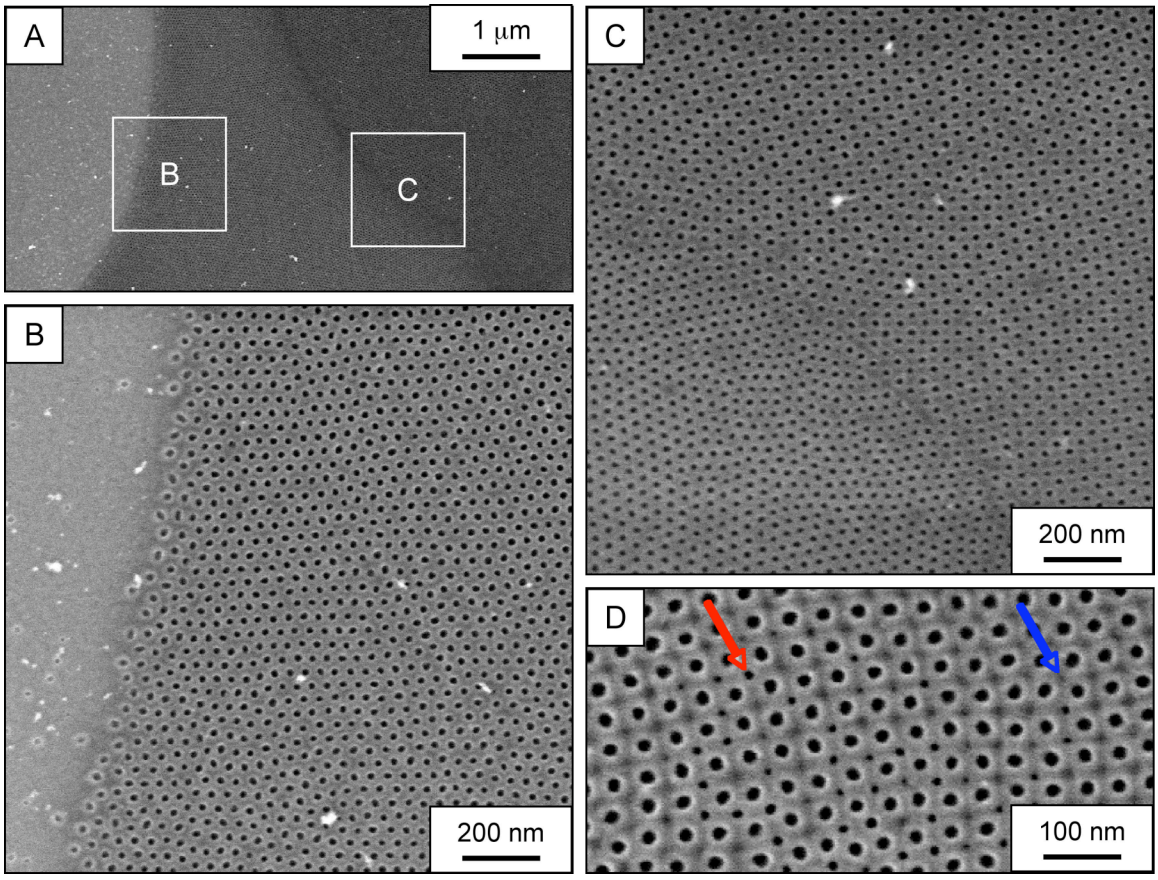

Figure 5.6. Films of PS-*b*-P2VP blended with 10% HABA after annealing in toluene. Terracing is present in thin films of incommensurate thicknesses, though due to defects this region displays 3 step heights (a). The white boxes indicate the location of images in b-c). The step between brush layer and single film thickness is observed in b), while the step height from hexagonally packed monolayer to square-packed bilayer is shown in c). Spacing for these two are observed to be nearly identical, 41 ± 1 nm for hexagonal dots and 42 ± 1 nm for square dots. As can be seen in the zoomed in region (d), in some regions of the square dot region, very small dots appear at the interstitial space (an example is marked with a red arrow), consistent with the very top of a sphere layer underneath; even in regions without small interstitial dots, depressions are observed (an example is marked with a blue arrow).

minimizes chain stretching required for filling interstitial spaces at interfaces.[17] Later work demonstrated that bcc packing forms for films thicker than 22 layers upon thermal annealing, but thinner thermally-annealed PS-*b*-P2VP films containing between 4 and 22 sphere layers change to a face-centered orthorhombic (fco) structure.[18,19] Below 4 layers a hexagonal packing is the most stable structure. The fco lattice observed in thickness 4-22 layers is more deformed closer to 4 layers and approaches bcc-like packing closer to 22 nm. As demonstrated in Scheme 5.1, the bcc lattice (110) crystal plane parallel to the substrate corresponds with an fco (100) crystal plane parallel to the substrate. This fco (100) would lead to rectangular packing of spheres in the bcc, but in the highly deformed lattice in thin films could form square packing.

Solvent vapor processing of the spherical-phase triblock copolymer of polystyrene-*block*-poly(ethylene oxide)-*block*-poly(methyl methacrylate) (PS-*b*-PEO-*b*-PMMA) in benzene and water results in square packing of PEO-*b*-PMMA spheres for films having 2.5 layers., which is described as a bcc arrangement with (100) orientation.[28] The behavior is believed to result from interactions between hydrophilic PEO segments and water during solvent evaporation. Films of PS-*b*-PEO-*b*-PMMA less than 2.5 layers thick also arrange hexagonally.

Our measurements of square domain packing in a diblock copolymer blended with HABA suggests the behavior may be more generally observable in other systems as well. The requirement of *both* a selective solvent (toluene) and HABA for square domain packing in PS-*b*-P2VP films suggests that decreased mobility within the minority spherical phase (compared to the PS majority) contributes to pattern formation.

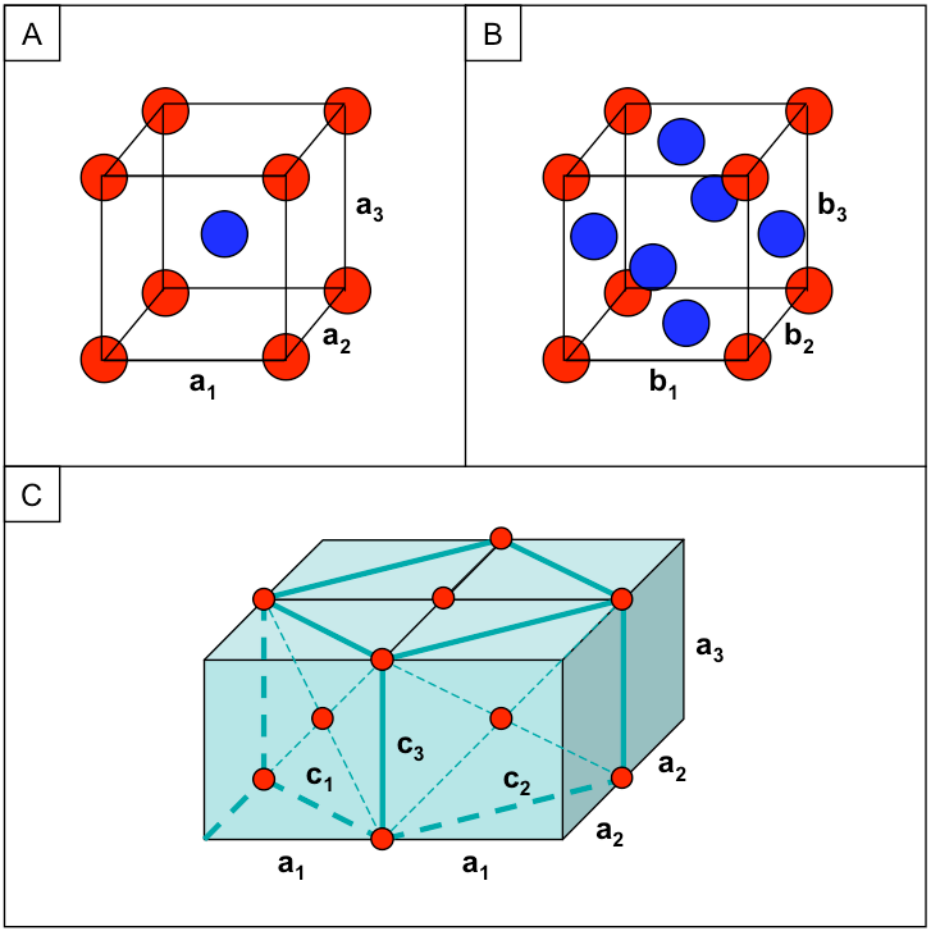

Scheme 5.1. a) A body-centered cubic (bcc) unit cell, where $a=a_1=a_2=a_3$. For clarity, the spheres located on lattice corners are red, while the sphere located at the center of cube is blue. b) A face-centered cubic (fcc) unit cell, where $b=b_1=b_2=b_3$. A face-centered orthorhombic (fco) unit cell has the same arrangement of spheres as an fcc, but b_1, b_2 and b_3 need not be equal. For clarity, spheres located on lattice corneers are red, while spheres located on lattice faces are blue. c) Projection of an fco lattice existing within a layer of 4 bcc lattices, in which the lattice parameters $c_1=c_2=a*2^{1/2}$ and $c_3=a$. In thick films, a spherical morphology possesses bcc packing with the (110) lattice plane parallel to the substrate.[17-19] In the fco contained within the bcc crystal plane, the fco (100) and bcc (110) are the same plane. Stein et al showed that in films approaching 22 layers of spheres, the fco morphology approached the structure shown in c, while for thinner films it was more deformed.[25,26] Deformation of the lattice in thin films could lead to square packing of the fco morphology displayed in thin films.

The observed square packing in bilayers of PS-*b*-P2VP/HABA films annealed in toluene is consistent with an fco (100) lattice (Scheme 5.2). It could also be consistent with an fcc (100), or a bcc (100) packing, which are specific equilateral cases of an fco lattice (Scheme 5.1). These lattices could be determined by comparing the ratio of the spacing of the dots on the surface to the distance between the layers of the spheres in the swollen state (Scheme 5.2). In dried films, however, the spacing between layers does not reflect the layer spacing of a solvent swollen film due to contraction of the film upon evaporation.[7,29] This structure could be elucidated by performing grazing incidence small angle X-ray scattering on solvent-swollen films.

5.3.4 Templating Applications

We have demonstrated the utility of blending HABA with PS-*b*-P2VP material for both controlling the resulting self-assembled pattern dimensions and also the domain packing pattern. Here we demonstrate a further benefit of the blend material for templating applications. Previous experiments have demonstrated the selective infiltration of the P2VP block in PS-*b*-P2VP with oxide precursors or metal salt complexes.[30-33] Metal salt infiltration of a P2VP cylindrical phase of PS-*b*-P2VP film followed by reduction to metallic form has been demonstrated to create patterns of gold, platinum, and other metals.[30,31] We have adopted this approach in templating P2VP domains with gold. Gold coating is achieved by soaking films in gold chloride in acidic solution, and then an oxygen plasma etch removes the polymeric material and reduces the gold precursor. Use of PS-*b*-P2VP films annealed in both dioxane (Figure 5.7a) and toluene (Figure 5.7d) as a template results in gold in line and dot patterns corresponding the self-assembled morphology. Blend films of PS-*b*-P2VP/HABA contain larger exposed P2VP surface area after HABA removal (with

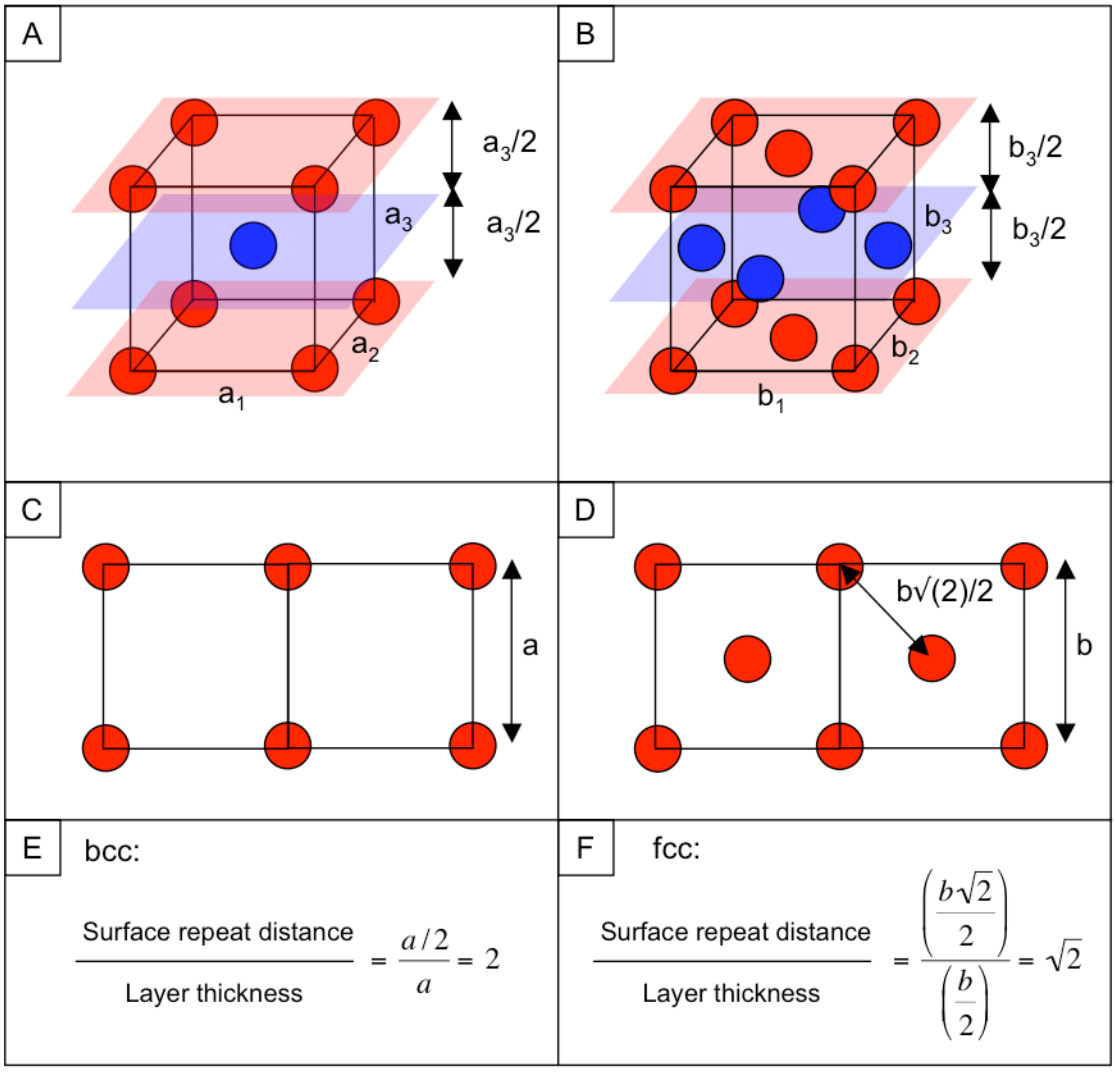

Scheme 5.2. Bilayers of PS-*b*-P2VP containing 10% HABA possess a square packing after annealing in toluene. This could be explained as the substrate-parallel alignment of the (100) crystal plane of (a) a bcc lattice with $a=a_1=a_2=a_3$, (b), an fcc lattice (with $b=b_1=b_2=b_3$, or an fco lattice (with $b=b_1=b_2\neq b_3$). The (100) crystal planes are indicated by the shaded parallelograms; a projection of the (100) crystal plane for bcc (c) and fcc and fco (d) is shown here. Distinguishing the lattice structure for the square bilayer region would require comparing the spacing between the spheres at the surface to the spacing between the sphere layers, as described in e) and f). An fco packing would exist if the ratios for bcc or fcc are not observed.

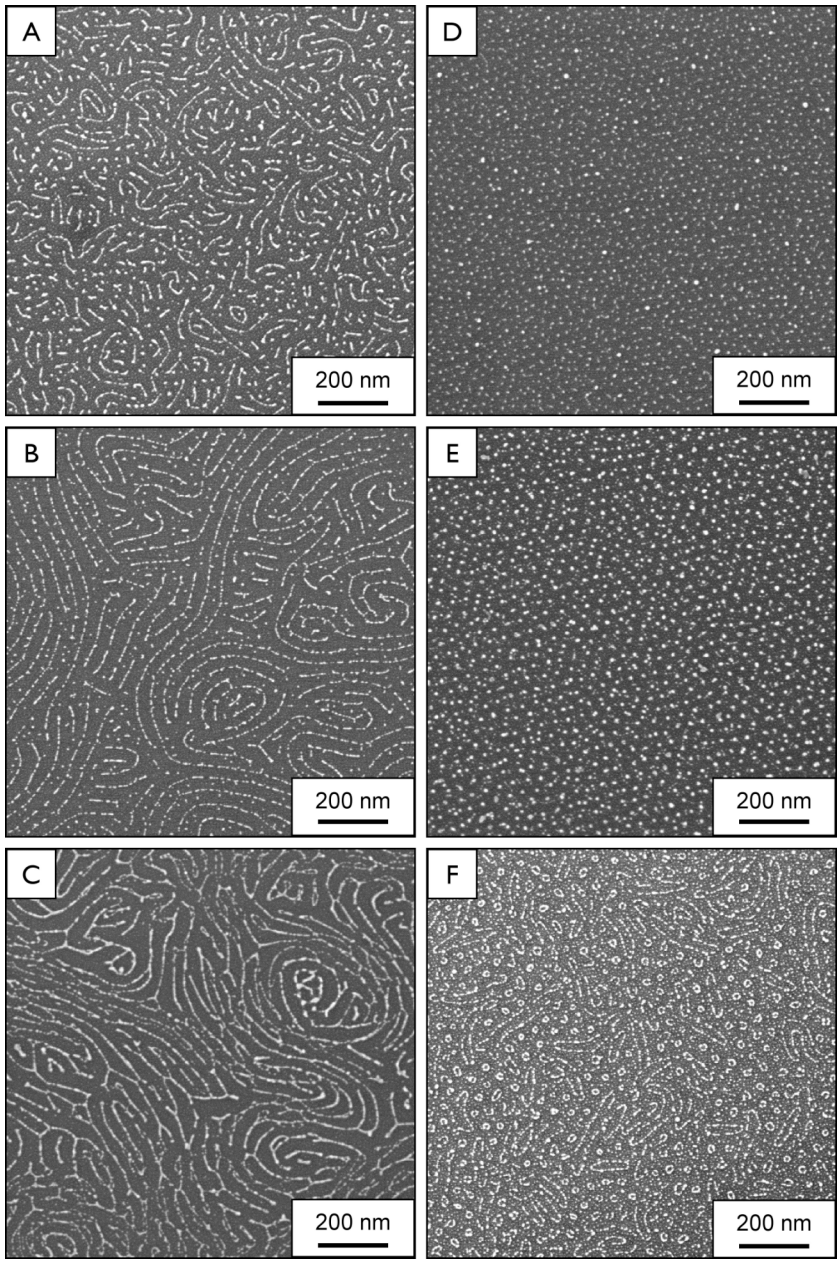

Figure 5.7. Gold patterns after organic material removal from PS-*b*-P2VP films containing 0% HABA (a, d), 10% HABA (b, e) and 20% HABA (c, f) were annealed in dioxane (left: a, b, c) and toluene (right: d, e, f). Patterns containing 0% HABA follow P2VP pattern, but with low pattern fidelity. Films containing 10% HABA display significantly increased pattern fidelity. Films with 20% HABA demonstrate pattern fidelity, but block copolymer self assembly is less controlled. The 20% HABA dioxane annealed film (c) has severl sets of parallel lines, indicating a bilayer of parallel cylinders; monolayer regions did not display patterns with any fidelity at all. The 20% HABA toluene annealed film possesses a gold pattern that is a direct match to the disordereted pattern after annealing displayed in Figure 5.2f.

methanol), and show improved fidelity of gold patterning (Figures 5.7b-c and 5.7e-f) because of improved accessibility of gold chloride ions in solution to the P2VP phase.

We have also templated a new material, germanium oxide, using a PS-*b*-P2VP/HABA film by dipping porous (post-HABA extraction) films into aqueous GeO_2 solution and removing the remaing polymer with UV/ozone treatment (Figure 5.8). As with gold patterning, HABA-extracted films give better patterning than those without HABA due to the increase in pore size after HABA extraction. The size of the germanium domains within the PS-*b*-P2VP voids is observed to increase as the HABA content of the PS-P2VP increases, indicating larger pores formed in films blended with more HABA. Furthermore, the periodicity of the germanium oxide patterns is found to mimic the increased periodicity of PS-*b*-PVP blended with HABA. Thus, use of HABA to tune periodicity and pore size provides a method to tune the size and spacing of germanium oxide patterns. Finally, the germanium oxide pattern may be formed both on hexagonally-packed and cubically-packed regions of films containing HABA and annealed in toluene; in Figure 5.8f, the germanium pattern formed on 10% HABA film after annealing in toluene shows a region with square packing.

The use of HABA blended with PS-*b*-P2VP to control periodicity and to form pores in PS-P2VP after its selective extraction holds promise for tuning domain patterns, as demonstrated here with gold and germanium oxide patterning. In both cases, assembly of PS-*b*-P2VP containing HABA promotes increased pattern fidelity due to larger pore formation after HABA extraction. The above results indicate that templating techniques that make use of backfilling pores (as for GeO_2) as well as selective attraction of a salt to the polar P2VP phase (as for gold), benefit from inclusion of HABA during the self assembly step followed by its extraction. Furthermore, changing the HABA concentration allows tuning of the pore size and domain spacing, which is transferred to the patterned materials.

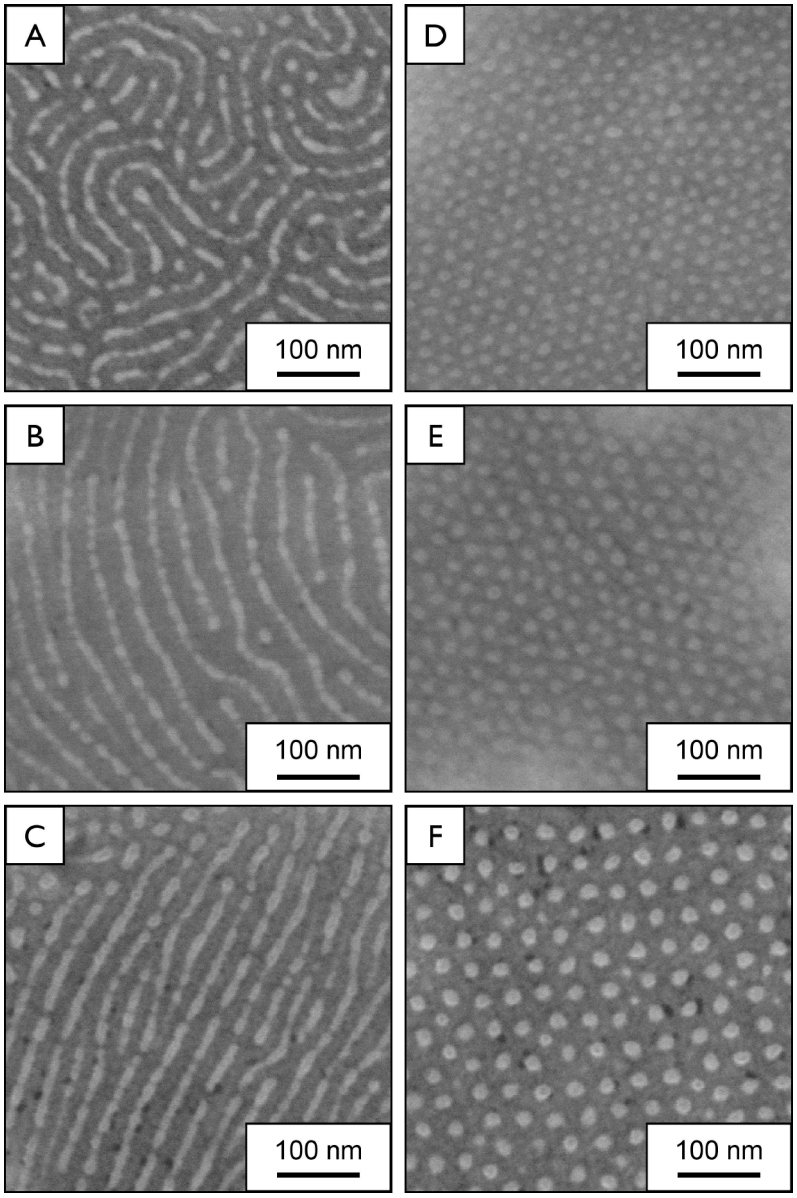

Figure 5.8. Germanium oxide patterns created on PS-*b*-P2VP films containing 0% HABA (a, d), 5% HABA (b, e) and 10% HABA (c, f) annealed in dioxane (left: a, b, c) and toluene (right: d, e, f). We observe Germanium oxide deposited in pores with a high degree of fidelity, as well as a thin GeO_2 layer present at the top surface.

5.4 Conclusion

Solvent annealing of PS-*b*-P2VP allows control of morphology formed by choice of solvent: annealing in dioxane yields parallel cylinders, while annealing in toluene gives spherical morphology. Inclusion of HABA in films prior to solvent annealing leads to the same morphologies as for HABA-free films, but the spatial period of the films is found to vary significantly. In the case of the increase of d_0 in dioxane-annealed films, the bulk of the increase may be attributed to the increase in HABA volume. For toluene-annealed films, however, the increase of spacing is found not only due to increased HABA volume but also to increased swelling of toluene needed for mobility of the PVP block. Finally, inclusion of HABA is found to improve templating of both void-filling templating techniques (GeO_2) as well as single-block swelling techniques (P2VP), as well as to provide tunability of periodicity.

5.5 Acknowledgements

Research carried out in primarily at the Center for Functional Nanomaterials, Brookhaven National Laboratory, which is supported by the U.S. Department of Energy, Division of Materials Sciences and Division of Chemical Sciences, under Contract No. DE-AC02-98CH10886. The authors would like to thank Chang-Yong Nam for his assistance in the lab and Marvin Y. Paik for discussion of sphere packing. This work was supported by the National Science Foundation Materials World Network (award DMR 0602821), the NSF NIRT (award CTS 0304159), and the Semiconductor Research Consortium, and J.K.B. was supported by fellowships from Motorola and IBM. This work was performed using facilities at the Cornell Center for Materials Research (CCMR), supported by NSF award DMR 0520404, part of the NSF MRSEC Program

REFERENCES

(1) Bates, F. S.; Fredrickson, G. H. *Phys. Today* **1999**, *52*, 32-38.

(2) Fukunaga, K.; Elbs, H.; Magerle, R.; Krausch, G. *Macromol.* **2000**, *33*, 947-953.

(3) Kim, S. H.; Misner, M. J.; Xu, T.; Kimura, M.; Russell, T. P. *Adv. Mater.* **2004**, *16*, 226-231.

(4) Cavicchi, K. A.; Russell, T. P. *Macromol.* **2007**, *40*, 1181-1186.

(5) Sidorenko, A.; Tokarev, I.; Minko, S.; Stamm, M. *J. Am. Chem. Soc.* **2003**, *125*, 12211–12216.

(6) Tokarev, I.; Krenek, R.; Burkov, Y.; Schmeisser, D.; Sidorenko, A.; Minko, S.; Stamm, M. *Macromol.* **2005**, *38*, 507–516.

(7) Bosworth, J. K.; Paik, M. Y.; Ruiz, R.; Schwartz, E. L.; Huang, J. Q.; Ko, A. W.; Smilgies, D.-M.; Black, C. T.; Ober, C. K. *ACS Nano* **2008**, *2*, 1396-1402.

(8) Rauch, J.; Koehler, W. *J. Chem. Phys.* **2003**, *119*, 11977-11988.

(9) Zielinski, J. M.; Duda, J. L. *AIChE Journal* **1992**, *38*, 405-415.

(10) Mori, K.; Hasegawa, H.; Hashimoto, T. *Polymer* **1990**, *31*, 2368-2376.

(11) Whitmore, M. D.; Vavasour, J. D. *Macromol.* **1992**, *25*, 2041-2045.

(12) Lodge, T. P.; Hanley, K. J.; Pudil, B.; Alahapperuma, V. *Macromol.* **2003**, *36*, 816-822.

(13) Huang, C.-I.; Lodge, T. P. *Macromol.* **1998**, *31*, 3556-3565.

(14) Hanley, K. J.; Lodge, T. P.; Huange, C.-I. *Macromol.* **2000**, *33*, 5918-5931.

(15) Lai, C.; Russel, W. B.; Register, R. A. *Macromol.* **2002**, *35*, 841-849.

(16) Xu, T.; Goldbach, J. T.; Misner, M. J.; Kim, S. H.; Gibaud, A.; Gang, O.; Ocko, B.; Guarini, K. W.; Black, C. T.; Hawker, C. J.; Russell, T. P. *Macromol.* **2004**, *37*, 2972-2977.

(17) Yokoyama, H.; Mates, T. E.; Kramer, E. J. *Macromol.* **2000**, *33*, 1888-1898.

(18) Stein, G. A.; Cochran, E. W.; Katsov, K.; Fredrickson, G. H.; Kramer, E. J.; Li, X.; Wang, J. *Phys. Rev. Lett.* **2007**, *98*, 158302.

(19) Stein, G. A.; Kramer, E. J.; Li, X.; Wang, J. *Macromol.* **2007**, *40*, 2453-2460.

(20) Guarini, K.; Black, C. T.; Yeung, S. H. I. *Adv. Mater.* **2002**, *14*, 1290-1294.

(21) Xu, T.; Stevens, J.; Villa, J. A.; Goldbach, J. T.; Guarini, K. W.; Black, C. T.; Hawker, C. J.; Russell, T. P. *Adv. Funct. Mater.* **2003**, *13*, 698-702.

(22) Bratton, D.; Yang, D.; Dai, J.; Ober, C. K. *Polym. Adv. Technol.* **2006**, *17*, 94-103.

(23) de Silva, A.; Felix, N. M.; Ober, C. K. *Adv. Mater.* **2008**, *20*, 3355-3361.

(24) Whitmore, M. D.; Noolandi, J. *J. Chem. Phys.* **1990**, *93*, 2946-2955.

(25) Lai, C.; Russel, W. B.; Register, R. A. *Macromol.* **2002**, *35*, 4044-4049.

(26) Park, S. M.; Craig, G. S. W.; La, Y.-H.; Solak, H. H.; Nealey, P. F. *Macromol.* **2007**, *40*, 5084.

(27) Tang, C.; Lennon, E. M.; Fredrickson, G. H.; Kramer, E. J.; Hawker, C. J. *Science* **2008**, *322*, 429.

(28) Tang, C.; Bang, J.; Stein, G. A.; Fredrickson, G. H.; Hawker, C. J.; Kramer, E. J.; Sprung, M.; Wang, J. *Macromol.* **2008**, *41*, 4328-4339.

(29) Kim, G.; Libera, M. *Macromol.* **1998**, *31*, 2569-2577.

(30) Chai, J.; Wang, D.; Fan, X.; Buriak, J. M. *Nature Nanotech.* **2007**, *2*, 500-506.

(31) Chai, J.; Buriak, J. M. *ACS Nano* **2008**, *2*, 489-501.

(32) Hayward, R. C.; Chmelka, B. F.; Kramer, E. J. *Adv. Mater.* **2005**, *17*, 2591-2595.

(33) Hayward, R. C.; Chmelka, B. F.; Kramer, E. J. *Macromol.* **2005**, *38*, 7768-7783.